Tesi di dottorato in Bioingegneria industriale, di Roberto Barone,
discussa presso l'Università Campus Bio-Medico di Roma in data 04/03/2017.
La disseminazione e la riproduzione di questo documento sono consentite per scopi di didattica e ricerca,
a condizione che ne venga citata la fonte.

matr: 20187

UNIVERSITÀ
CAMPUS BIO–MEDICO DI ROMA

FACULTY OF ENGINEERING
Ph.D IN BIOMEDICAL ENGINEERING

Design and control of a dexterous upper-limb prosthetic system

Thesis Supervisor
Prof. Loredana Zollo

Thesis Co-supervisor
Prof. Eugenio Guglielmelli

Author
Roberto Barone

ACADEMIC YEAR 2016/2017

Tesi di dottorato in Bioingegneria industriale, di Roberto Barone,
discussa presso l'Università Campus Bio-Medico di Roma in data 04/03/2017.
La disseminazione e la riproduzione di questo documento sono consentite per scopi di didattica e ricerca,
a condizione che ne venga citata la fonte.

Tesi di dottorato in Bioingegneria industriale, di Roberto Barone,
discussa presso l'Università Campus Bio-Medico di Roma in data 04/03/2017.
La disseminazione e la riproduzione di questo documento sono consentite per scopi di didattica e ricerca,
a condizione che ne venga citata la fonte.

Abstract

The human hand is considered as the highest example of dexterous system capable of interacting with different objects and adapting its manipulation abilities to them. The control of poliarticulated prosthetic hands represents one important research challenge, typically aiming at replicating the manipulation capabilities of the natural hand. The success of grasping and manipulation tasks of commercial prosthetic hands is mainly related to amputee visual feedback since they are not provided either with tactile sensors or with sophisticated control. As a consequence, slippage and object falls often occur.
Another important issue to consider is the preshaping of the hand, in fact it is very important to avoid injuries for the amputees giving them a prosthetic wrist. Literature studies highlight the importance of the active pronosupination and passive flexion-extension for an upper limb amputee.
This thesis wants to address the specific issue of enhancing grasping and manipulation capabilities of existing prosthetic hands, by changing the control strategy and designing a new prosthetic wrist. For this purpose it proposes a multilevel control based on two distinct levels: a high and a low level. The low level control is a parallel force-position control and directly communicate with the actuators of the prosthetic hand while the high level could be a policy search learning algorithm or an actor-critic reinforcement learning (RL) combined with central pattern generators.
With the RL as high level, it was carried out the control of a commercial biomechatronic hand (the IH2 hand) including the main features of recent poliarticulated prosthetic hands. The training phase of the hand was performed in simulation, the parallel force/position control was tested in simulation whereas preliminary tests were performed on the real IH2 hand. The results obtained in simulation and on the real hand provide an important evidence of the applicability of the bio-inspired neural control to real biomechatronic hand with the typical features of a hand prosthesis.
With the policy search learning algorithm as high level, the control has been tested on an anthropomorphic robotic hand with prosthetic features (the IH2 hand) equipped with force sensors. Bi-digital and tri-digital grasping tasks with and without slip information have been carried out. The KUKA-LWR has been employed to perturb the grasp stability inducing controlled slip events. The acquired data demonstrate that the proposed control has the potential to

Tesi di dottorato in Bioingegneria industriale, di Roberto Barone,
discussa presso l'Università Campus Bio-Medico di Roma in data 04/03/2017.
La disseminazione e la riproduzione di questo documento sono consentite per scopi di didattica e ricerca,
a condizione che ne venga citata la fonte.

adapt to changes in the environment and guarantees grasp stability, by avoiding object fall thanks to prompt slippage event detection.

For what concerns the wrist, an active prono-supination and passive flexion-extension modules are designed in order to avoid compensatory movements during grasps.

The main intention of this thesis is to develop the control strategies and the mechanical design of the wrist previously described. A wrist/hand combined control is proposed and preliminary tests on the prono-supination module have been carried out.

Tesi di dottorato in Bioingegneria industriale, di Roberto Barone,
discussa presso l'Università Campus Bio-Medico di Roma in data 04/03/2017.
La disseminazione e la riproduzione di questo documento sono consentite per scopi di didattica e ricerca,
a condizione che ne venga citata la fonte.

Contents

Tesi di dottorato in Bioingegneria industriale, di Roberto Barone,
discussa presso l'Università Campus Bio-Medico di Roma in data 04/03/2017.
La disseminazione e la riproduzione di questo documento sono consentite per scopi di didattica e ricerca,
a condizione che ne venga citata la fonte.

Tesi di dottorato in Bioingegneria industriale, di Roberto Barone,
discussa presso l'Università Campus Bio-Medico di Roma in data 04/03/2017.
La disseminazione e la riproduzione di questo documento sono consentite per scopi di didattica e ricerca,
a condizione che ne venga citata la fonte.

Chapter 1

Introduction

Upper limb prosthetics is a hot topic in the research scenario because of the the high number of amputees each year: the amputation incidence is 3.9 citizens per 100000 [1]. Upper limb prostheses can be divided in two main groups: passive and active prostheses. Passive prostheses can be cosmetic or for work, while active can be body powered or myoelectric. Active prostheses are also called externally powered and have components that are moved by motors and powered by batteries. The system is controlled by a microprocessor that uses signals from the body to command the prosthesis. Signals are generated one of two ways: body movement or, more commonly, electrical signals generated by the user's muscles [2]. In the clinical practice the control of upper limb prostheses is nowadays achieved thanks to electromyographic sensors put on agonist-antagonist muscles and proportional control. On the other hand, control of upper limb prostheses in the research field builds on control approaches for robotic hands.

In literature many attempts to improve the state of the art of the prosthetic hands have been done, trying to improve the mechanical aspects of the prosthesis [3], [4], [5], [6], [7] rather than the controller [8], [9]. Results are encouraging for the development of noninvasive EMG interfaces for the control of dexterous prostheses, but there are still things to improve, such as the simultaneous control of more degrees of freedom, improving the dexterity and the manipulation capabilities of the hands.

In this thesis we propose to improve the dexterity and the manipulation abilities of hand prostheses through two main ways: (i) developing control strategies grounded on sensory-motor coordination, thanks to tactile sensors for force and slippage sensing embedded in the fingertips; (ii) designing an innovative wrist for active prono-supination and passive flexion-extension to improve dexterity

Tesi di dottorato in Bioingegneria industriale, di Roberto Barone,
discussa presso l'Università Campus Bio-Medico di Roma in data 04/03/2017.
La disseminazione e la riproduzione di questo documento sono consentite per scopi di didattica e ricerca,
a condizione che ne venga citata la fonte.

and reduce the side effects of body compensation movements.
The lack of dexterity and manipulation ability is one of the main limitations of currently available prosthetic hands. This thesis wants to face this challenge by developing a new controller able to adapt to the different circumstances of grasp and manipulation and a novel prosthetic wrist to enable most of grasping and manipulation tasks requiring the wrist degrees of freedom in a more natural way than currently available solutions.

This thesis is structured as follows:

- Chapter 2 presents an overview of the systems at the moment present on the market and in the literature divided in hand prostheses, wrist modules and control strategies; pros and cons of solutions are analysed for defining the requirements of the developed hardware and software technologies.

- Chapter 3 presents the proposed force-and-slippage control, aimed at improving the manipulation and dexterity abilities of a prosthetic hand by means of a distributed high-level/low-level approach for sensori-motor coordination of fingers in grasping and manipulation tasks.

- In chapter 4 the design of an innovative wrist for active prono-supination and passive flexion-extension is presented. It is conceived to be embedded in the user's socket and easily interfaced with already available commercial hand prostheses.

Tesi di dottorato in Bioingegneria industriale, di Roberto Barone,
discussa presso l'Università Campus Bio-Medico di Roma in data 04/03/2017.
La disseminazione e la riproduzione di questo documento sono consentite per scopi di didattica e ricerca,
a condizione che ne venga citata la fonte.

Chapter 2

Overview on upper-limb prostheses: hand, wrist, and control

2.1 Prosthetic Hands

There are three main types of prostheses in the upper limb scenario:

1. cosmetic;
2. kinematic;
3. myoelectric.

Cosmetic prostheses are just objects that substitute the missing limb and hand but with no functions. They are very realistic and assure a psychological support to permit the amputees to live in the society avoiding to be shy for their difference with people having sound limbs.
Kinematic prostheses are typically composed of an elbow and a hook as hand and are moved by the sound limb of the user by cables.
Myoelectric prostheses are instead devices very similar to the human hand, with 5 fingers and are moved thanks to surface electromyography sensors with the so-called myoelectric control.
On the market there are three main prostheses: Michelangelo, Bebionic and iLimb. The Michelangelo hand [10] (Fig. 2.1) is an anthropomorphic prosthesis with three degrees of actuation: one to open-close the hand, one to adduct-abduct the thumb and the last to rotate the wrist. It is one of the most advanced device. Bebionic hand [11] (Fig. 2.2) is a five fingered pros-

Tesi di dottorato in Bioingegneria industriale, di Roberto Barone,
discussa presso l'Università Campus Bio-Medico di Roma in data 04/03/2017.
La disseminazione e la riproduzione di questo documento sono consentite per scopi di didattica e ricerca,
a condizione che ne venga citata la fonte.

Figure 2.1: The Michelangelo hand.

thetic device with one actuator for each finger. It can achieve 14 different grip patterns and is designed to handle almost anything that the amputee need to do in an average day, from eating meals and carrying bags, to opening doors, switching on lights and typing. Thumb and wrist are moved by the sound hand of the user.

At last, the iLimb prosthesis [12] (Fig. 2.3) features powered rotating thumb

Figure 2.2: The Bebionic hand.

and individually active articulating fingers offering unparalleled dexterity and reliable access to precision grip patterns. With 24 grip options and extra sensitive electrodes, is the first upper limb prosthesis that can be controlled via a

Tesi di dottorato in Bioingegneria industriale, di Roberto Barone,
discussa presso l'Università Campus Bio-Medico di Roma in data 04/03/2017.
La disseminazione e la riproduzione di questo documento sono consentite per scopi di didattica e ricerca,
a condizione che ne venga citata la fonte.

mobile application.

In literature there are some examples of prosthetic hands. One example is

Figure 2.3: The iLimb hand.

the Southampton Hand [3], which has six degrees of freedom and is shown in Figure 2.4. The hand consists of six small electrical motors, two of which are used to actuate the extension-flexion, and rotation movements of the thumb with each of the remaining four motors being assigned to individual fingers. Each finger is made from six bar linkages, which when extended or flexed curl in a fixed anthropomorphic trajectory. To reduce the power required to hold an object, the fingers are driven via a worm wheel gear configuration. This also has the additional advantage that it prevents the fingers being back driven after power is removed from the motor. The drive from the worm wheel configuration also increases the torque produced from the small motors to provide a 9 N grip force at the end of each finger. On each fingertip is an array of thick-film sensors which can be used to monitor the force exerted by the fingertip as well as detect the onset of object slip and measure temperature.

Another example is the MARCUS hand: a two degree of freedom hand prosthesis with hierarchical grip control [5]. The control is arranged in a hierarchical manner and the lower levels' detailed control is performed by a microprocessor, so it is possible to control a number of degrees with little direct intervention by the operator.

An experimental hand prosthesis 2.5 design is presented in [6] with 8 small fluidic actuators at the digit joints. With the objective of addressing consumers' requirements, functionality was increased and cosmetic appearance became more natural. Moreover, a vibrotactile feedback system makes the prosthesis controllable without visual attention.

Tesi di dottorato in Bioingegneria industriale, di Roberto Barone,
discussa presso l'Università Campus Bio-Medico di Roma in data 04/03/2017.
La disseminazione e la riproduzione di questo documento sono consentite per scopi di didattica e ricerca,
a condizione che ne venga citata la fonte.

Figure 2.4: The Southampton hand.

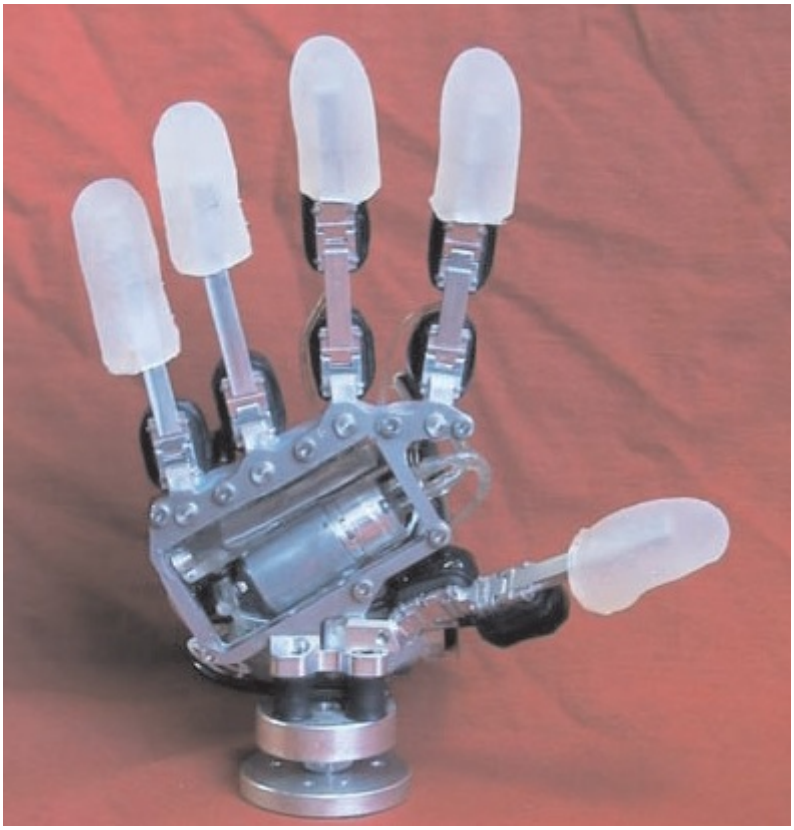

Figure 2.5: Multifunctional hand prosthesis.

Tesi di dottorato in Bioingegneria industriale, di Roberto Barone,
discussa presso l'Università Campus Bio-Medico di Roma in data 04/03/2017.
La disseminazione e la riproduzione di questo documento sono consentite per scopi di didattica e ricerca,
a condizione che ne venga citata la fonte.

In [7] the design and analysis of a multi-fingered hand prosthesis (YOWA hand) is presented (Figure 2.6). The hand has multi-actuated fingers, four

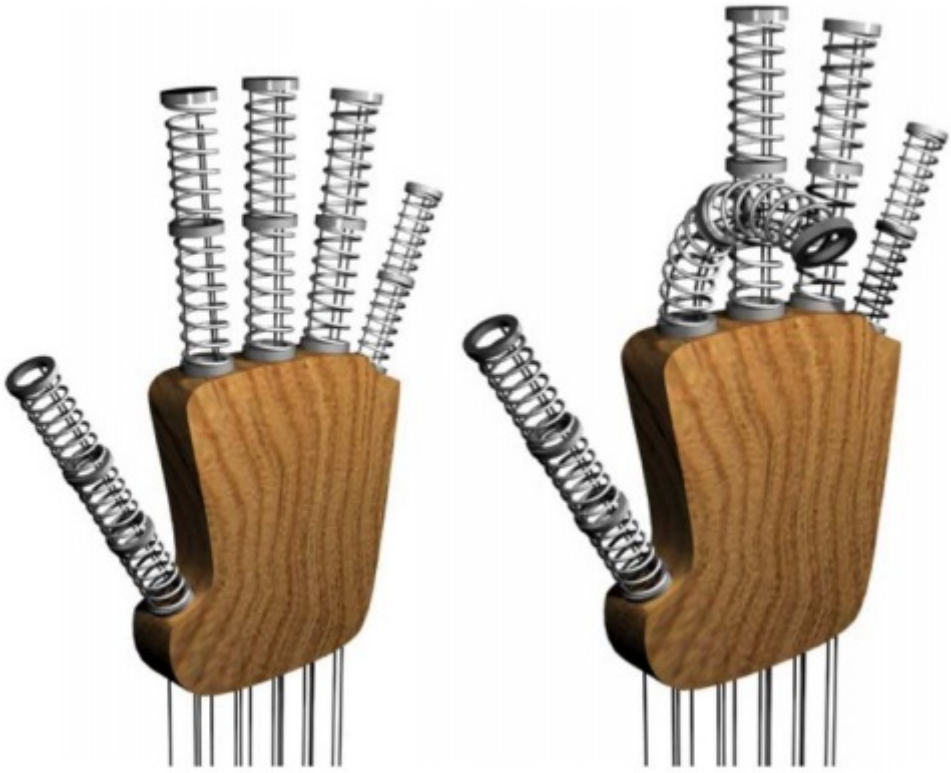

Figure 2.6: Prototype of the IOWA prosthesis.

with two joints and the thumb with three joints. Each joint is designed using a novel flexible mechanism based on the loading of a compression spring in both transverse and axial directions and using cable-conduit systems. The rotational motion is transformed to tendon-like behavior, which enables the location of the actuators far from the arm (e.g., on a belt around the waist). This new design, while presents a low cost alternative, enables the actuation and control of a multi-fingered hand with relatively high degrees of freedom.
In [13] is reported a taxonomy of different grasps that were referenced in the literature and are arranged in a systematic way (Figure 2.7).
Actual prostheses can perform only few of these grasps, and no manipulation ability is implemented.

2.2 Prosthetic Wrist

In an upper-limb prosthesis, a very important role is played by the wrist because it allows the prepositioning and orientation of the hand in the space.

Tesi di dottorato in Bioingegneria industriale, di Roberto Barone,
discussa presso l'Università Campus Bio-Medico di Roma in data 04/03/2017.
La disseminazione e la riproduzione di questo documento sono consentite per scopi di didattica e ricerca,
a condizione che ne venga citata la fonte.

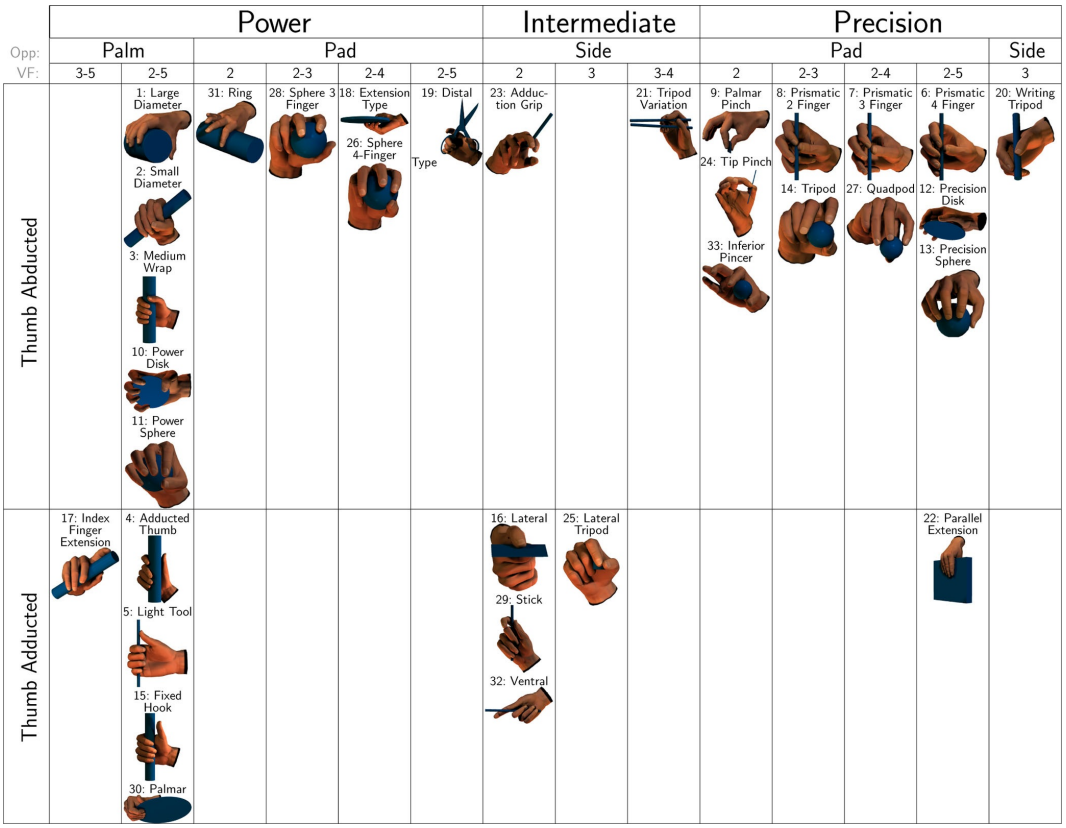

Figure 2.7: The GRASP Taxonomy proposed by Feix et al.

This is also confirmed by the taxonomy shown in Fig. 2.7.

In the following an in-depth analysis of wrist prosthetic module is reported and a taxonomy of the wrist modules is proposed in Figure 2.8. Main difference is between passive and active wrists; the latter are able to generate movements autonomously, because they have an independent actuation.

Most delicate aspects to consider during the design of prosthetic systems for the wrist are:

1. Length, which is added to the socket because wrist modules are thought to be mounted at the end of the socket and before the prosthetic hand. This is particularly critical when the subject has a distal amputation.

2. Weight that, if not limited, can bring to frustration and the abandonment of the module;

3. Prosthetic control, because there is the necessity of enabling simultaneous control of more dofs trying to find the right compromise between ease of use and computational burden of the control algorithm.

Tesi di dottorato in Bioingegneria industriale, di Roberto Barone,
discussa presso l'Università Campus Bio-Medico di Roma in data 04/03/2017.
La disseminazione e la riproduzione di questo documento sono consentite per scopi di didattica e ricerca,
a condizione che ne venga citata la fonte.

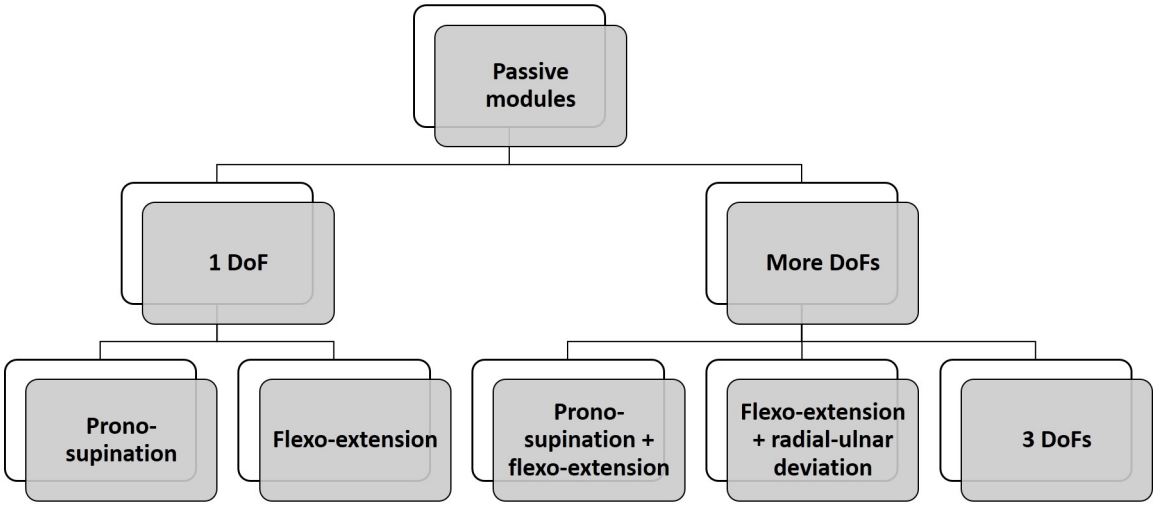

(a) *Taxonomy of the passive wrist.*

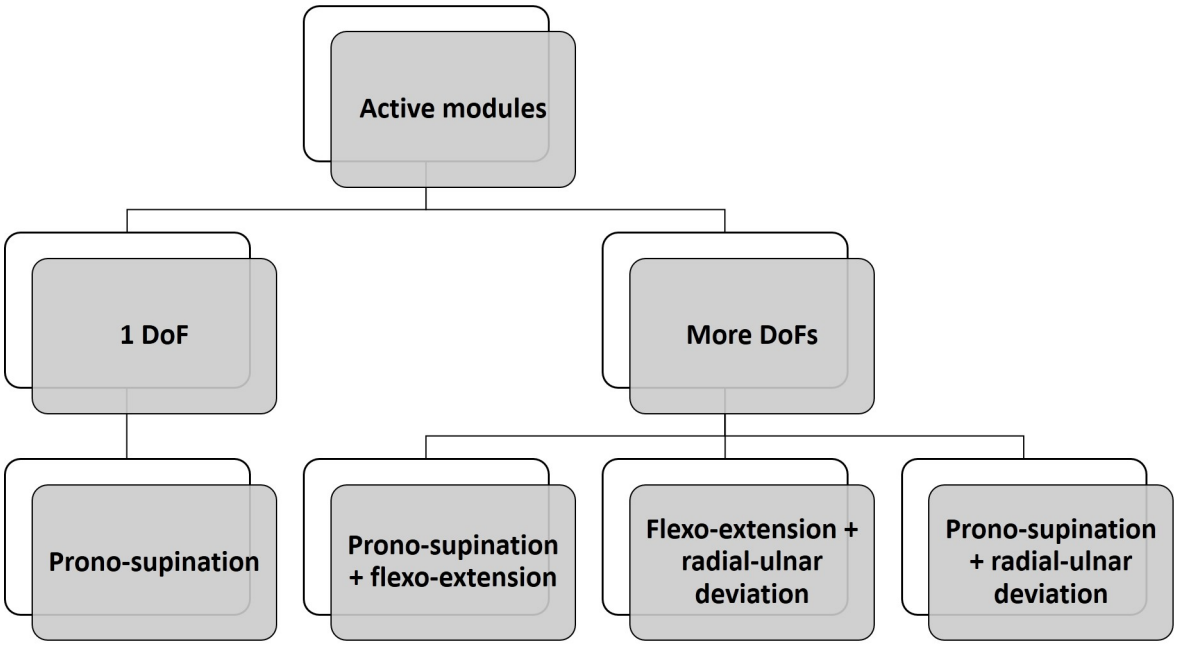

(b) *Taxonomy of the active wrist.*

Figure 2.8: Taxonomy of the wrist modules.

2.2.1 Passive modules with one degree of freedom

Modules for the passive prono-supination

This typology of modules comprises commercial products that can be grouped in the following categories:

Tesi di dottorato in Bioingegneria industriale, di Roberto Barone,
discussa presso l'Università Campus Bio-Medico di Roma in data 04/03/2017.
La disseminazione e la riproduzione di questo documento sono consentite per scopi di didattica e ricerca,
a condizione che ne venga citata la fonte.

- Friction modules;
- Rapid unfasten modules;
- Rotational modules.

Friction modules (fig. 2.9(a)) allow the user to do a prono-supination of the wrist rotating the prosthesis with the sound limb. Application of these devices on bilateral amputees results not so feasible. Typical materials used for the

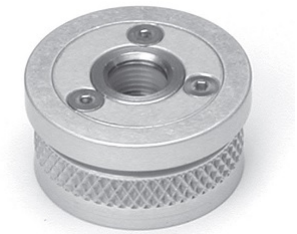

(a) *Standard friction wrist module.*

(b) *Oval module.*

(c) *Module for the disarticulation of the wrist.*

Figure 2.9: Friction modules.

realization of the prono-supination modules are the aluminum, the steel and the titanium. These devices are sold, for example, by Hosmer. The catalog is visible in [14].
Different sizes are available, starting from the child size of 32 mm of diameter and 28 g of mass, until the adult size characterized by 51 mm of diameter and 74 g of mass.
This functioning principle is utilized also by wrist prostheses with oval shape in Fig. 2.9(b) and in that for wrist disarticulation (fig. 2.9(c)).
RSL-Steeper company, which produces Bebionic 3 prosthetic hand, give different possibilities as wrist modules [15]. One of these (Fig. 2.10) is a wrist

Tesi di dottorato in Bioingegneria industriale, di Roberto Barone,
discussa presso l'Università Campus Bio-Medico di Roma in data 04/03/2017.
La disseminazione e la riproduzione di questo documento sono consentite per scopi di didattica e ricerca,
a condizione che ne venga citata la fonte.

with just 10 mm of thickness which permits passive prono-supination with adjustable friction. Another company leader in selling wrist modules is Ottobock

Figure 2.10: "Short" module for Bebionic 3 hand.

[16]. Friction wrist modules for disarticulation are sold in different sizes. In Fig. 2.11 an example of Ottobock friction wrist is reported. Available dimensions are: 28, 34, 40, 45 e 50 mm of diameter.

Another module for passive prono-supination produced by Hosmer is the

Figure 2.11: Ottobock frction module.

"Wedge-Grip" available in circular and oval shape (Fig. 2.12). Only the adult size is available (51 mm of diameter for the circular and 57x41 mm for the oval).

Hosmer also produces the "Economy-Wrist", available in aluminum, steel or titanium only in a big size (51 mm of diameter); near in the figure 2.13 there is the version with metallic bands which, attached to the socket, allow the amputee to lift more load in comparison to the other wrist modules. On the market there are also light passive wrist modules for prono-supination. There is Hosmer module (Fig. 2.14(a)) realized in ABS and available in small, medium

Tesi di dottorato in Bioingegneria industriale, di Roberto Barone,
discussa presso l'Università Campus Bio-Medico di Roma in data 04/03/2017.
La disseminazione e la riproduzione di questo documento sono consentite per scopi di didattica e ricerca,
a condizione che ne venga citata la fonte.

Figure 2.12: "Wedge-Grip" Hosmer modules.

Figure 2.13: "Economy-Wrist"Hosmer modules.

and large sizes. It has controllable friction and can be modeled on the amputee, in order to let the transition between prosthesis and socket smoother.

LTI [17] also produces a light wrist module, realized in metallic material,

(a) *Hosmer light wrist module in ABS.*

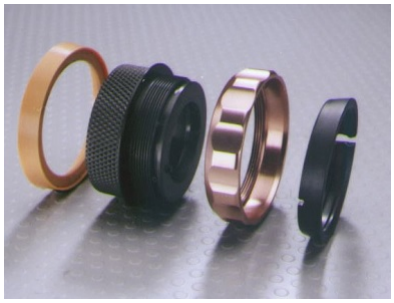

(b) *Passive light module of the LTI.*

Figure 2.14: Light passive modules.

available in 4 sizes. (Fig. 2.14(b)).

Quick release wrist modules are designed in order to allow a rapid substitution of the prosthesis, typically hook and prosthetic hand.
Main actions these modules allow are:

- removing hand prosthesis from the wrist module;
- substituting one prosthetic hand with another one;

Tesi di dottorato in Bioingegneria industriale, di Roberto Barone,
discussa presso l'Università Campus Bio-Medico di Roma in data 04/03/2017.
La disseminazione e la riproduzione di questo documento sono consentite per scopi di didattica e ricerca,
a condizione che ne venga citata la fonte.

- manually positioning prosthetic hand in different prono-supiantion configurations;
- blocking prosthetic hand in different prono-supination positions.

These modules are sold by Hosmer, Ottobock and LTI.
Bebionic 3 hand, other than "short" module earlier presented, can be furnished with a quick release module (Fig. 2.15). It allows a quick substitution between different terminal devices and passive prono-supination. There is a version

Figure 2.15: Quick release module for Bebionic 3 hand.

from the Hosmer (Fig. 2.16(a)) which functioning is controlled by a lever. A little pressure allows locking and unlocking to manage prono-supination, while a stronger pressure allows the expulsion of the prosthesis.
Also exists a Hosmer version with no lever (fig. 2.16(b)) where prosthesis unfasten rather then rotation depends on the rotation direction.
In figure 2.17 is presented the quick disconnect module of the Ottobock, but

(a) *Quick disconnect module with lever.*

(b) *Quick disconnect module with no lever.*

Figure 2.16: Hosmer quick disconnect modules.

Tesi di dottorato in Bioingegneria industriale, di Roberto Barone,
discussa presso l'Università Campus Bio-Medico di Roma in data 04/03/2017.
La disseminazione e la riproduzione di questo documento sono consentite per scopi di didattica e ricerca,
a condizione che ne venga citata la fonte.

Figure 2.17: Ottobock quick disconnect module.

no technical information are given. LTI quick disconnect module [18] is similar to the other and has 4 different diameters: 40, 45, 50 and 54 mm.

Wrist modules described so far can create difficulties to that subjects that, for personal or work reasons, exert high torques on the prosthesis. These devices allow involuntary rotations if loads are bigger than a certain value.
Hosmer rotational wrists (Fig. 2.18) are devices with the control of the passive prono-supination, but with active blocking mechanism. In the unlocked modality is possible to rotate the wrist about 360°. In the locked modality the resistance to the rotation is much larger than in the previous wrists.
There are 18 blocking positions and only one size, the adult one, with a diameter of 51 mm.

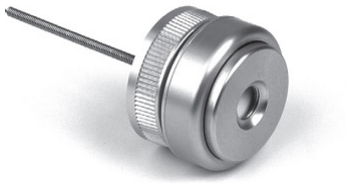

Figure 2.18: Moduli di polso rotazionali.

Modules for the passive prono-supination

Flexion-extension is a very important degree of freedom of the wrist because it allows activities of daily living like getting dressed, eating, shaving, personal hygiene. Flexion-extension modules are an alternative to prono-supination friction modules and they allow the manual positioning in different flexion-extension positions.
There exist three products from the Hosmer company: the *APRL* (Fig. 2.19(a)),

Tesi di dottorato in Bioingegneria industriale, di Roberto Barone,
discussa presso l'Università Campus Bio-Medico di Roma in data 04/03/2017.
La disseminazione e la riproduzione di questo documento sono consentite per scopi di didattica e ricerca,
a condizione che ne venga citata la fonte.

(a) *APRL Hosmer unit.* (b) *Hosmer Sierra flexion wrist module of the wrist.* (c) *Hosmer* FW *flexion wrist module.*

Figure 2.19: Wrist modules with integrated flexion-extension.

the *Sierra* (Fig. 2.19(b)) and *FW* wrist. First module is for the children, with a diameter of 27 mm and a weight of 42 g. It can be manually flexed between 0° and 36° but it doesn't allow fixed positions. At the contrary, *Sierra* module allows fixing the module at $0°, 25°$ and 50° of flexion thanks to a lever. It has a diameter of 36 mm ad a weight of 113 g. The last wrist, figure 2.19(c), can be blocked at $0°, 30°$ and 50° of flexion but also allows regulating the friction resistance. It is recommended the usage only with hook prostheses. It is available in three sizes: small, medium and large. Ottobock also has on the market a wrist for the flexion-extension (Fig. 2.20), that is able to block in 5 positions between $-40°$ e $+40°$. It has a diameter of 36 mm and a weight of 85 g.

Figure 2.20: Ottobock flexion-extension module.

2.2.2 Passive wrist modules with more degrees of freedom

Prono-supination and flexion-extension modules

These modules allow the amputee to passively control 2 degrees of freedom: prono-supination and flexion-extension. Hosmer *4-Function* (Fig. 2.21) is the

Tesi di dottorato in Bioingegneria industriale, di Roberto Barone,
discussa presso l'Università Campus Bio-Medico di Roma in data 04/03/2017.
La disseminazione e la riproduzione di questo documento sono consentite per scopi di didattica e ricerca,
a condizione che ne venga citata la fonte.

combination of the rotational wrist and of the *Sierra* module. It permits 360° of rotation and 3 flexing positions: $0°, 25°$ e $50°$. Ottobock proposes 3 modules

Figure 2.21: Hosmer *4-Function* wrist module for flexion-extension and prono-supination module.

which integrate these degrees of freedom: the *MyoWrist 2 Act* (Fig. 2.22(a)), the *MovoWrist* (Fig. 2.22(b)) and the *10V25 Friction Wrist* (Fig. 2.22(c)).

First module allows passive rotation and flexion-extension in the following

(a) *MyoWrist 2 Act.*

(b) *Module MovoWrist.*

(c) *Module 10V25 Friction Wrist.*

Figure 2.22: Ottobock modules of prono-supination and flexion-extension.

positions: $-40°, -20°, 0°, 20°$ *e* $40°$. It has a diameter of 36 mm and a weight of 55 g. Also the second module allows passive prono-supination, and the blocking position in flexion-extension are 5, between $-10°$ *and* $45°$. The diameter is of 45 mm. The last module has not technical information, except the diameter that is 50 mm.

A very interesting prosthetic wrist is the module integrated in the Ottobock *Michelangelo* hand [19].

This wrist (Fig. 2.23) is formed by two modules, one for the flexion-extension and one for the prono-supination, both passive.

Prono-supination can cover 360°, with 24 blocking positions with a step of 15°. Flexion can approximately reach 70° with 5 ratchet positions. Maximum

Tesi di dottorato in Bioingegneria industriale, di Roberto Barone,
discussa presso l'Università Campus Bio-Medico di Roma in data 04/03/2017.
La disseminazione e la riproduzione di questo documento sono consentite per scopi di didattica e ricerca,
a condizione che ne venga citata la fonte.

extension is 45° with 3 ratchet positions. Weight is about 180 g. This device has 2 main functioning modalities: flexible and rigid. In the first case the wrist can't stop at the ratchet positions and a relaxed natural wrist behaviour is reproduced. In the rigid modality, the wrist is locked in the different configurations of flexion-extension and prono-supination.

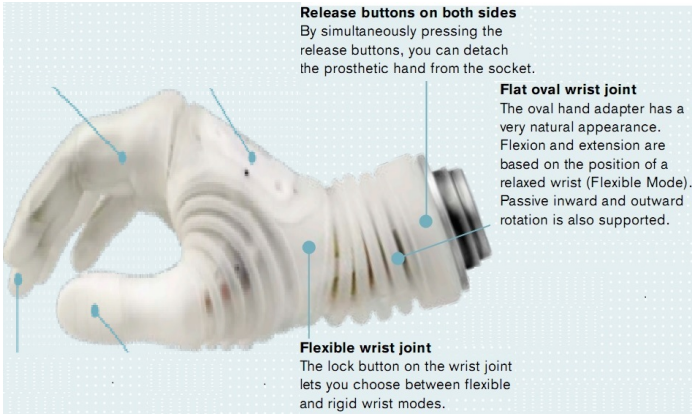

Figure 2.23: Michelangelo prosthetic wrist

Wilmer prosthetic wrist [20] (Fig. 2.24) has been designed for child amputee. A child of 4 years old has been selected as reference. Total dimensions

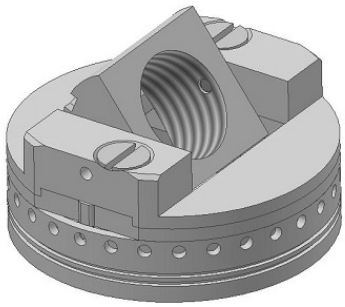

Figure 2.24: Wilmer prosthetic wrist

are 35 mm of diameter and 15 mm of width. Dofs implemented are passive prono-supination and flexion-extension, with the possibility to lock the device in different positions. In particular there are 5 ratchet positions for flexion-extension: $-60°, -30°, 0°, 30°$ and $60°$. In prono-supination the wrist can be locked in 30 positions, every 12°. Maximum torque for the rotation is 24 Nm, in flexion 21 Nm. The weight is about 22 g.
This prosthesis is strong enough to be similar to the others available on the market but maintaining low weight and dimensions although it has 2 passive dofs.

Tesi di dottorato in Bioingegneria industriale, di Roberto Barone,
discussa presso l'Università Campus Bio-Medico di Roma in data 04/03/2017.
La disseminazione e la riproduzione di questo documento sono consentite per scopi di didattica e ricerca,
a condizione che ne venga citata la fonte.

Passive wrist modules for flexion-extension and adduction-abduction

To this category belong to the Multi-Flex module for the Bebionic 3 (Fig. 2.25) which permits passive flexion-extension and guarantees the absorption of the impacts. It is also possible to lock the hand in neutral position, in 30° of flexion or 30° of extension. When the wrist is locked it is possible the passive adduction-abduction.

Figure 2.25: Bebionic 3 multi-Flex prosthetic wrist.

Passive wrist modules with 3 degrees of freedom

These wrist prostheses are characterized by the presence of a ball-joint that allows the prepositioning of all the degrees of freedom with constant friction. Friction che be modified by the user.

A commercial module which belong to this category is LTI OmniWrist (Fig. 2.26) [21], available for children and adults. Ottobock *Myolino Wrist 2000*

Figure 2.26: LTI OmniWrist module.

(Fig. 2.27) is sold in two models: 40 mm of diameter, 32 of length and 47 of

Tesi di dottorato in Bioingegneria industriale, di Roberto Barone,
discussa presso l'Università Campus Bio-Medico di Roma in data 04/03/2017.
La disseminazione e la riproduzione di questo documento sono consentite per scopi di didattica e ricerca,
a condizione che ne venga citata la fonte.

weight and 40 mm of diameter, 40 mm of length, 50 g of weight. They are both available on the Ottobock catalogue [16].

Figure 2.27: Ottobock Myolino 2000 module.

Tesi di dottorato in Bioingegneria industriale, di Roberto Barone,
discussa presso l'Università Campus Bio-Medico di Roma in data 04/03/2017.
La disseminazione e la riproduzione di questo documento sono consentite per scopi di didattica e ricerca,
a condizione che ne venga citata la fonte.

2.2.3 Active wrist modules with 1 dof

Active prono-supination modules

This typology of wrists allows an active prono-supination controllable by the user. In figure 2.28 are shown two examples of rotational modules with active control, commercialized by Ottobock [16]. In the module of figure 2.28(a)

(a) *Electric wrist 10S17.* (b) *Electric wrist 13E205 MyoRotronic.*

Figure 2.28: Wrist modules with active actuation by Ottobock.

the power supply can be 6 or 7.2 Volt. MyoRotronic module (Fig. 2.28(b)) allows, in combination with EMG electrodes, proportional control of prono-supination. This module is compatible with *MyoWrist 2 Act* seen before to simultaneously furnish also the passive flexion-extension and can be utilized with all "Quick Disconnect" devices.
A very interesting active rotational wrist module is commercialized by Motion Control [22], with the name *MC Wrist Rotator* (Fig. 4.3(a)). It is available in two versions: Standard (Fig. 4.3(b)) and Pro (Fig. 4.3(c)). Standard module has a diameter of 50 mm and length 67 mm. It has a weight of 143 g and can be powered between 7.2 and 14.4 V. When the power supply iis 7.2 V, it has a torque of 1.13 $N \cdot m$ and a velocity of 32 rpm; when the power supply is 12 V it has a torque of 1.58 $N \cdot m$ and 61 rpm of velocity. Pro module has the same characteristics but the length and weight that are higher (70 mm and 168 g). The producer says the torque and the speed to be twice the value of the other commercial modules when the power supply is 7.2 V.

Standard module has been modified by LTI [23] (Fig. 2.30) to be compatible with tha *Boston Digital* arm.

Tesi di dottorato in Bioingegneria industriale, di Roberto Barone,
discussa presso l'Università Campus Bio-Medico di Roma in data 04/03/2017.
La disseminazione e la riproduzione di questo documento sono consentite per scopi di didattica e ricerca,
a condizione che ne venga citata la fonte.

(a) *Motion Control rotational module.*

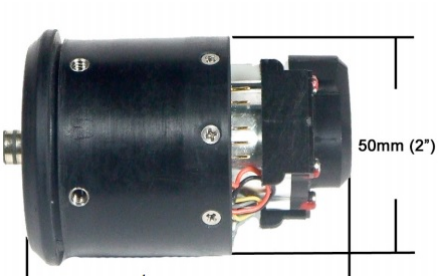

(b) *Standard module.*

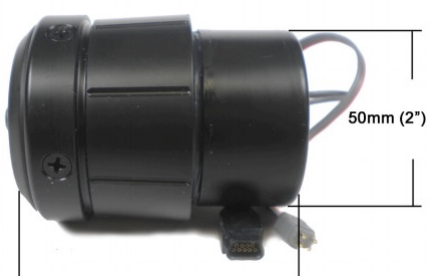

(c) *Pro module.*

Figure 2.29: Motion control active prono-supination modules.

2.2.4 Active modules with more degrees of freedom

Active prono-supination and flexion-extension modules In the research field there is a paper of Kyberd et al. [24] which presents a prototype with actuated prono-supination and flexion-extension thanks to two motors in differential configuration (Fig. 2.31).

The two motors are parallel and oriented in opposite directions. Functioning of the differential mechanism is as follows (Fig. 2.32): when the two motors rotates in the same direction the terminal parts of the differential mechanism counter-rotate, and the prono-supination is possible. Flexion-extension is guaranteed when motors rotate in different directions.

Main advantages using a differential mechanism is the higher output torque and the compactness of the device. The control is performed by a micro-controller (model 18F454, Microchip Technology, Inc; Chandler, Arizona) able to manage the two rotations. The micro-controller receives as input angles measured by two potentiometers and guarantees a physiological range of the two dofs.

The subject can manage the 2 dofs independently, with two different commands. Subject motor intention is managed by an EMG classifier. There are 7 commands to perform: flexion, extension, pronation, supination, opening

Tesi di dottorato in Bioingegneria industriale, di Roberto Barone,
discussa presso l'Università Campus Bio-Medico di Roma in data 04/03/2017.
La disseminazione e la riproduzione di questo documento sono consentite per scopi di didattica e ricerca,
a condizione che ne venga citata la fonte.

Figure 2.30: Active rotational wrist of LTI.

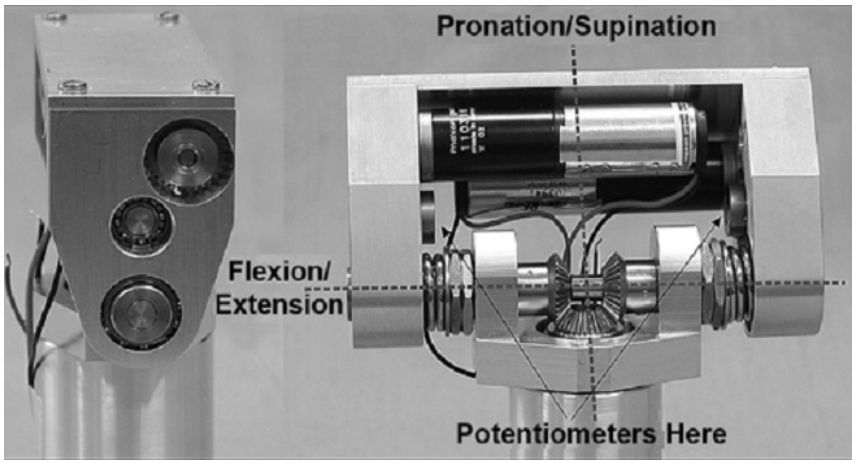

Figure 2.31: Wrist module with differential actuation.

and closing of the hand, no movement. Rotation speed of the motors is proportional to the EMG intensity.
The device occupies 32 mm in the hand utilized as end-effector leaving 16 mm of thickness, so it is possible to use it also on distal amputees. Weight is 200 g. Available torque at 7 V and 500 mA is 0.073 Nm, and it is very low for a practical usage. Maximum angular speed (250 $^{\circ}s^{-1}$ both in flexion-extension that in prono-supination) is comparable with the commercial devices but the high backdriveability doesn't allow the application in the prosthetic field.

Modules for active flexion-extension and adduction-abduction There are no commercial modules with these dofs. Otherwise, in the literature there are some prototypes.

The paper of Ahmad et al. [25] describes the mechanical design of a wrist module with actuated flexion-extension and adduction-abduction. Mechanical

Tesi di dottorato in Bioingegneria industriale, di Roberto Barone,
discussa presso l'Università Campus Bio-Medico di Roma in data 04/03/2017.
La disseminazione e la riproduzione di questo documento sono consentite per scopi di didattica e ricerca,
a condizione che ne venga citata la fonte.

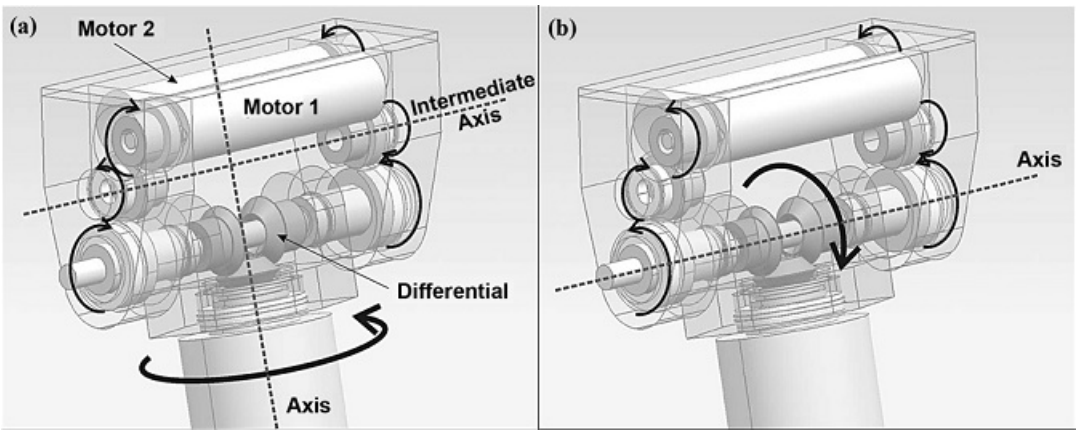

Figure 2.32: Working principle of the differential mechanism. a) Prono-supination b) Flexion-extension.

structure is a modified version of a ball joint (Fig. 2.33). Modifications consist of higher range of motion and in the creation of 4 anchoring points for the cables. Dofs are controlled by 2 actuators.

Materials like steel and bronze cannot be used because of their weight. PTFE

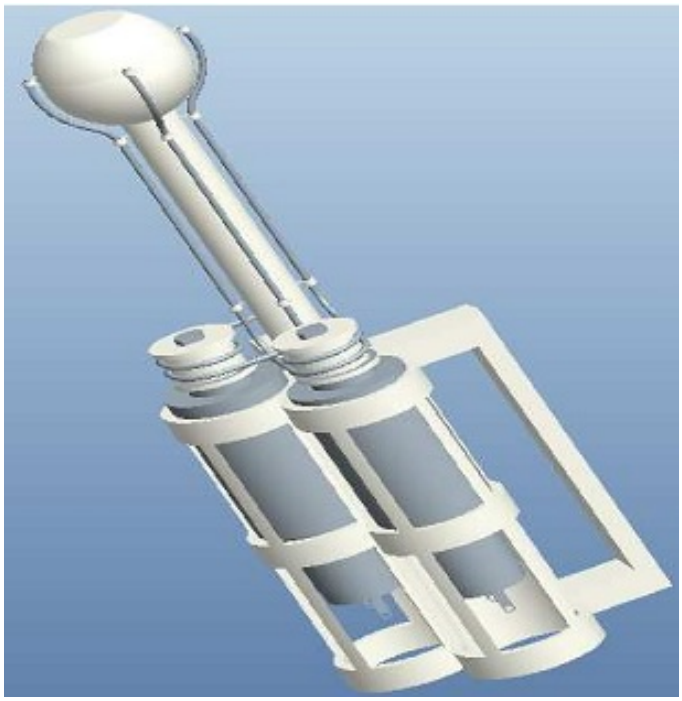

Figure 2.33: Ball-joint actuated thanks to cables.

is a material that guarantees a good resistance to wear, low friction and low weight. The authors of the paper have collected data to evaluate the necessary torque resulted in 4 Nm. Thanks to this value it has been designed the section of the cables and actuators have been selected.

Tesi di dottorato in Bioingegneria industriale, di Roberto Barone,
discussa presso l'Università Campus Bio-Medico di Roma in data 04/03/2017.
La disseminazione e la riproduzione di questo documento sono consentite per scopi di didattica e ricerca,
a condizione che ne venga citata la fonte.

Range of motion of the dofs implemented are very close to human one (Fig. 2.34), but final dimensions and weight are too high.

CHARACTERISTICS OF WRIST ACTUATOR

Characteristics	Wrist Actuator
Actuator Forearm Circumferance	28.274 (cm)
Actuator Wrist Circumferance	14.76 (cm)
Actuator Wrist Breadth	4.7 (cm)
Actuator Weight	870 (gm)
Max. Lift Capacity	3.9 (Nm)
Flexion/Extension axis	85°/90°
Abduction/Adduction axis	15°/45°

Figure 2.34: Final characteristics of the wrist module with actuated ball-joint.

In Tropea et al. [26] is presented an active solution for the flexion-extension (25°-35°) and adduction-abduction (30°-25°). Range of motion is limited and cannot cover the physiological one. Figure 2.35 shows the functioning of the

Figure 2.35: ARTS robotic wrist.

wrist. There is a spring which link two circular plates, and 3 motors linked to the upper plate thanks to cables. Combining the actuation of the 3 motors it is possible to obtain the desired dof. Total dimensions are 120 mm of diameter and 150 mm of thickness.
The spring wants to substitute a cardan joint. Motors works in direct current and they have a worm-gear reduction which converts the movement from rotational to linear and make the system non backdriveable.

Tesi di dottorato in Bioingegneria industriale, di Roberto Barone,
discussa presso l'Università Campus Bio-Medico di Roma in data 04/03/2017.
La disseminazione e la riproduzione di questo documento sono consentite per scopi di didattica e ricerca,
a condizione che ne venga citata la fonte.

Modules for active prono-supination and adduction-abduction Below is described a wrist module integrated in a proshtetic arm [27].

The wrist has prono-supination and adduction-abduction dofs. Prono-supination

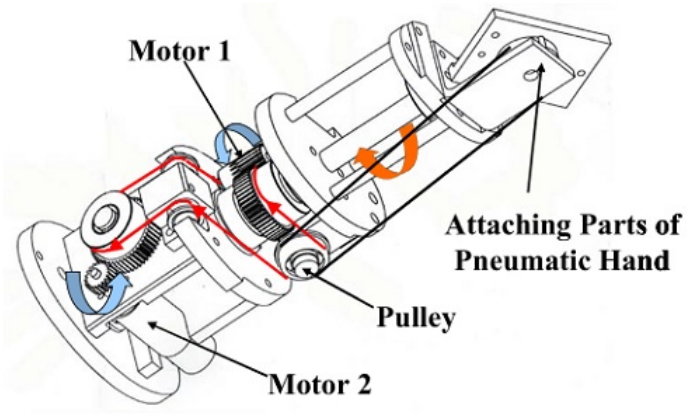

(a) *Prono-supination mechanism.*

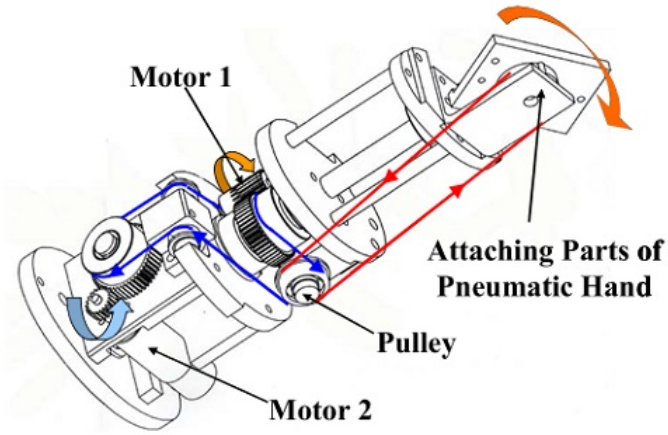

(b) *Adduction-abduction mechanism.*

Figure 2.36: Dofs actuation of the wrist.

mechanism is depicted in figure 2.36(a). When it is applied the same voltage to both motors, a rotation around the main axis is performed.

When an opposite voltage is applied to the motors (Fig. 2.36(b)), the cable linked to the hand is pulled. Thanks to this mechanism is possible the adduction-abduction of the terminal device depending on the rotational direction of the actuators.

Using two motors allow increasing the output torque. The paper does not provide numerical data and dimension of the device.

The movement of the wrist relies on a fuzzy control modeled on Matlab/Simulink environment. After simulations the control has been implemented on DSP (DS1005;dSPACE Inc.).

Experimental trials have given confirmation of the functioning of the control

Tesi di dottorato in Bioingegneria industriale, di Roberto Barone,
discussa presso l'Università Campus Bio-Medico di Roma in data 04/03/2017.
La disseminazione e la riproduzione di questo documento sono consentite per scopi di didattica e ricerca,
a condizione che ne venga citata la fonte.

on the real system.

2.3 Control of prosthetic hands

One of the first solutions of myoelectric control is the on-off control: when the EMG signals exceed a threshold, a certain prosthesis function is activated [28]. This simple and intuitive control modality requires many sites to extract the EMG signal, one for each function to control. This condition is often prohibitive in proximal amputees and hugely restricts the number of functions to select. One way to overcome this drawback is to have different activation thresholds, but this solution (called Double-Command Control) affects the simplicity of use [29] and limits its application. As an alternative, the Agonist/Antagonist Control can be used. It consists of using a couple of electrodes on agonist-antagonist muscle pairs [30]. The contraction of one muscle is associated to the motion of opening with constant speed, while the contraction of the other muscle controls the closure; simultaneous muscle pair contraction(co-contraction) allows switching from one function to another. Setting an intermediate threshold of the muscle contraction it is possible to obtain a two-speedmotion (i.e., Two-SpeedControl) of the prosthesis (slow and fast) to accommodate fine movements.

Proportional control [31] permits to vary force and speed proportionally to the amplitude of the recorded EMG signal. Hence, the voltage command for the motors is taken as proportional to the contraction intensity. Measuring EMG signals from agonist/antagonist muscles is a common procedure in proportional control and co-contraction of the muscle pair is used to select the degree of freedom to control. The main limitation of agonist/antagonist control consists of the limited number of independently controllable DoFs (far from the multi-functional control of the human hand). Anyway, thanks to its simplicity and robustness, it results to be the most adopted control option for myoelectric prostheses in commercially available systems as well as in clinical applications [32].

Two additional techniques have been developed in the framework of myoelectric control, i.e. the Targeted Muscle Reinnervation (TMR) [33] and the recent nerve transfer in brachial plexus injury [34]. In the TMR [33], the remaining arm nerves are reallocated to residual chest or upper-arm muscles that are no longer biomechanically functional due to the amputation. Once re-innervated, these muscles serve as biological amplifiers of motor commands

Tesi di dottorato in Bioingegneria industriale, di Roberto Barone,
discussa presso l'Università Campus Bio-Medico di Roma in data 04/03/2017.
La disseminazione e la riproduzione di questo documento sono consentite per scopi di didattica e ricerca,
a condizione che ne venga citata la fonte.

from the transferred arm nerves and provide physiologically appropriate EMG signals for the arm control. This procedure is especially applied to subjects with very proximal amputation, which usually control the motors of the prosthetic arm through switches actuated with residual shoulder movement or myoelectric signals acquired from muscles of the chest and back. With respect to these control techniques, TMR presents several advantages, such as improvements in function (measured both objectively and subjectively), ease of use, simultaneous control of more than one DoF, fast and seamless motion [35]. In [34] nerve transfer in brachial plexus injury is presented. It is defined "bionic reconstruction." After free functioning muscle transfer procedure for the restoration of shoulder and elbow functions, the hand muscle activity has been restored selectively transferring the nerves in order to optimize the number of electromyographic sites. The surgical procedure and the rehabilitation program allowed the improvement of EMG activity and the maximization of the prosthetic hand functions.

Over the years, several studies for improving myoelectric control performance have been carried out. The development of pattern recognition techniques aimed at increasing the number of controllable DoFs (and consequently the number of feasible functions) keeping low the number of utilized electrodes ([36]). Myoelectric control based on pattern recognition techniques resorts to supervised machine learning algorithms ([37]): in an initial training phase the system learns to associate different hand gestures to different myoelectric patterns based on the phantom limb effect. This association is then adopted in the daily use of the prosthesis.

This thesis work is focused on the study of the controller that follows the EMG analysis and builds on robotic controls and also deals with the design of a new prosthetic wrist in order to improve the dexterity of the system. In chapter 3 is reported a state of the art of the most common controllers found in literature.

Tesi di dottorato in Bioingegneria industriale, di Roberto Barone,
discussa presso l'Università Campus Bio-Medico di Roma in data 04/03/2017.
La disseminazione e la riproduzione di questo documento sono consentite per scopi di didattica e ricerca,
a condizione che ne venga citata la fonte.

Chapter 3

Multilevel control of an anthropomorphic prosthetic hand for grasp and slip prevention

The human hand is considered as the highest example of dexterous system capable of interacting with different objects and adapting its manipulation abilities to them. The control of poliarticulated prosthetic hands represents one important research challenge, typically aiming at replicating the manipulation capabilities of the natural hand.
This chapter wants to propose a multi-level control architecture for prosthetic hands, capable of learning both cyclic manipulation and grasping capabilities. To this purpose, it is focused on the control of a commercial biomechatronic hand (the IH2 hand by Prensilia s.r.l.) including the main features of recent poliarticulated prosthetic hands and, at the same time, offering an open platform for research.

3.1 Grasping tasks

3.1.1 Introduction

The success of grasping and manipulation tasks of commercial prosthetic hands is mainly related to amputee visual feedback, since they are not provided either with tactile sensors or with sophisticated control. As a consequence slippage and object falls often occur. This paragraph wants to address the specific issue of enhancing grasping and manipulation capabilities of existing prosthetic hands, by changing the control strategy. To this purpose, it pro-

Tesi di dottorato in Bioingegneria industriale, di Roberto Barone,
discussa presso l'Università Campus Bio-Medico di Roma in data 04/03/2017.
La disseminazione e la riproduzione di questo documento sono consentite per scopi di didattica e ricerca,
a condizione che ne venga citata la fonte.

poses a multilevel control based on two distinct levels consisting of i) a policy search learning algorithm combined with Central Pattern Generators in the higher level, and ii) a parallel force/position control managing slippage events in the lower level. The control has been tested on an anthropomorphic robotic hand with prosthetic features (the IH2 hand) equipped with force sensors. Bi-digital and tri-digital grasping tasks with and without slip information have been carried out. The KUKA-LWR has been employed to perturb the grasp stability inducing controlled slip events. The acquired data demonstrate that the proposed control has the potential to adapt to changes in the environment and guarantees grasp stability, by avoiding object fall thanks to prompt slippage event detection.

Commercial prostheses are typically velocity- or position-controlled; no tactile system is integrated in the hand and the success of the grasp is based on the visual feedback of the amputee [38],[39]. On the other hand, control solutions of prosthetic hands based on tactile feedback are borrowed from robotics, where the tactile sensing allows endowing the robotic hands with autonomous dexterous manipulation features. In robotic applications, tactile systems are used for objects recognition tasks, control forces, grasp objects and to servo surfaces [40]. The control approaches can control fingers torque, force, velocity and trajectory and include classical PID, adaptive, robust, neural, fuzzy sliding-mode and their combinations [41],[42]. In addition, a well-consolidated approach to ensure grasp stability relies on the concept of friction cone, thus implying that the ratio between the normal force and the tangential force during grasping, multiplied by the static coefficient of friction, has to exceed one. This method is very effective; however, it suffers from some limitations that make it unsuitable for prosthetics, e.g. it requires sensors able to measure both normal and tangential forces (even though estimations of the latter can be used as in [43]) and requires to a priori know the static friction coefficient.

Alternative and more recent approaches able to still guarantee grasp stability rely on force control schemes that allow recognizing slippage events by the decrease of the measured normal force. An example of this approach can be found in [44], where a PID control is used to preshape a multi-fingered underactuated hand, and a simultaneous force control is applied to all the fingers during grasping. In [70] a PI force control with an inner velocity loop has been proposed, but no experimental tests on real prosthetic hands have been done. A hybrid approach has been tested in [45], where a PI force control is adopted for the outer loop, while a fuzzy position control is used in the inner loop. In [46] a control strategy based on a neural network has been implemented in

Tesi di dottorato in Bioingegneria industriale, di Roberto Barone,
discussa presso l'Università Campus Bio-Medico di Roma in data 04/03/2017.
La disseminazione e la riproduzione di questo documento sono consentite per scopi di didattica e ricerca,
a condizione che ne venga citata la fonte.

order to compensate for sensors and hardware non-linearities. The control was divided into two stages: the former was a velocity control to grasp the object, the latter was a force control. Lately, further studies have been proposed where controls based on slippage prevention are implemented. The idea to prevent slippage in robotics is not new [47]; however, the first example of prosthetic device with force control and slip prevention algorithm has been presented in [48]. In it, a sliding mode force control with slippage detection was successfully compared with a simple PD force control and a sliding mode with no slippage detection. In [49] a position proportional control has been used to grasp the object, and a fuzzy logic based algorithm was complementary implemented to prevent slippage.

Recent algorithms have proposed to use neural networks [50] and fuzzy logic [51] to modulate grasping force of a prosthetic hand.

In this work a new control architecture for prosthetic hands is proposed with the following two main features:

- It is distributed on two levels: an high level based on learning, for trajectory planning and finger coordination, and a low-level for force and position control;
- The low level is made of a parallel force/position control endowed with slippage prevention capability.

A preliminary feasibility study of such a control architecture has been provided in [52]. An actor-critic reinforcement learning paradigm and a classical parallel force/position control have been implemented. The architecture was validated in simulation in a cyclic manipulation tasks with a multi-fingered prosthetic hand.

Here, the high-level control has been grounded on a policy search learning algorithm (Policy Improvement Black Box); the low-level control has been based on a parallel force/position control able to manage also slip events. Moreover, the control architecture is implemented and experimentally validated on a real multifingered prosthetic hand, i.e. the IH2 hand (by Prensilia s.r.l.), purposely equipped with force sensors on the distal phalanxes.

In the literature different control architectures based on learning algorithms have been proposed to control robotic hands during grasping or manipulation tasks [53], [54], [55], [56]. Such architectures have been typically based on hierarchical reinforcement learning [57], policy search [54], [55], [56] and other learning paradigms (e.g. ligand-receptor [53] and neuro-fuzzy inference system [58]). Despite these architectures have been conceived to confer a good

Tesi di dottorato in Bioingegneria industriale, di Roberto Barone,
discussa presso l'Università Campus Bio-Medico di Roma in data 04/03/2017.
La disseminazione e la riproduzione di questo documento sono consentite per scopi di didattica e ricerca,
a condizione che ne venga citata la fonte.

level of autonomy upon the robot, they typically yield a huge increase of the computational burden of the control architecture, thus causing long learning phases, which can hardly be implemented on real robots and cannot be used for on-line learning.

The learning paradigm adopted in this work, based on Policy Improvement Black Box (PIBB) paradigm has been demonstrated to have moderate computational burden [55], [56] and high efficiency, with the consequent advantage of enabling on-line learning [59]. In [59] Central Pattern Generators have been demonstrated to generate simple motor primitives able to produce both rhythmic and discrete movements. Furthermore in [59] a first experimental evidence is provided of the learning algorithm coupled with Central Pattern Generators in discrete and rhythmic tasks as finger tapping and object rotation.

For the low-level control, a parallel force/position control is adopted; such a control is able to manage forces as well as motion during interaction, and track the desired motion when interaction does not occur (e.g., during preshaping)[60]. The usefulness of this control strategy has been studied in the prosthetic field through simulation tests [61]. Here, it is tested in a real experimental setting and enriched with the slippage information provided by force/tactile sensors in order to enable slippage prevention. To this purpose, force sensors have been embedded into the distal phalanxes of the multi-fingered hand. Moreover, in order to demonstrate the potential of the proposed two-level control, comparative experimental tests with respect to a traditional position control (without learning capabilities) have been carried out.

Strain gauges have largely been utilized on prostheses, but more than one sensor per finger is often needed [62]. Further, temperature compensation is always required to achieve correct force measurements [44]. Force Sensing Resistors (FSRs) represent an alternative solution though their functioning principle requires additional sensing units (e.g., piezoelectric [47]) or supplementary equipment [49], or signal processing for slippage detection. For example, in [46] signal derivatives have been computed for slip detection, with not negligible noise. In some cases, Force/Torque (F/T) sensors have been employed [70], although they provide complex information that are not required by the application with high costs. In this paper, one FSR sensor has been positioned on the fingertip of thumb, index and middle and used for the twofold purpose of measuring the normal force component and detecting slippage. Therefore, FSR force signal is properly processed to extract information about slippage events.

Tesi di dottorato in Bioingegneria industriale, di Roberto Barone,
discussa presso l'Università Campus Bio-Medico di Roma in data 04/03/2017.
La disseminazione e la riproduzione di questo documento sono consentite per scopi di didattica e ricerca,
a condizione che ne venga citata la fonte.

3.1.2 Matherials and methods

The control architecture distributed on high and low level control is shown in Fig. 3.1. The high level control has the aim of planning the desired grasping

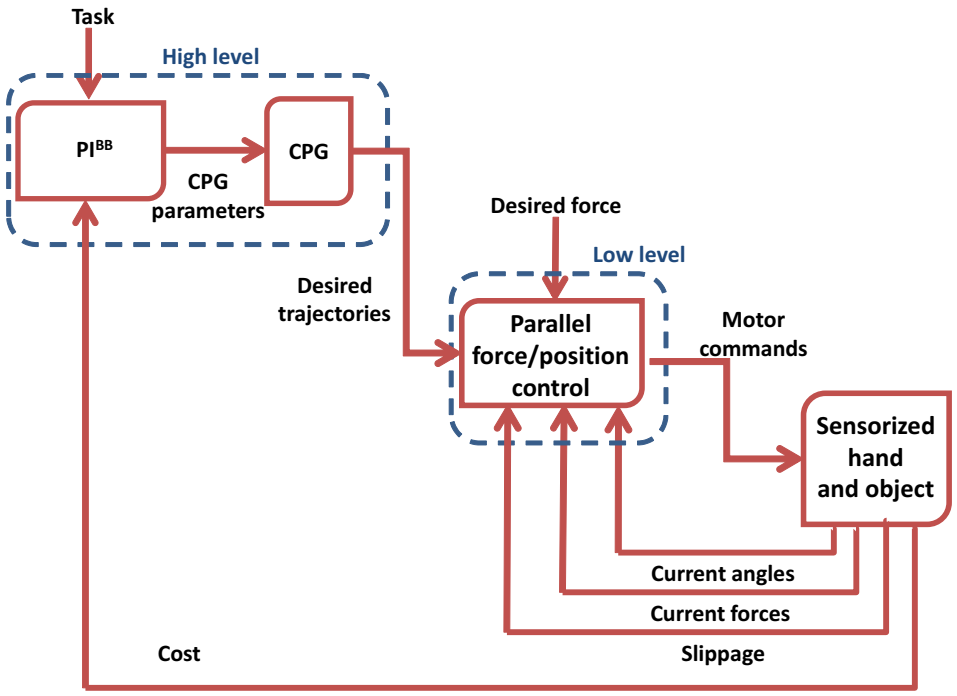

Figure 3.1: Control architecture characterized by the following components: Policy Improvement with Black Box, Central Pattern Generators, Parallel force/position control, sensorized hand and object.

task and identifying the optimal strategy for finger coordination. The PIBB learning algorithm has been employed in order to autonomously search the CPG parameters necessary to define the desired finger trajectory suitable for the grasping task. The learning phase has been characterized by several repetitions of the trial, grouped into periods. During one period, for each trial, the corresponding set of CPG parameters have been tested, thus producing the desired trajectories the hand needs to interact with the object.

The parallel force/position control (i.e. the low level control) has been devoted to the definition of the motor commands for the hand actuation system starting from force and position references and proprioceptive and tactile sensory feedback.

The proposed architecture aims at being used both during grasping and (rhythmic and discrete) manipulation tasks. The desired forces have been experimentally retrieved with the prosthetic hand while the position references have been generated by the high level control. The control aims to regulate

Tesi di dottorato in Bioingegneria industriale, di Roberto Barone,
discussa presso l'Università Campus Bio-Medico di Roma in data 04/03/2017.
La disseminazione e la riproduzione di questo documento sono consentite per scopi di didattica e ricerca,
a condizione che ne venga citata la fonte.

i) finger motion during preshaping and ii) force applied to the object during grasping based on position, force and slippage information coming from the sensorized hand.

High Level Control

The Policy Improvement Black Box (PIBB) algorithm has been used to search the CPG parameters necessary to define the optimal trajectories for the desired task. The learning phase has been characterized by several repetitions of the trial. K trials have been grouped in a period.

At the beginning of learning an initial set of CPG parameter μ_0 is defined. When each period starts, the CPG parameters of K trials μ_k are generated based on current parameter set μ. After evaluating the performance of each parameter, a new parameter set is computed.

The PIBB learning method grounds its functioning on the following phases [55], [56], [59]:
a) Parameter set: in this phase the K parameters sets are defined on the basis of a Gaussian distribution expressed as

$$\mu_k = N(\mu, \sigma) \tag{3.1}$$

with μ and σ representing the mean vector and covariance matrix of the distribution respectively. The K sets of parameters are delineated starting from the mean parameter set μ. A constant exploration noise is employed considering a diagonal σ matrix with elements 0.1.
b) Test: each possible set of CPG parameters (μ_k) is tested on the prosthetic hand interacting with the object. The cost function, quantifying the performance of the executed task, is calculated as difference between the ideal and real results of the task

$$J_{dk} = J_{max} - J \tag{3.2}$$

where J quantifies the performance of the current trial and J_{max} indicates the maximum achievable performance (ideal result) during the single trial.
c) Performance evaluation and parameters update: the cost value J_{dk} (obtained testing the parameter set μ_k during task b) is transformed in probabilities in order to contribute to the new mean parameter set by means of the soft-max

Tesi di dottorato in Bioingegneria industriale, di Roberto Barone,
discussa presso l'Università Campus Bio-Medico di Roma in data 04/03/2017.
La disseminazione e la riproduzione di questo documento sono consentite per scopi di didattica e ricerca,
a condizione che ne venga citata la fonte.

function

$$p_{dk} = \frac{e^{-\frac{1}{\lambda} J_{dk}}}{\sum_{k=1}^{K} e^{-\frac{1}{\lambda} J_{dk}}} \tag{3.3}$$

where the "temperature parameter" λ allows regulating the effect of different performance on the probabilities and is empirically chosen as $\lambda = 10$. Higher probabilities are associated to parameter set causing lower costs, while lower probabilities are calculated with higher costs. The new mean parameter set (μ_n) is computed averaging the tested samples by means of the calculated probabilities (p_{dk}).

$$\mu_n = \sum_{k=1}^{K} p_{dk} \mu_k \tag{3.4}$$

The phases a), b), c) are iterated for all the M periods in order to train the system. The number of successive periods is experimentally defined as $M = 50$ in order to allow stabilizing learning performance. Cost function J_{dk} depends on the grasping or manipulation task and has been calculated on the basis of interaction information between fingers and objects.

In grasping task the cost function needs to take into account the contact points between fingers and object. During bi-digital and tri-digital grasps only fingertips of thumb, index and middle (during tri-digital) are in contact with the object for the whole task. For this reason the cost function needs to know the happened contact and the contact duration during object and finger interaction. Three counters have been used to calculate the contact time between each fingertips (index, thumb, middle) and the object. The lowest cost has been obtained when the finger involved in the task have been in contact with the object for the whole grasp. The counters have updated their values at each step. The maximum performance (J_{max}) have been expressed by

$$J_{max} = n_{max} \ \Lambda \ tc_{max} \tag{3.5}$$

where n_{max} indicates the maximum number of contacts and tc_{max} defines the maximum time of contact (depending from the single trial duration).

The current performance value has been defined as the sum of the counters related to each contact point (tc_{finger}) as follows

$$J = \sum_{i=0}^{n_{max}} tc_{finger} \tag{3.6}$$

Tesi di dottorato in Bioingegneria industriale, di Roberto Barone,
discussa presso l'Università Campus Bio-Medico di Roma in data 04/03/2017.
La disseminazione e la riproduzione di questo documento sono consentite per scopi di didattica e ricerca,
a condizione che ne venga citata la fonte.

The counters update has been carried out at each trial step for each possible hand contact point, increasing the counter if the correct possible contact point is in contact with the object and decrease the counter in the opposite case. This has avoided the contact of the object from the wrong fingers.

The CPGs have been modeled as coupled oscillators and the theoretical formulation have been presented in (Ciancio, 2013)[65]. As detailed in (Meola, 2016), where a first application of the high level control is presented, the CPG algorithm has been preferred to DMP to facilitate the initialization and the transition from discrete and rhythmic movements, e.g. transition from grasping and manipulation tasks. The number of adopted oscillators has been directly related to the number of Degrees of Actuation (DoAs) of the prosthetic hand (Fig. 3.2). The trajectory of each DoA has been defined by the output of the corresponding oscillator.

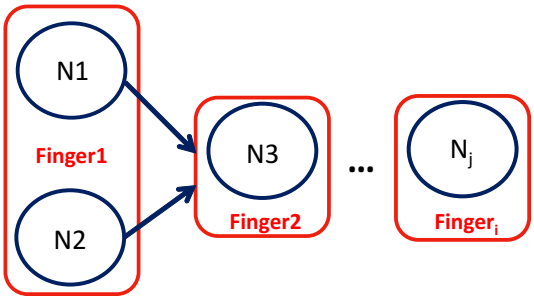

Figure 3.2: Central Pattern Generation architecture: the number of oscillators has been directly related to the number of Degrees of Actuation of the prosthetic hand.

Low Level Control

The implemented low level control is a parallel force/position control equipped with a slippage detection and control. Figure 3.3 shows the block diagram of the control.

The proposed control law for each finger is expressed as follows

$$\tau = \tau_g + k_p(q_f + q_d - e_{qs} - q) - k_d\dot{q} + J^t f_a \tag{3.7}$$

$$q_f = C_f(\tau_d - \tau_a) = k_{fp}(\tau_d - \tau_a) + k_{fi}\int_0^{t_f}(\tau_d - \tau_a)\,dt. \tag{3.8}$$

The parallel force/position control consists of two loops: the outer, with C_f

Tesi di dottorato in Bioingegneria industriale, di Roberto Barone,
discussa presso l'Università Campus Bio-Medico di Roma in data 04/03/2017.
La disseminazione e la riproduzione di questo documento sono consentite per scopi di didattica e ricerca,
a condizione che ne venga citata la fonte.

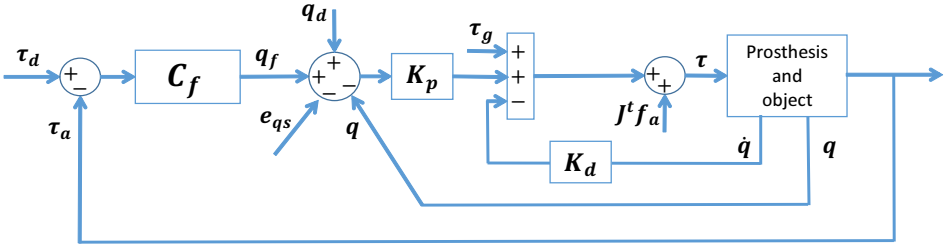

Figure 3.3: Parallel force/position with slippage prevention feature control scheme.

as a gain, is a PI force control (with k_{fp} and k_{fi} as proportional and integral gains, respectively) while the inner loop is a PD position control, where k_p and k_d are the proportional and derivative gains. q_f is the position reference from the outer loop, τ_d and τ_a the desired and the actual torques respectively. τ is the actuation torque to command each joint of the hand (q), τ_g is the torque needed to compensate the gravity action. q_d is the desired joints position, e_{qs} the slippage signal (the integral signal) which acts as an additional error of the position inner control loop as shown in (Engeberg, 2013)[48]. $\dot{q}$ is the joint velocities vector and $J^t f_a$ is the term needed to compensate the force between the fingers and the object, being J the Jacobian matrix of the robotic finger.

Implementation on the prosthetic hand

In this study, the IH2 prosthetic hand [72] was used (Fig. 3.4). The IH2 anthropomorphic robotic hand, is a 5-finger biomechatronic hand with a human-sized dimension. It has 5 DC brushed motors (integrated in the palm) with, correspondingly, 5 Degrees of Actuation (DoAs) not back-driveable and 11 degrees of freedom. Each finger has 2 phalanxes connected by means of 2 joints. The single DC motor transmits the movement to the 2 phalanxes by means of a slider mechanism. Two motors actuate respectively thumb abduction/adduction (A/A) and flexion-extension (F/E) of all the thumb phalanxes. Two motors are used to independently activate F/E of index and middle fingers. Finally, the fifth motor is used to move in a coupled way the ring and the little fingers. The underactuated mechanisms, adopted for all the fingers to enable phalanxes F/E, consists of a tendon that runs inside the phalanxes and is wrapped around the pulleys placed at the joints. The fingers automatically adapt to the object shape while closing. Finger position is measured by means of incremental encoders and varies between 0 (totally open) and 255 (totally closed). One FSR for fingertips of thumb, index and middle fingers was applied

Tesi di dottorato in Bioingegneria industriale, di Roberto Barone,
discussa presso l'Università Campus Bio-Medico di Roma in data 04/03/2017.
La disseminazione e la riproduzione di questo documento sono consentite per scopi di didattica e ricerca,
a condizione che ne venga citata la fonte.

Figure 3.4: Ih2 hand

Tesi di dottorato in Bioingegneria industriale, di Roberto Barone,
discussa presso l'Università Campus Bio-Medico di Roma in data 04/03/2017.
La disseminazione e la riproduzione di questo documento sono consentite per scopi di didattica e ricerca,
a condizione che ne venga citata la fonte.

and then the fingers were covered with prosthetic silicon caps (Fig. 3.5).

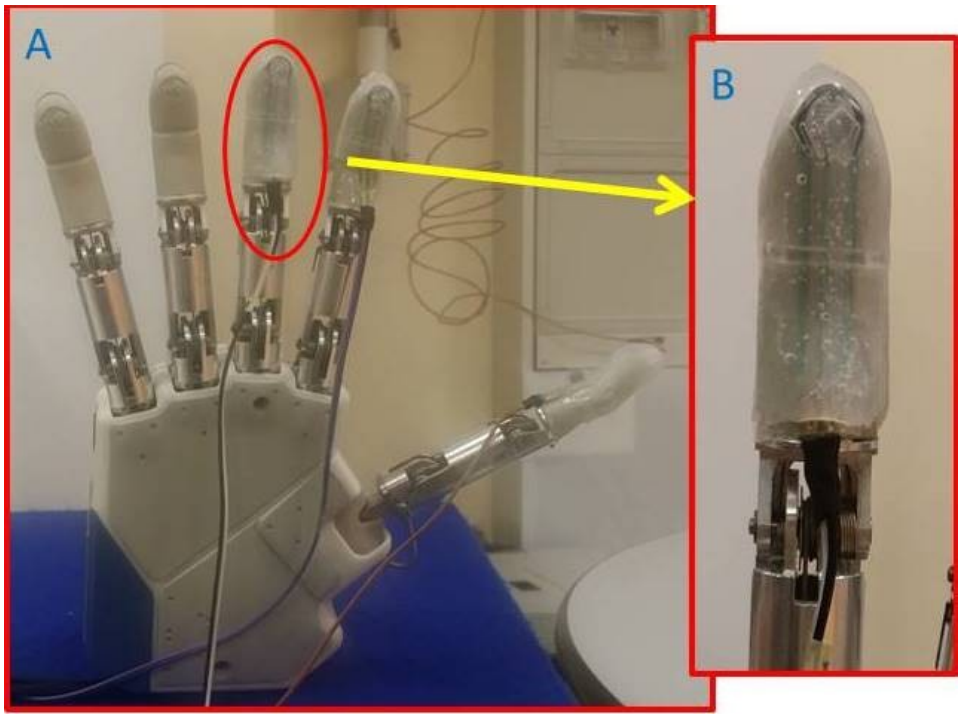

Figure 3.5: Prosthetic hand IH2 mounted with FSRs on the fingertips of thumb, index and middle finger (A). The sensorized fingertips are covered with prosthetic silicon caps, as detailed in (B).

The learning phase (high-level control) has been carried out in simulation with the defined simulated objects in order to avoid overwork and exclude unexpected behavior or damages in the real setting with the IH2 hand. The learned parameters have been tested on the real robotic hand during the object grasp. The learning phase is characterized by a period with K=8 trials, experimentally retrieved. At each trial a different set of CPG parameters has been tested, and at the end of each period new K parameter sets have been calculated on the basis of the performance of the previous K trials.

The adopted CPG is presented in Fig. 3.6. It consists of 5 different oscillators, each one devoted to the definition of the desired trajectory for one degree of actuation involved in the task. Five different oscillators have been adopted with a total of 15 parameters to search (5 amplitudes, 5 centers of oscillation, 4 phases and a common frequency). As shown in Fig. 3.6 N1 oscillator has been associated to index flexion/extension, N2 has been in charge of middle flexion/extension, N3 has been responsible for thumb flexion/extension, N4 has been associated to thumb adduction/abduction and N5 has been affiliated to ring/little flexion/extension. Because of the under-actuation, the control

Tesi di dottorato in Bioingegneria industriale, di Roberto Barone,
discussa presso l'Università Campus Bio-Medico di Roma in data 04/03/2017.
La disseminazione e la riproduzione di questo documento sono consentite per scopi di didattica e ricerca,
a condizione che ne venga citata la fonte.

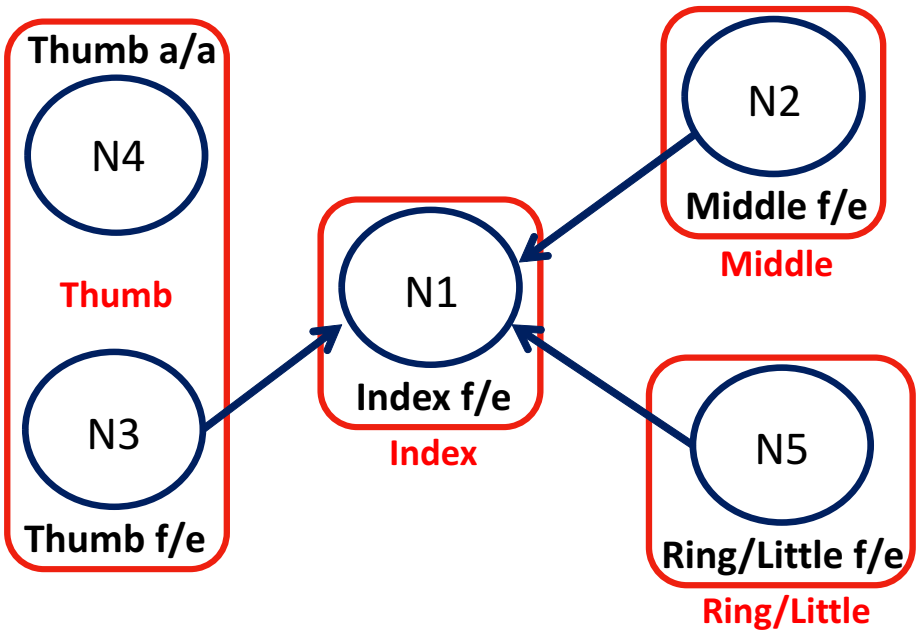

Figure 3.6: Central Pattern Generator scheme composed by 5 oscillators each defining the trajectory of one Degree of Actuation (DoA): N1 defining index flexion/extension trajectory, N2 defining middle flexion/extension trajectory, N3 defining thumb flexion/extension trajectory, N4 defining thumb adduction/abduction trajectory and N5 defining ring/little flexion/extension trajectory.

law has been reformulated in terms of slider variable x_s, related to the joint variables q_1 and q_2 as follows [73]

$$x_S = r_1(q_1 - q_{01}) + r_2(q_2 - q_{02}) \tag{3.9}$$

with r_1 and r_2 the radii of MCP (metacarpophalangeal) and PIP (proximal interphalangeal) joint pulleys, respectively and q_{01} and q_{02} the initial equilibrium joint angles (equal to 0).
The parallel force/position control law suited to the IH2 Hand can be expressed as

$$\tau = [T_g + T_e - k_d\dot{x}_s + k_p(x_{fs} + x_{ds} - x_s - e_s)]\mathbf{r} + J^t\mathbf{f_a} \tag{3.10}$$

being x_{fs} related to the joint variable $\mathbf{q_f}$ through $\mathbf{q_f} = C_f(\tau_\mathbf{d} - \tau_\mathbf{c})$, with $\tau_\mathbf{d}$ and $\tau_\mathbf{c}$ the desired and the current torque vectors respectively. The unique difference with respect to the control scheme in Fig. 3.3 is the presence of slider variables converted in joint variables multiplying by $\mathbf{r}$, the pulley radii

Tesi di dottorato in Bioingegneria industriale, di Roberto Barone,
discussa presso l'Università Campus Bio-Medico di Roma in data 04/03/2017.
La disseminazione e la riproduzione di questo documento sono consentite per scopi di didattica e ricerca,
a condizione che ne venga citata la fonte.

vector. e_{qs} is now called e_s, $\dot{x}_s$ is the slider velocity, x_{fs} is the position reference computed from $\mathbf{q_f}$, which is the vector of reference joint position computed on the basis of torque error. x_s is the current slider position, x_{ds} is the reference slider position computed by means of CPGs. T_g is the contribution of the gravitational torque at the level of slider, T_e is the elastic contribution in order to compensate for the preloaded spring. Other terms remain unvaried compared to the control law in Eq. 3.7. To set the control of the slippage in the "off" condition, variable e_s was set to zero by means of a dedicated user interface.

Tactile sensing

Forces exerted by the prosthetic fingers onto the objects during the experimental trials have been collected by three FSR sensors (Model 400 by Interlink Electronics, Inc.), each one mounted respectively on the distal phalanx of thumb, index and middle finger (Fig. 3.5). The selected FSR model, has a circular active area with a diameter of 5.08 mm, a discrimination threshold of 0.2 N and a measurement range up to 20 N.

Voltage V_{out}, obtained through the differential amplification of a Wheatstone bridge output can be expressed as

$$V_{out} = \frac{c}{R_w + 10^{a \log_{10} F + b}} - d \tag{3.11}$$

where a, b, c and d are constants that depend on the sensor response, whereas R_w indicates the value of the three electrical resistances of the bridge, chosen so as to guarantee a good tradeoff between sensitivity at low forces and resolution at high forces in the whole range of interest (i.e., up to 10 N). A quasi-static calibration of the three sensors used has been carried out over the range [0.2-8] N [63]. Each sensor has been covered with a prosthetic silicon cap in order to stably locate the sensor on the fingertip (Fig. 3.5). Therefore, the whole structure made of fingertip/sensor/cap has been characterized. Table 3.1 and Fig. 3.7 show the results of the best fitting procedure for the three sensors. Experimental data showed high coherence with the non-linear theoretical model (equation 3.11). As regards the slip signal, after preprocessing and rectification, a threshold mechanism has been adopted to extract a binary slip signal.

Tesi di dottorato in Bioingegneria industriale, di Roberto Barone,
discussa presso l'Università Campus Bio-Medico di Roma in data 04/03/2017.
La disseminazione e la riproduzione di questo documento sono consentite per scopi di didattica e ricerca,
a condizione che ne venga citata la fonte.

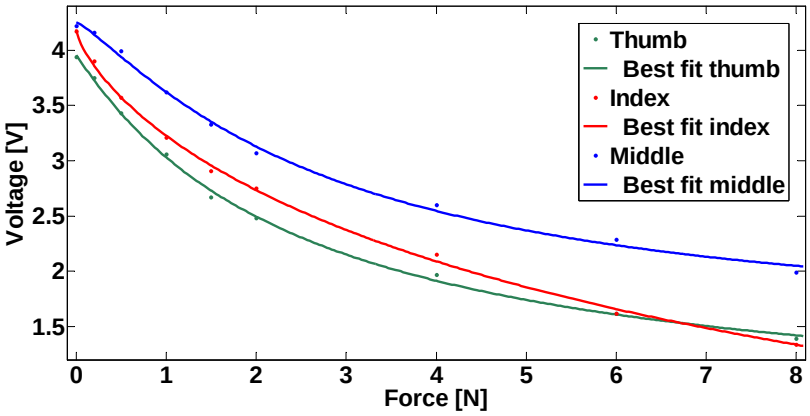

Figure 3.7: Best fitting curves for the three FSRs placed on the prosthetic hand and covered with silicon caps.

Table 3.1: Results from quasi-static calibration.

Sensor	a	b	c	d	R^2	RMSE [V]	Sm [V/N]
Thumb	1.028	2.766	4955	-0.652	0.9986	0.0438	0.31
Index	0.77	2.474	8526	1.491	0.9987	0.0446	0.35
Middle	1.191	2.628	4233	-1.423	0.9969	0.0575	0.27

Experimental setup

A first experimental setup has been realized for validating the high-level layer and demonstrate its potentials, especially for managing coordinated fingers grasping and achieve successful grasp also when experimental conditions are varied (e.g. size or shape of the objects). To this purpose, the preshaping phase has been in-depth investigated (thus not including the force control) and compared with a traditional position control made of a PD action on the slider position error. In the case of learning architecture, CPGs generated proper joint reference trajectories (converted in slider position references) for a given object, thanks to the training made in simulation. No a priori knowledge on the object precise location was needed. In the case of traditional PD control, slider position references were planned thanks to a priori knowledge of the object size and position.

In order to demonstrate the added value provided by the high-level control with learning, the effect of size changes on the control performance was investigated. In particular, cylindrical objects of different sizes were tested with a tri-digital grasp. It is worth observing that, due to the hand underactuation,

Tesi di dottorato in Bioingegneria industriale, di Roberto Barone,
discussa presso l'Università Campus Bio-Medico di Roma in data 04/03/2017.
La disseminazione e la riproduzione di questo documento sono consentite per scopi di didattica e ricerca,
a condizione che ne venga citata la fonte.

the traditional PD control is expected to grasp also objects larger than those used for trajectory planning. On the other hand, it is expected to fail with objects of smaller size. The objects considered for these experimental tests were a plastic cup of 7 cm of diameter and other three cylindrical objects of respectively 8, 3.4 and 2 cm of diameter). Control performance have been measured by means of the success rate during the different grasps.

The experimental set-up for the validation of the complete two-level control is depicted in Fig. 3.8. Three widely used objects during activities of daily

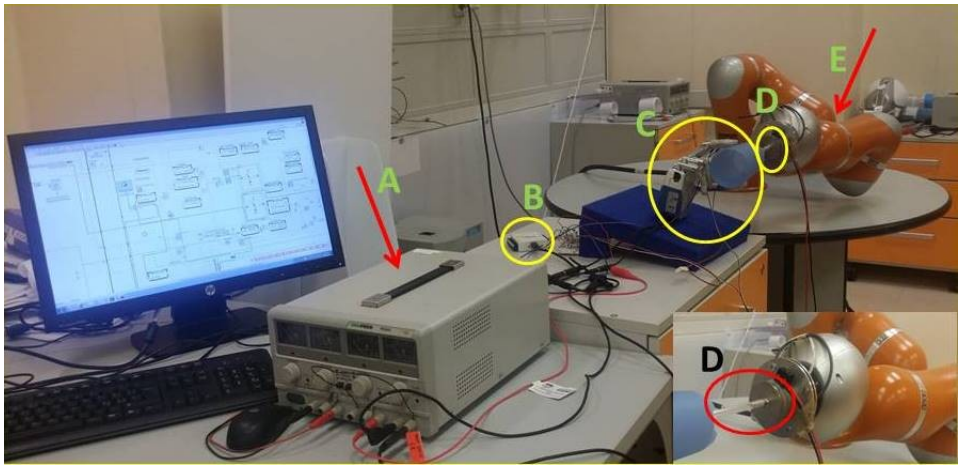

Figure 3.8: Experimental set-up. DC power supply for electronics, sensors and prosthetic hand (A); NI-DAQ device (B) for data acquisition; prosthetic hand grasping a cup (C); end effector inducing slippage (D); KUKA-LWR 4 robotic arm (E).

living (ADLs) have been selected for performing two kinds of grasp: bi-digital and tri-digital (Fig. 3.9). The former has been performed with an egg (Fig. 3.9B) and a highlighter (Fig. 3.9D), the latter with the same egg (Fig. 3.9A) and with a cylindrical plastic cup (Fig. 3.9C). The masses of the objects were around: 60 g (egg), 50 g (cup) and 10 g (highlighter). The purpose of the experimental tests was to investigate the stability of the grasp when an external perturbation is applied in the two cases of presence or absence of slip detection, and to verify system robustness with respect to the type of perturbation. Slippage has been automatically induced by means of a seven degrees of freedom robotic arm (KUKA-LWR 4+), whose end effector has been a thin, cylindrical probe. Slip experiments have been executed by actuating the probe for 1 cm at two different speeds (i.e. 2 cm/s and 4 cm/s (maximum speed possible)), in order to assess control stability and robustness at increasing velocities.

Tesi di dottorato in Bioingegneria industriale, di Roberto Barone,
discussa presso l'Università Campus Bio-Medico di Roma in data 04/03/2017.
La disseminazione e la riproduzione di questo documento sono consentite per scopi di didattica e ricerca,
a condizione che ne venga citata la fonte.

Experiments without considering the sensory slip information (i.e., only relying on the force/position control) have been carried out only at 4 cm/s, in order to demonstrate the efficacy of the proposed slippage control also when control laws that do not manage slippage fail. In all cases, six repetitions have been performed, resulting in a total of 72 trials. All the data have been acquired at a sampling frequency of 2 kHz by a NI DAQ (NI-6009) device, and the slip signal has been recorded even when not employed for the control; the prosthetic hand has been supplied by a DC power supply at 8 V, while all the sensors and acquisition electronics at 5 V. The gains of the PD position control loop have been set to the following values: $k_p = 210000$, $k_d = 1000$. The gains of the PI force control loop have been fixed to the following values: $k_f i = 1000$, $k_f p = 50000$.

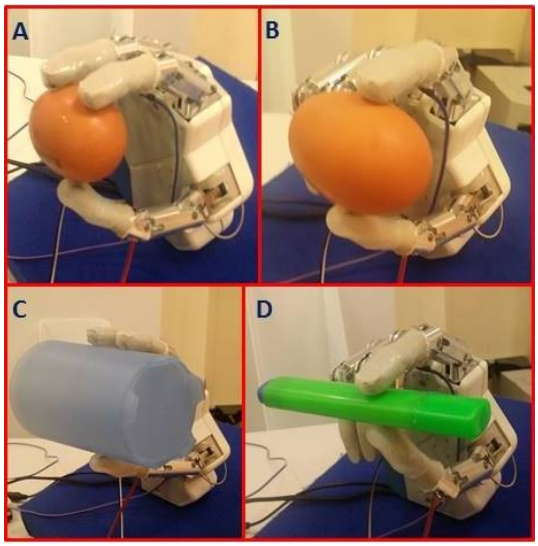

Figure 3.9: Grasps performed by the IH2 hand during the experiments: tri-digital with egg (A) and cup (C), bi-digital with egg (B) and highlighter (D).

3.1.3 Results

Training results

The training phase has been carried out in simulation, by modelling the IH2 hand and the objects, with the same tools described in [65]. The training of the high-level control has been performed for the tridigital grasp of a plastic cup with 7 cm of diameter. Afterwards, the high-level control has also been applied to other three objects with smaller and larger diameters (i.e. 3.4 cm,2 cm and 8 cm).

Tesi di dottorato in Bioingegneria industriale, di Roberto Barone,
discussa presso l'Università Campus Bio-Medico di Roma in data 04/03/2017.
La disseminazione e la riproduzione di questo documento sono consentite per scopi di didattica e ricerca,
a condizione che ne venga citata la fonte.

The performance of the high-level control architecture has been evaluated in two cases: 1) learning is carried out for each object separately (namely *learning from zero*), 2) learning of smaller objects benefits from the learning of the plastic cup (namely *learning from plastic cup*) (Table 3.2). Control performance has been assessed through the mean cost value (the lower is the value, the better is the hand behavior), and the number of trials, which provides a measure of the time needed for learning.

The training of the high-level control during grasp of larger object (i.e. 8 cm diameter) has been carried out only in the case of learning from zero. As for the case of traditional PD control, it is expected that the underactuation of IH2 fingers makes the hand adapt to larger objects.

Table 3.2: Mean cost values and number of trials at the end of the learning. Two types of learning have been carried out: Learning starting from zero, Learning starting from plastic cup .

Objects	Learning from zero		Learning from plastic cup	
	Mean Cost values	Number of trials	Mean Cost values	Number of trials
Cylindrical object (8 cm of diameter)	1.7	40	-	-
Plastic cup (7 cm of diameter)	4	52	-	-
Cylindrical object (3.4 cm of diameter)	4.1	55	0.1	18
Cylindrical object (2 cm of diameter)	5.7	60	0.3	30

As shown in Table 3.2 the performance of the task decreased with the object size. Moreover, the number of trials required for training the high-level control increased during grasp of smaller objects. It is interesting to observe that, although the training was always successful, the incremental training of the high-level control architecture from the plastic cup learning led to improved performance with respect to learning from zero, with lower values of both the mean cost and the number of trials necessary to conclude the training phase.

The training results demonstrate that the high-level control is able to successfully face changes in the experimental scenario, such as object dimensions, with a quicker learning phase if it starts from previously trained parameters. Furthermore, performance obtained with the incremental training from the previously learned situation also exceeded performance achieved by a new learning from zero.

Tesi di dottorato in Bioingegneria industriale, di Roberto Barone,
discussa presso l'Università Campus Bio-Medico di Roma in data 04/03/2017.
La disseminazione e la riproduzione di questo documento sono consentite per scopi di didattica e ricerca,
a condizione che ne venga citata la fonte.

Preshaping results

Experimental tests have been carried out in order to verify that the trajectories provided by the high-level control were able to correctly grasp the objects (i.e. plastic cup, cylinders 3.4 and 2 cm of diameters, respectively) and to compare results with a traditional PD control with predefined slider positions (and correspondingly joint positions) required to stably grasp the object. In particular, Table 3.3 reports the predetermined slider positions to grasp the object (experimentally retrieved), the slider positions provided by the high-level control, the slider positions actually achieved by the fingers and the success rate of the grasping task.

The hand has been able to grasp the four objects using trajectories furnished by the high-level control with a success rate of 100% during 10 trials. As expected, for the traditional PD control, the same results have been achieved only in the case of plastic cup (as the real slider positions correspond to the planned ones) and larger object (thanks to the underactuation). The experimental results confirm the correctness of simulation outcomes after re-learning process and demonstrate the applicability of a high-level structure to provide suitable trajectories during grasps of objects with different dimensions.

Results of the complete control architecture: the training phase

The evolutions of the cost during the learning of bi-digital and tri-digital grasp of an egg are shown in Fig. 3.10. The decrease of the cost values during training clearly indicates the improvement of the performance during learning.

The performance of the high level control architecture during each grasping task before and after the learning have been summarized in Table 3.4. Mean values have been calculated on the first and last 5 periods of the training. In Table 3.4 the increase of the performance during the learning of the four grasping tasks can be observed. Table 3.5 reports the CPG parameters extracted at the end of the learning in simulation and adopted in the test phase on the real hand.

Results of the complete control architecture: the test phase

In this section the results of the experimental tests on grasping are shown. For sake of brevity the plot of four trials is reported, as the trend is similar during the different grasps of the different objects. Figures 3.11 and 3.12 show: (a), (c) the measured forces compared with the desired force; (b), (d) the slider positions compared with the desired positions. When slippage control

Tesi di dottorato in Bioingegneria industriale, di Roberto Barone,
discussa presso l'Università Campus Bio-Medico di Roma in data 04/03/2017.
La disseminazione e la riproduzione di questo documento sono consentite per scopi di didattica e ricerca,
a condizione che ne venga citata la fonte.

Table 3.3: Predetermined slider positions to grasp the object, slider positions actually achieved and success rate of the grasping tasks for the traditional PD control and the high-level control.

	Traditional PD control						
Objects diameters [m]	Index Desired Position [m]	Actual Index Position (mean±SD) [m]	Middle Desired Position [m]	Actual Middle Position (mean±SD) [m]	Thumb Desired Position [m]	Actual Thumb Position (mean±SD) [m]	Grasps success rate
d=0.08	$16.8 \cdot 10^{-3}$	$15.4 \pm 0.1 \cdot 10^{-3}$	$16.8 \cdot 10^{-3}$	$16.1 \pm 0.1 \cdot 10^{-3}$	$9.3 \cdot 10^{-3}$	$9.1 \pm 0.2 \cdot 10^{-3}$	100%
d=0.07	$16.8 \cdot 10^{-3}$	$16.7 \pm 0.1 \cdot 10^{-3}$	$16.8 \cdot 10^{-3}$	$16.7 \pm 0.1 \cdot 10^{-3}$	$9.3 \cdot 10^{-3}$	$9.4 \pm 0.1 \cdot 10^{-3}$	100%
d=0.034	$16.8 \cdot 10^{-3}$	$17.0 \pm 0.1 \cdot 10^{-3}$	$16.8 \cdot 10^{-3}$	$16.7 \pm 0.1 \cdot 10^{-3}$	$9.3 \cdot 10^{-3}$	$9.3 \pm 0.3 \cdot 10^{-3}$	0%
d=0.02	$16.8 \cdot 10^{-3}$	$17.0 \pm 0.1 \cdot 10^{-3}$	$16.8 \cdot 10^{-3}$	$16.8 \pm 0.1 \cdot 10^{-3}$	$9.3 \cdot 10^{-3}$	$9.6 \pm 0.4 \cdot 10^{-3}$	0%
Objects diameters [m]	High-level control						
d=0.08	$16.5 \cdot 10^{-3}$	$15.5 \pm 0.1 \cdot 10^{-3}$	$16.5 \cdot 10^{-3}$	$16.1 \pm 0.1 \cdot 10^{-3}$	$8.8 \cdot 10^{-3}$	$8.6 \pm 0.1 \cdot 10^{-3}$	100%
d=0.07	$16.5 \cdot 10^{-3}$	$16.5 \pm 0.2 \cdot 10^{-3}$	$16.5 \cdot 10^{-3}$	$16.4 \pm 0.1 \cdot 10^{-3}$	$8.8 \cdot 10^{-3}$	$9.0 \pm 0.1 \cdot 10^{-3}$	100%
d=0.034	$18.4 \cdot 10^{-3}$	$18.4 \pm 0.2 \cdot 10^{-3}$	$18.4 \cdot 10^{-3}$	$18.4 \pm 0.2 \cdot 10^{-3}$	$14.7 \cdot 10^{-3}$	$14.8 \pm 0.2 \cdot 10^{-3}$	100%
d=0.02	$20.2 \cdot 10^{-3}$	$20.2 \pm 0.1 \cdot 10^{-3}$	$20.2 \cdot 10^{-3}$	$20.0 \pm 0.3 \cdot 10^{-3}$	$17.6 \cdot 10^{-3}$	$17.7 \pm 0.1 \cdot 10^{-3}$	100%

is off, the grasped object is perturbed by two identical perturbations of 1 cm at the maximum speed possible (4 cm/s) so as to demonstrate that the object

Tesi di dottorato in Bioingegneria industriale, di Roberto Barone,
discussa presso l'Università Campus Bio-Medico di Roma in data 04/03/2017.
La disseminazione e la riproduzione di questo documento sono consentite per scopi di didattica e ricerca,
a condizione che ne venga citata la fonte.

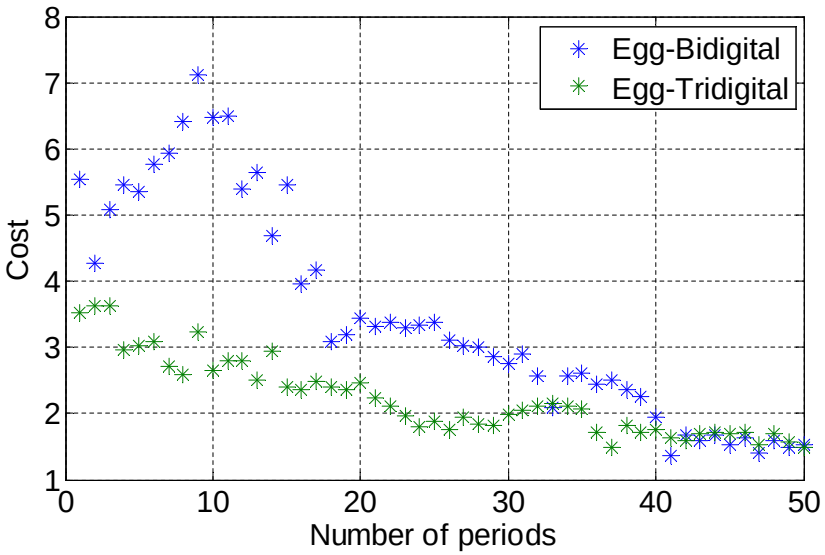

Figure 3.10: Cost during the learning of two grasping tasks of an egg: bi-digital grasp (blue) and tri-digital grasp (green). The stars indicates the cost value at each period of the training.

Table 3.4: Mean cost values at the start and at the end of the learning for each object and grasp.

Object	Grasp	Mean cost values	
		Start of learning	End of learning
Plastic Cup	Tridigital	16.1	4.0
Egg	Bidigital	5.1	1.53
Egg	Tridigital	3.3	1.61
Highlighter	Bidigital	12.9	8.0

falls, or at least is unstably grasped. When the slippage control is active, one perturbation of 1 cm at different velocities (2 cm/s and 4 cm/s) is produced; as expected, the system is able to immediately detect slippage as shown in Figs 3.11 and 3.12. The activation command for the robotic arm was given as soon as the forces reached a steady state; hence, perturbations were not applied at the same time instants in all the trials.

In Figs 3.11(a) and 3.11(b) it is shown a trial of the tri-digital grasp of the plastic cup with the slip prevention algorithm disabled and perturbation set to 4 cm/s. After the forces reached the steady state, a first disturbance is applied and the controller avoids the cup fall thanks exclusively to the parallel force/position control. The grasp is maintained but it is no longer stable.

Tesi di dottorato in Bioingegneria industriale, di Roberto Barone,
discussa presso l'Università Campus Bio-Medico di Roma in data 04/03/2017.
La disseminazione e la riproduzione di questo documento sono consentite per scopi di didattica e ricerca,
a condizione che ne venga citata la fonte.

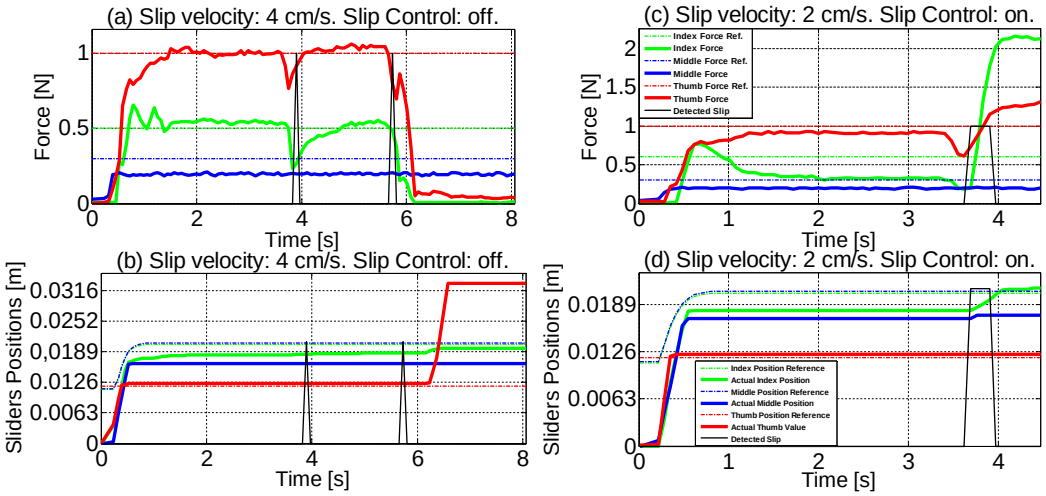

Figure 3.11: Experimental results with the plastic cup. (a) and (b): Slippage control: off. (c) and (d): Slippage control: on.

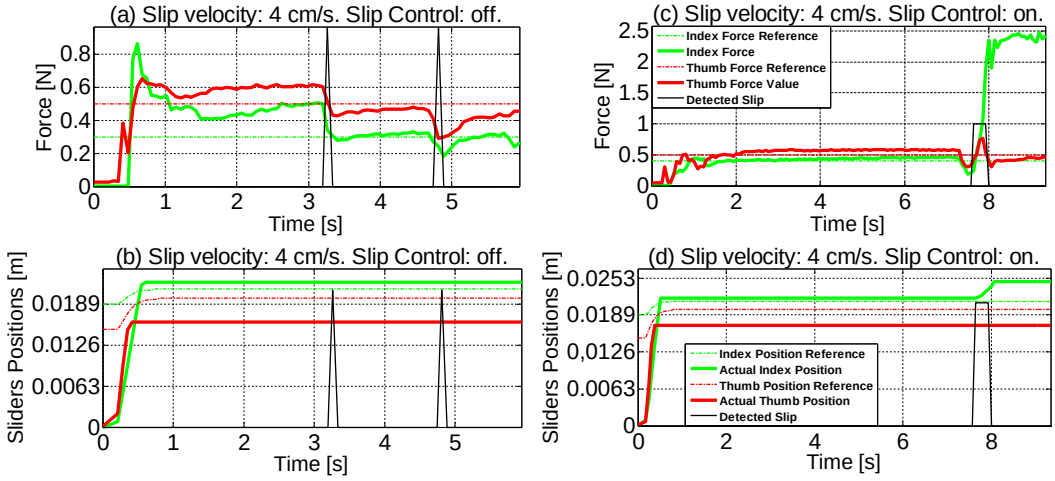

Figure 3.12: Experimental results with the highlighter. (a) and (b): Slippage control: off. (c) and (d): Slippage control: on.

Tesi di dottorato in Bioingegneria industriale, di Roberto Barone,
discussa presso l'Università Campus Bio-Medico di Roma in data 04/03/2017.
La disseminazione e la riproduzione di questo documento sono consentite per scopi di didattica e ricerca,
a condizione che ne venga citata la fonte.

Table 3.5: Parameters learned in simulation for each object and grasp.

Objects		Plastic cup	Egg	Egg	Highlighter
Grasp		Tridigital	Bidigital	Tridigital	Bidigital
CPG parameters	***f1***	0.01	0.12	0.12	0
	$\mathbf{\Phi_{12}}$	3.11	-1.9	-2.24	2.65
	$\mathbf{\Phi_{13}}$	3.14	2.81	-0.94	3.14
	$\mathbf{\Phi_{15}}$	3.14	-0.24	3.14	3.14
	R1	0.18	0.13	0.09	1
	R2	0.2	0	0.11	0.59
	R3	0.3	0	0.08	1
	R4	0.42	0.2	0	0.88
	R5	0.35	0	0.1	1
	C1	2	2	1.9	1.25
	C2	2	0.8	2	0
	C3	1	2	2	2
	C4	1.9	2	1.02	2
	C5	0	0.51	0.07	0

In fact, as the subsequent perturbation occurs, index and thumb fingertips lose their contact with the object and the precision grasp fails. The middle fingertip accidentally continues touching the object because the object remains unstably grasped. The force references have appositely been chosen quite low in order to achieve a precarious grasp and to demonstrate the effectiveness of the slippage control. The positions graph highlights the precariousness of the grasp since after the second perturbation the thumb is completely flexed.

Figures 3.11(c) and 3.11(d) show a further trial of the tri-digital grasp of the cup, but this time the slippage prevention algorithm is active and the perturbation set to 2 cm/s. As the slip event due to perturbation is detected, the grip is strengthened and the grasp becomes stable. From both force and position graphs it can be noticed that index finger, on which the slippage prevention algorithm is computed, mostly contributes to grasp stability; its applied force evidently arises and, as a reaction, also thumb increases its force value while middle finger does not modify its action.

In Fig. 3.12 the bi-digital grasp task of the highlighter is reported. In this case, when the control of the slippage is inactive (i.e 3.12(a) and 3.12(b)) the force references are well-kept after the first as well as the second perturbation, but there is no incisive increase in the grasp forces. Rather, forces diminution can be observed in the force graph, confirming that the object is not grasped in

Tesi di dottorato in Bioingegneria industriale, di Roberto Barone,
discussa presso l'Università Campus Bio-Medico di Roma in data 04/03/2017.
La disseminazione e la riproduzione di questo documento sono consentite per scopi di didattica e ricerca,
a condizione che ne venga citata la fonte.

a stable manner as a consequence of the perturbations. Slider positions remain unvaried; forces change is uniquely due to the under-actuated behaviour of the fingers. Figures 3.12(c) and 3.12(d) illustrate the reaction of the controller to a disturbance as fast as 4 cm/s, in order to show its capability of reacting also to the maximum velocity of the robotic arm. More seconds are needed to reach the steady state. In this trial the slip event is followed by a quick, high response of the index finger force and also the thumb increases its force in reaction. After the adjustment due to slippage, a grasp stability of the object is clearly reached.

Table 3.6 summarizes the overall performances of the control architecture for all the 72 trials. As a confirmation of the results depicted in Figures 3.11 and 3.12, it can be seen that when the slippage control is off, the failure percentage often comes to be high. Oppositely, the enabled slippage control allows the prosthesis to stably hold the object in every perturbation condition with rare exceptions. Table 3.7 indicates the mean force and position errors

Table 3.6: Complexive results over the 72 trials.

Object	Mass [g]	Trial	Failure percentage (No Slip Control, 4 cm/s)	Failure percentage (Slip Control, 2 cm/s)	Failure percentage (Slip Control, 4 cm/s)
Plastic cup	50	6	83%	0%	16%
Highlighter	10	6	16%	0%	0%
Egg Tri-digital	60	6	33%	0%	0%
Egg Bi-digital	60	6	50%	0%	0%

along with standard deviation computed for all the 72 trials. The most influent level of the control is the position one, as its gains are much higher than the force gains. Indeed, the fingers closed quickly, taking around 0.5 s to reach a steady position; thus the mean position error is always quite low. Force errors resulted little when slip control was off, but rose up significantly when the control could rely on the slip information; this fact can be easily explained considering the force augmentation in case of slip detection.

Tesi di dottorato in Bioingegneria industriale, di Roberto Barone,
discussa presso l'Università Campus Bio-Medico di Roma in data 04/03/2017.
La disseminazione e la riproduzione di questo documento sono consentite per scopi di didattica e ricerca,
a condizione che ne venga citata la fonte.

Table 3.7: Mean position and force error and standard deviation over the 72 trials.

Mean force error ± SD [N]	**Plastic cup**	**Highlighter**	**Egg Tri-digital**	**Egg Bi-digital**
No Slip Control (4 cm/s)	0.15±0.03	0.12±0.01	0.21±0.03	0.21±0.02
Slip Control (2 cm/s)	0.28±0.02	0.22±0.01	0.40±0.03	0.41±0.03
Slip Control (4 cm/s)	0.30±0.02	0.28±0.03	0.41±0.01	0.36±0.03
Mean position error ± SD [m]				
No Sip Control (4 cm/s)	0.0027 ± 0.0001	0.0014 ± 0.0001	0.0013 ± 0.0001	0.0011 ± 0.0001
Slip Control (2 cm/s)	0.0026 ± 0.0001	0.0001 ± 0.0001	0.0013 ± 0.0001	0.0015 ± 0.0001
Slip Control (4 cm/s)	0.0026 ± 0.0001	0.0018 ± 0.0001	0.0015 ± 0.0001	0.0011 ± 0.0001

Tesi di dottorato in Bioingegneria industriale, di Roberto Barone,
discussa presso l'Università Campus Bio-Medico di Roma in data 04/03/2017.
La disseminazione e la riproduzione di questo documento sono consentite per scopi di didattica e ricerca,
a condizione che ne venga citata la fonte.

3.1.4 Conclusions

A novel control architecture to improve grasp stability has been tested on an anthropomorphic hand for prosthetic applications. The control was distributed on two different levels; the high-level control provided the fingers with the optimal trajectories learnt by a PIBB algorithm, whereas the low-level control was directly interfaced with the hand actuators. Potentialities of the high-level control have been analyzed and compared with a traditional approach based on PD control; in particular, the generalization capabilities of a hierarchical control architecture where verified by means of experimental trials involving grasping tasks of objects with different sizes.
FSR sensors put onto the fingertips of thumb, index, and middle fingers and covered with silicon caps have been employed for forces estimation, as well as for slippage detection. An ad hoc experimental setup exploiting a robotic arm has been set to evaluate system performance: results confirmed the architecture capability of stably grasp objects of different sizes and shapes, also in presence of slippage. The added value of the two-layer architecture is especially evident in scenarios where the experimental conditions cannot be predefined, and the environment is highly unstructured, as in the ADLs. In these situations, learning is undoubtedly crucial, above all if grounded on incremental learning with respect to an already performed offline training. Future works will be addressed to (1) extract the slip sensory information from more than one sensor, paying attention not to excessively slow down the control loop; (2) add more force sensors on the prosthetic hand in order to extend the approach to other grasping tasks and to manipulation; and (3) implement online learning on the prosthetic hand and possibly test the developed architecture on different prosthetic hands.

3.2 Cyclic tasks

3.2.1 Introduction

This paragraph describes the application and the experimental validation of a bio-inspired control on a prosthetic hand during tasks of cyclic manipulation (e.g. unscrewing the cup to open a bottle). In the last years great attention has been dedicated to prosthetic hands and huge efforts have been lavished in activities related to mimicking human manipulation capabilities. Despite the recent technological advancements, well-represented by the anthropomorphic

Tesi di dottorato in Bioingegneria industriale, di Roberto Barone,
discussa presso l'Università Campus Bio-Medico di Roma in data 04/03/2017.
La disseminazione e la riproduzione di questo documento sono consentite per scopi di didattica e ricerca,
a condizione che ne venga citata la fonte.

poliarticulated hands (e.g. Touch Bionics iLimb, Ottobock Michelangelo and RSL Steeper BeBionic3), human grasping and (mainly) manipulation capabilities are still far away. This section wants to address the challenge of making a prosthetic hand develop manipulation capabilities by means of a learning architecture grounded on Reinforcement Learning (RL), coupled with Central Pattern Generators (i.e. CPGs) and force control, with special attention to cyclic manipulation tasks. The dynamic interaction between fingers and object is managed by a low-level parallel force/position control. Cyclic manipulation can be regarded as one of the more widespread activities of daily living [64] requiring the motion of an object (e.g. turning a key to open a door, turning a handle to open a wardrobe or unscrewing the cup to open a bottle). In this work, the bio-inspired control proposed in [65] is modified in order to account for kinematics and dynamic issues involved in the interaction between fingers and object during a cyclic manipulation task. Information about the normal force exerted by the fingers on the object, neglected in [65], are taken into account in the implementation of a parallel force/position control. In the literature the first computational architecture for cyclic manipulation tasks was proposed by Kurita in [66] to replicate the contact between the two involved fingers. Afterwards a bio-inspired hierarchical neural architecture based on a RL model was presented in [65] with the goal of mimicking the human learning mechanisms and replicating them on two simulated robotic hands. Most of the grasp control strategies of prosthetic hands resort to the computed torque feed-forward control, inverse dynamics and other model based controls. On the other hand, examples of controls that don't need to model the dynamics of the system, such as the finger thumb opposition for pinching objects by Arimoto [67], were proposed. In a recent paper [68] an intrinsically passive control (IPC) was compared to position, admittance and impedance controls. It just needs fingertip position information while succeeding in compliantly grasping different objects and dynamically accommodating the object's motion. In [69], thanks to a position control and a mechanical design based on springs it was possible to control the grasping force. On the other hand, in [70] a classic force control with inner velocity loop was implemented, thus demonstrating the benefits deriving from force sensory feedback. Although many efforts have been spent in studying grasping tasks, in literature there are no examples of force control applied to cyclic manipulation. This work has a twofold purpose: on one hand, it wants to demonstrate the applicability of the proposed control based on learning architecture and parallel force/position control to cyclic manipulation, and on the other hand, it intends to verify the viability of the

Tesi di dottorato in Bioingegneria industriale, di Roberto Barone,
discussa presso l'Università Campus Bio-Medico di Roma in data 04/03/2017.
La disseminazione e la riproduzione di questo documento sono consentite per scopi di didattica e ricerca,
a condizione che ne venga citata la fonte.

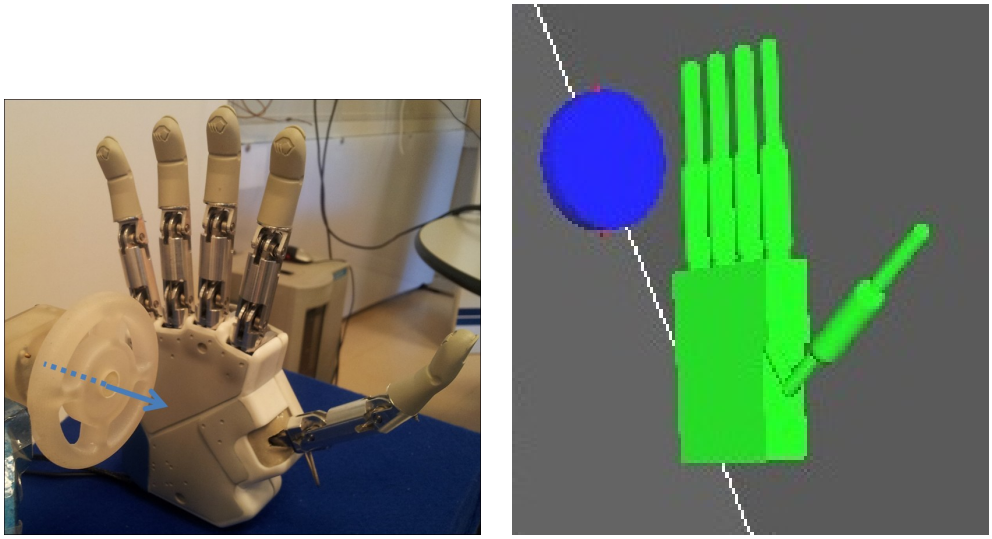

(a) *Setup for the experimental tests with the rotating object.*

(b) *Simulated hand and object.*

Figure 3.13: Real and simulate IH2 hand.

control in the prosthetic field where many constraints have to be accounted for, e.g.: (i) the reduced number of active DOFs, (ii) the usual choice of using underactuated mechanisms for driving the fingers and (iii) the necessity to carry out the training of the hand before providing the amputee with it, in order to guarantee high levels of dependability, reliability and safety. Two simulated models of the hand were developed, taking into account kinematic and dynamic parameters of the real IH2 hand. First, the open-source physical-engine software OPAL interfacing with the NEWTON physical engine library was used for simulating the hand and the environment during the training phase. Secondly, a simulated model of the IH2 fingers was developed in Matlab/Simulink in order to test the parallel force/position control, based on the results of the training phase. The choice of implementing the training phase in simulation has a twofold motivation: (i) it facilitates learning, thus avoiding problems of damages and overwork on the real hardware; (ii) it avoids making the real hand learn when mounted on the patient socket, thus excluding the possibility to have unexpected behavior.

3.2.2 Materials and methods

The control architecture (Fig. 3.14) consists of the actor-critic RL neural network, the CPG, the parallel force/position control and a robotic hand interacting with the object . The theoretical details on the neural architec-

Tesi di dottorato in Bioingegneria industriale, di Roberto Barone,
discussa presso l'Università Campus Bio-Medico di Roma in data 04/03/2017.
La disseminazione e la riproduzione di questo documento sono consentite per scopi di didattica e ricerca,
a condizione che ne venga citata la fonte.

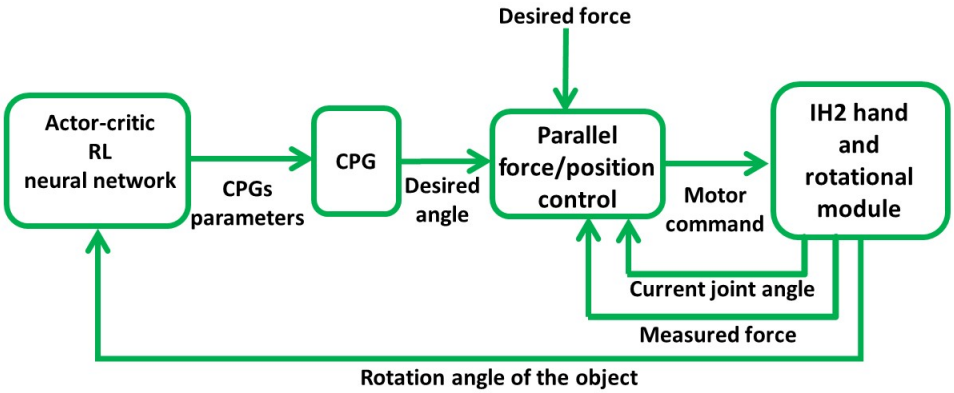

Figure 3.14: The overall control system architecture characterized by the following components: actor-critic RL neural network, CPG, parallel force/position control, hand and object.

ture with RL and CPGs are reported in [65]. Therefore, a brief description is reported in the following. The trial-and-error process characterizing the RL neural network (based on actor-critic model [65], [71]) allows the system to autonomously define the CPG parameters that maximize the object rotation. The reinforcement signal, i.e. the object rotation used as reward, was calculated at each trial, lasting 3000 cycles. Accordingly the RL neural network computed 4 different types of parameters: amplitude, center of oscillation, frequency and phase of the CPG every 3000 cycles and joint desired angles were generated. The training phase lasted 5000 trials. The cyclic trajectories are computed by means of coupled oscillators. The adopted CPG (Fig. 3.15) has 3 oscillators and requires the computation of 9 parameters: a common frequency, 3 amplitudes (one for each neuron), 3 centers of oscillation (one for each neuron), 2 phases. Each oscillator is associated to the control of a single

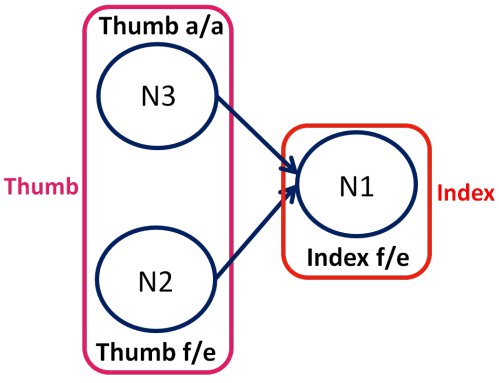

Figure 3.15: The CPG is formed by 3 different neurons each defining the trajectory of one DoA.

DoA as follows: N1 defines the desired angle of index F/E; N2 generates the

Tesi di dottorato in Bioingegneria industriale, di Roberto Barone,
discussa presso l'Università Campus Bio-Medico di Roma in data 04/03/2017.
La disseminazione e la riproduzione di questo documento sono consentite per scopi di didattica e ricerca,
a condizione che ne venga citata la fonte.

desired angle of thumb F/E and N3 defines the thumb A/A desired angle. The neuron in charge of generating the F/E desired angles is also responsible for this coupling between the two phalanxes. The dynamic model of the manipulator is expressed as

$$B(\mathbf{q})\ddot{\mathbf{q}} + C(\mathbf{q}, \dot{\mathbf{q}})\dot{\mathbf{q}} + g(\mathbf{q}) + e(\mathbf{q}) = \tau \tag{3.12}$$

where $B(\mathbf{q})$ is the inertia matrix, $C(\mathbf{q}, \dot{\mathbf{q}})$ is the vector of centrifugal and Coriolis torques, $g(\mathbf{q})$ is the gravitational torque vector, $e(\mathbf{q})$ is the joint elastic torque vector and $\mathbf{q}$ $\dot{\mathbf{q}}$ $\ddot{\mathbf{q}}$ are respectively vectors of joint position, velocity and acceleration. The coupling relation between joint kinematics and slider kinematics is expressed as [73]

$$x_S = r_1(q_1 - q_{01}) + r_2(q_2 - q_{02}) \tag{3.13}$$

with r_1 and r_2 the radii of MCP and PIP joint pulleys, respectively, q_1 and q_2 the joint positions, q_{01} and q_{02} the initial equilibrium joint angles(equal to 0) and x_S the slider position. The parallel force/position control law, expressed in terms of slider position, is

$$\tau = [\mathbf{T_g} + \mathbf{T_e} - k_D\dot{x_s} + k_P(x_{fs} + x_{ds} - x_s)]\mathbf{r} + J^t\mathbf{h} \tag{3.14}$$

being x_{fs} related to the joint variable q_{fs} through the following relation

$$q_{fs} = C_f(\tau_\mathbf{d} - \tau_\mathbf{c}) \tag{3.15}$$

and k_D is the gain for the derivative action, k_P is the gain for the proportional action, $\dot{x_s}$ is the slider velocity, x_{fs} is the position reference computed from q_{fs} (thanks to equation 3.15), x_s is the current slider position, x_{ds} is the reference slider position computed by means of CPG, $\mathbf{T_g}$ is the contribution of the gravitational torque at the level of slider, $\mathbf{T_e}$ is the elastic contribution in order to compensate the preloaded spring, $\mathbf{r}$ is the pulley radii vector, $\mathbf{q_{fs}}$ is the vector of reference joint position computed on the basis of torque error, C_f is the proportional-integral torque control [73], $\mathbf{h}$ is the vector of forces exerted on the environment, $\tau_\mathbf{d}$ is the desired torque vector and $\tau_\mathbf{c}$ is the vector of current torques computed as follows

$$\tau_\mathbf{c} = J^t\mathbf{h_{FSR}} \tag{3.16}$$

Tesi di dottorato in Bioingegneria industriale, di Roberto Barone,
discussa presso l'Università Campus Bio-Medico di Roma in data 04/03/2017.
La disseminazione e la riproduzione di questo documento sono consentite per scopi di didattica e ricerca,
a condizione che ne venga citata la fonte.

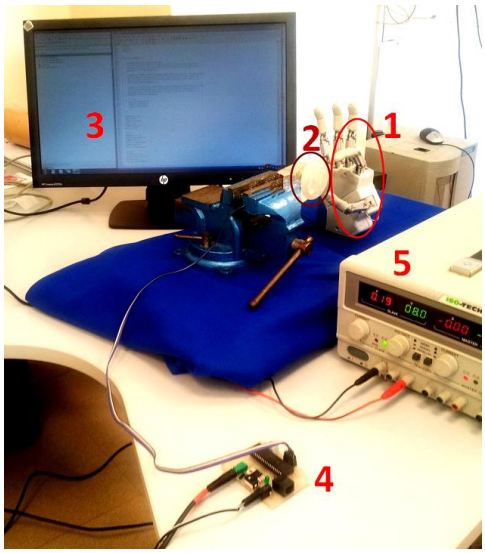

(a) *1) the IH2 robotic hand 2) the ring-shaped object 3) the workstation for the IH2 hand control 4) the rotation angle acquisition board 5) the power supply.*

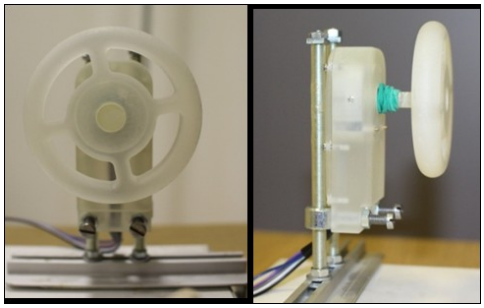

(b) *The rotating object used during the experimental tests on the IH2 hand.*

Figure 3.16: Experimental setup.

where $\mathbf{h_{FSR}}$ is the vector of measured interaction forces between finger and object. A typical task of everyday life, i.e. unscrewing the cup to open a bottle, was chosen to train the control architecture. The training phase was implemented in simulation and the extracted CPG parameters were used to control the IH2 hand during the same manipulation task. The parallel force/position control was implemented on a simulated model of the IH2 finger (in Matlab/Simulink) taking in input the desired positions from the CPG (properly converted in slider position) and a desired force value of 0.11 N experimentally retrieved. In the test phase, the CPG equations were implemented in Matlab for extracting joint desired trajectories. The goodness of the learning parameters was verified during the experimental tests through one encoder embedded into the rotating object (Fig. 3.16). The object is characterized by a ring-shaped interchangeable handle (diameter=6cm) connected to an optical encoder. The complete setup for the experimental tests is composed of: (i) the IH2 robotic hand; (ii) the ring-shaped object; (iii) one workstation for the hand control; (iv) a rotation angle acquisition board; (v) the power supply. Only three DoAs of the hand were controlled, as required by the task, in the learning as well as in the test phase: the F/E of the index finger and the two DoAs of the thumb (F/E and A/A).

Tesi di dottorato in Bioingegneria industriale, di Roberto Barone,
discussa presso l'Università Campus Bio-Medico di Roma in data 04/03/2017.
La disseminazione e la riproduzione di questo documento sono consentite per scopi di didattica e ricerca,
a condizione che ne venga citata la fonte.

3.2.3 Results of the learning and test phase

System performance during learning is shown in Fig. 3.17 in terms of rotation of the object. After a first period of exploration of all the possible

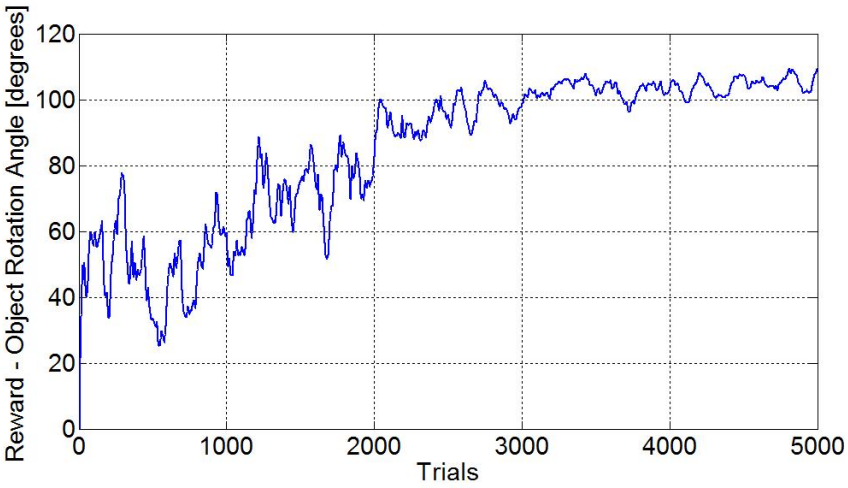

Figure 3.17: Reward signals (rotation angle of the object in degrees) during the complete learning of the cyclic manipulation task.

movements, the object rotation angle (Fig. 3.17) increased showing the enhanced capabilities of the hand to execute the required task. In Fig. 3.18 is shown the contact of index and thumb fingers in one trial at the end of the learning. At the end of the learning the hand controlled by the architecture

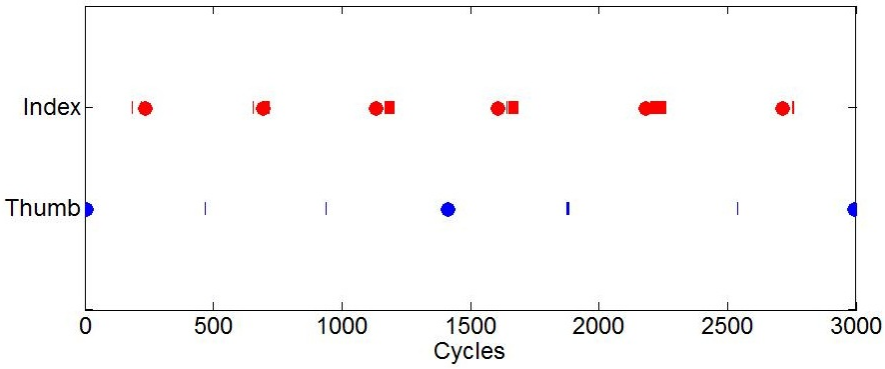

Figure 3.18: Contact of index and thumb fingers in one trial at the end of the learning.

using the CPG was able to rotate the object of 110° in one single trial as indicated in Fig. 3.19. Table 3.8 reports the parameters of the CPG extracted from the simulator and adopted in the test phase on the real hand. In Fig. 3.20 simulation results of the parallel force-position control are shown in terms

Tesi di dottorato in Bioingegneria industriale, di Roberto Barone,
discussa presso l'Università Campus Bio-Medico di Roma in data 04/03/2017.
La disseminazione e la riproduzione di questo documento sono consentite per scopi di didattica e ricerca,
a condizione che ne venga citata la fonte.

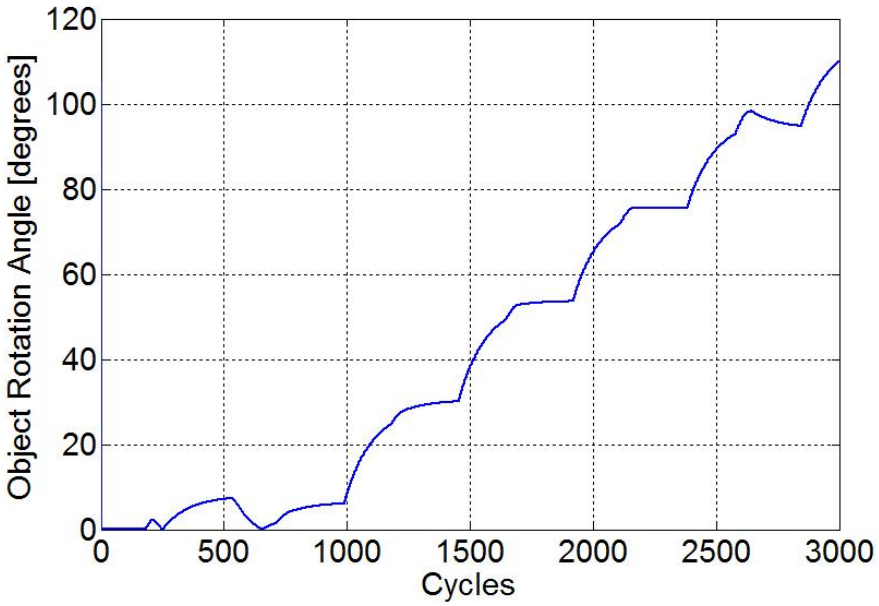

Figure 3.19: Rotation angle of the object (degrees) recorded at the end of the learning in a single trial (3000 cycles).

Table 3.8: Parameters learned in simulation.

$C1$	$C2$	$C3$	$R1$	$R2$	$R3$	f_1	Φ_{21}	$\Phi 31$
1.17	0.52	1.9	0.38	0.37	0.1	2.25	0.1	1

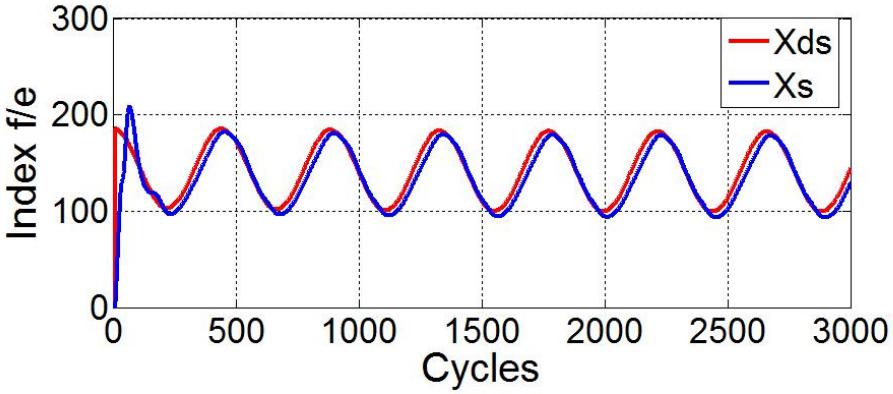

Figure 3.20: Desired and actual slider position responsible for index flexion/extension. The range of motion of the slider varies from 0 (extended index) and 255 (flexed index).

Tesi di dottorato in Bioingegneria industriale, di Roberto Barone,
discussa presso l'Università Campus Bio-Medico di Roma in data 04/03/2017.
La disseminazione e la riproduzione di questo documento sono consentite per scopi di didattica e ricerca,
a condizione che ne venga citata la fonte.

of overlapped desired and actual position of the slider. The mean error during one trial is 0.0007 m. Figure 3.21 shows the normal component of the force exerted between the index fingertip and the object, also the force reference is accurately reached (mean error of 0.024 N). The gains of the parallel

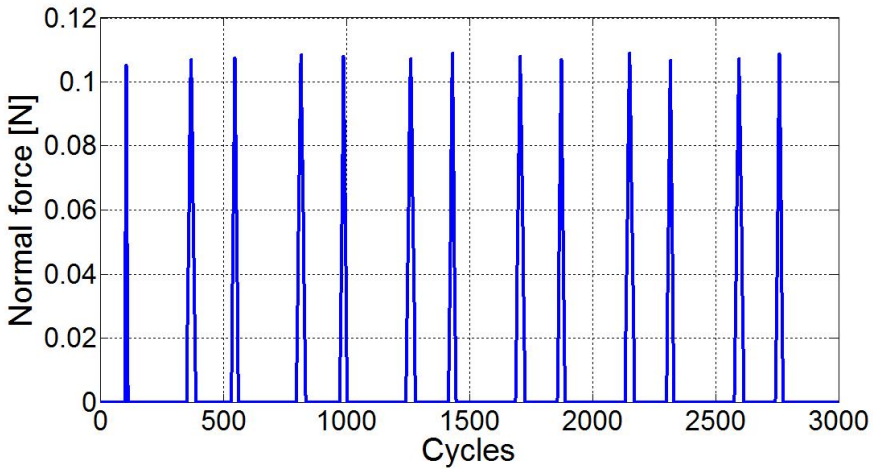

Figure 3.21: Normal contact force between the object and the index fingertip.

force/position control law had the following values: $k_D = 15$, $k_P = 950$. The gains of the proportional-integral torque control were fixed to: $k_P = 2$, $k_I = 4$. Preliminary experimental tests were carried out on the real IH2 hand as shown by snapshots of the task in Fig.3.22. The recorded ring rotation is shown in

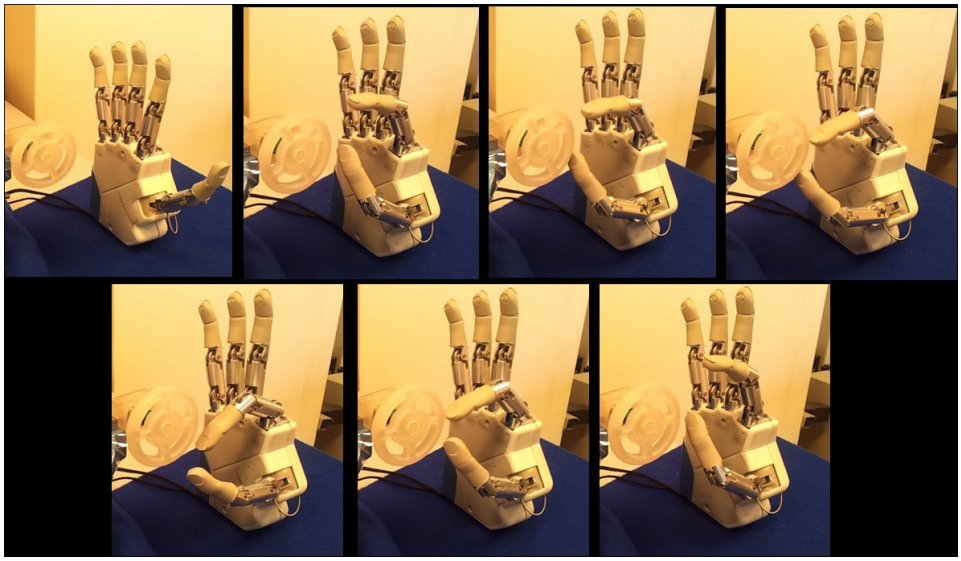

Figure 3.22: Snapshots of the cyclic manipulation task with the IH2 hand.

Fig. 3.23 after one trial. The IH2 hand was able to rotate the ring-shaped object of 294°. The experiments were repeated 5 times and the obtained performance are comparable (mean value 309° and standard deviation 9°), thus

Tesi di dottorato in Bioingegneria industriale, di Roberto Barone,
discussa presso l'Università Campus Bio-Medico di Roma in data 04/03/2017.
La disseminazione e la riproduzione di questo documento sono consentite per scopi di didattica e ricerca,
a condizione che ne venga citata la fonte.

demonstrating a good level of repeatability of the manipulation task.

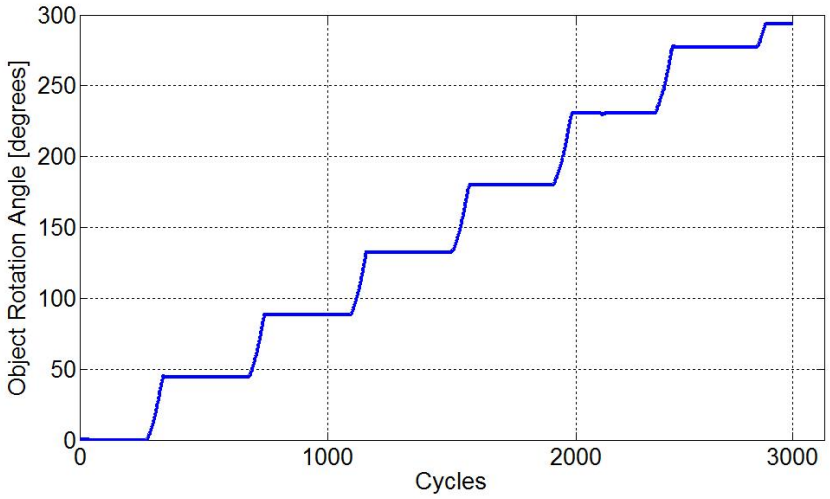

Figure 3.23: Snapshots of the cyclic manipulation task with the IH2 hand.

3.2.4 Conclusions

This work proposes the application and the experimental validation of a bio-inspired control on a prosthetic hand during tasks of cyclic manipulation (e.g. unscrewing the cup to open a bottle). In order to assure safety and avoid problems of damages and overwork, the training phase was conducted with a simulated model of the IH2 hand; the parallel force/position control was tested on simulated fingers interacting with simulated object and preliminary experimental tests were carried out on the real IH2 hand. The simulated and real IH2 hand learned to execute the manipulation task thanks to the coordinating action of index and thumb fingers. The rotational angle of the object reached 110° during training and 309° during experimental tests. The application of a parallel force/position control resulted in a satisfying behavior of the prosthetic hand, both the desired force and position targets are achieved in simulation with low errors. As a noteworthy result of this study simulator succeeded to find CPGs parameters despite two additional difficulties with respect to the study in [65]: the underactuated nature of IH2 hand and the lack of index A/A making the task more difficult to perform. However, despite these constraints, the control successfully found a solution to accomplish the task. As a future work, it is possible to imagine to use the Pibb algorithm also for manipulation with cyclic tasks because this algorithm is computationally less expensive than a RL neural network and this allows to implement an online framework.

Tesi di dottorato in Bioingegneria industriale, di Roberto Barone,
discussa presso l'Università Campus Bio-Medico di Roma in data 04/03/2017.
La disseminazione e la riproduzione di questo documento sono consentite per scopi di didattica e ricerca,
a condizione che ne venga citata la fonte.

Chapter 4

The design of a wrist prosthetic module for active prono-supination and passive flexion-extension

4.1 Introduction

Prosthetic system for the wrist are designed to perform a twofold function: (i) to connect the hand prosthesis to the forearm, and (ii) to define hand orientation before the execution of a task. Human wrist has 3 degrees of freedom (dofs): prono-supination, flexion-extension and adduction-abduction (fig. 4.1). Physiologically the wrist can cover the following ranges of motion [74]:

- pronation/supination: $-85°/+90°$;
- flexion/extension: $-80°/+70°$;
- adduction/abduction: $-30°/+20°$.

Prono-supination angle is zero when the palm of the hand is parallel to the sagittal plane of the subject. The zero angle for flexion-extension and adduction-abduction is obtained for totally opened fingers and are aligned with the forearm. In literature there are many studies pointing out the importance of the degrees of freedom of the wrist in grasping and manipulation, for increasing dexterity and reducing pathologies related to movement compensation, e.g . repetitive strain injuries (RSI)
RSI is a disorder that involves ligaments, muscles, tendons, joints or support structure of the body. Symptoms like pain, muscular weakness and tingling

Tesi di dottorato in Bioingegneria industriale, di Roberto Barone,
discussa presso l'Università Campus Bio-Medico di Roma in data 04/03/2017.
La disseminazione e la riproduzione di questo documento sono consentite per scopi di didattica e ricerca,
a condizione che ne venga citata la fonte.

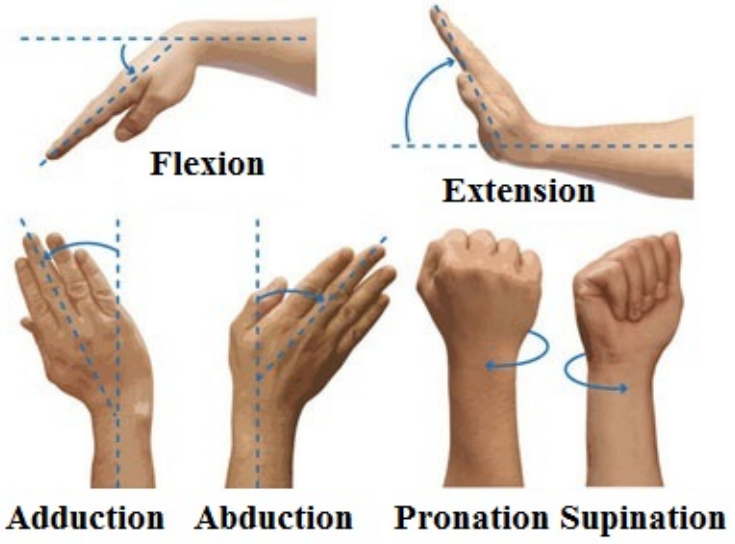

Figure 4.1: Degrees of freedom of the wrist.

with loose of strength in the considered arm are consequent. Although the name RSI makes someone think that the pathology is related to repetitive movements, instead, most common causes of the syndrome are anomalous postures and long work sessions.
In literature, there are few epistemological studies that show the incidence of this syndrome in unilateral upper limb amputees [75]. Moreover, the work in [76] has shown that the 57% of the unilateral upper limb amputees were affected by RSI syndrome on the sound limb. In [77] it is reported that 50% of the 60 involved unilateral upper-limb amputees suffered from RSI problems on the sound limb.
In [78] it is pointed out that using a prosthesis can help to prevent RSI syndrome with respect to the total absence of a prosthesis or to a cosmetic prosthesis.

An interesting study in [79] analyses the incidence of the RSI pathology on amputees thanks to a kinematic study on 3 groups of subjects during 4 tasks of daily living (drink from a glass and open a door, lift a box and rotate a steering wheel). This study provides two important results:

- Subjects with limited dofs of the wrist have a kinematic behaviour similar to subjects using a prosthesis with no wrist;
- compensatory movements, which precedent studies demonstrated to be present on the sound limb of amputees, are also present on the arm with the prosthesis during unilateral tasks.

Tesi di dottorato in Bioingegneria industriale, di Roberto Barone,
discussa presso l'Università Campus Bio-Medico di Roma in data 04/03/2017.
La disseminazione e la riproduzione di questo documento sono consentite per scopi di didattica e ricerca,
a condizione che ne venga citata la fonte.

From the aforementioned studies it emerges that the compensation due to the lack of the degrees of freedom of the wrist are related to the task to accomplish. This is also confirmed in [80] and [81] where it is demonstrated that, without the wrist, shoulder is the motor district more exposed to overload. Moreover, although it is clear the paramount role of the wrist during the execution of activities of daily living. Historically, the first dof implemented in a prosthesis is the prono-supination, because is intuitively the main responsible for the regulation of the orientation of the hand. So most examples of wrist prosthetic modules reproduce the prono-supination; also there exist solutions for the flexion-extension and adduction-abduction of the wrist. Anyway, it is important to note that all the solutions currently available are arranged between the socket and the hand prosthesis.

The restoration of the prono-supination through a prosthetic module is very important for the following reasons:

- Amputees with an amputation at the 50% or less of the initial length of the forearm cannot anymore perform prono-supination; moreover, in more distal transradial amputees this degree of freedom is seriously compromised;
- From a study on 1575 amputees [82] it emerges that users most requested dof is the prono-supination.

Two studies ([83] and [84]) highlights the importance of the flexion-extension after the prono-supination, because its presence reduces the compensatory movements and the articular kinematic is more physiological.
Respect to the state of the art, the wrist presented here has the active prono-supination embedded in the socket and passive flexion-extension with springs, which allow a flexible behavior of the module. There is no module on the market or in literature that has these characteristics. The chapter presents the choice of the prono-supination module and the design of a flexible wrist with passive flexion-extension.

4.2 Materials and methods

4.2.1 Choice of the prono-supination module

In this section, the choice of commercial components for the active prono-supination module is described. There are two main characteristics to be

Tesi di dottorato in Bioingegneria industriale, di Roberto Barone,
discussa presso l'Università Campus Bio-Medico di Roma in data 04/03/2017.
La disseminazione e la riproduzione di questo documento sono consentite per scopi di didattica e ricerca,
a condizione che ne venga citata la fonte.

fulfilled: the torque needs to be equal or greater than 1.7 Nm (in comparison with commercial and research active wrist torque) and dimensions and weight need to satisfy some requirements. In particular, the wrist need to be embedded in the socket, solving the problem of additional space required by standard commercial wrists and the weight need to be as small as possible.
Measuring a standard socket (Fig. 4.2) it was possible to find the following requirements: maximum 4.5 cm of diameter and maximum 10 cm of length.
Recapitulating, requirements for the wrist module are:

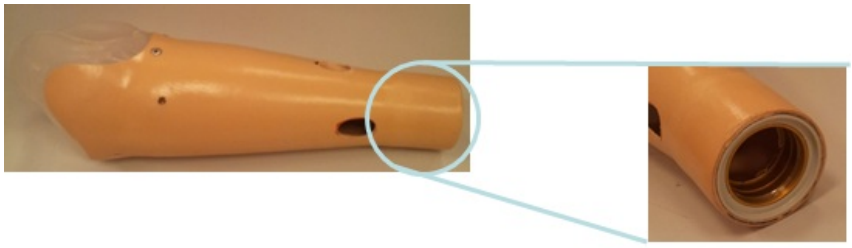

Figure 4.2: Prosthetic socket.

1. Nominal torque: 2 Nm;
2. Maximum length: 10 cm;
3. Maximum diameter: 4.5 cm;
4. Maximum weight: 150 g;
5. Angular speed: 32-61 rpm.

Searching the web for a solution, it was found a combination of actuator and gear that fulfilled our requirements. In particular, the EC 32 motor flat Ø32 mm, brushless, 6 Watt, with Hall sensors and Planetary gear GP 22 C Ø22 mm, 0.5 - 2.0 Nm were selected; an encoder MR 3 channels was added to better measure the position of the device. The device characteristics are:

1. Nominal torque: 1.5 Nm;
2. Length: 7.2 cm;
3. Diameter: 4.5 cm;
4. Weight: 113 g;
5. Angular speed: 14 rpm.

In figure 4.4 is reported the CAD of the prono-supination module.

Tesi di dottorato in Bioingegneria industriale, di Roberto Barone,
discussa presso l'Università Campus Bio-Medico di Roma in data 04/03/2017.
La disseminazione e la riproduzione di questo documento sono consentite per scopi di didattica e ricerca,
a condizione che ne venga citata la fonte.

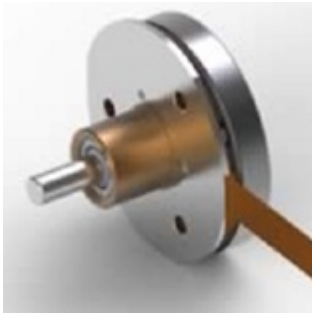

(a) *Actuator.*

(b) *Gear.*

(c) *Encoder.*

Figure 4.3: Selected components for the wrist module.

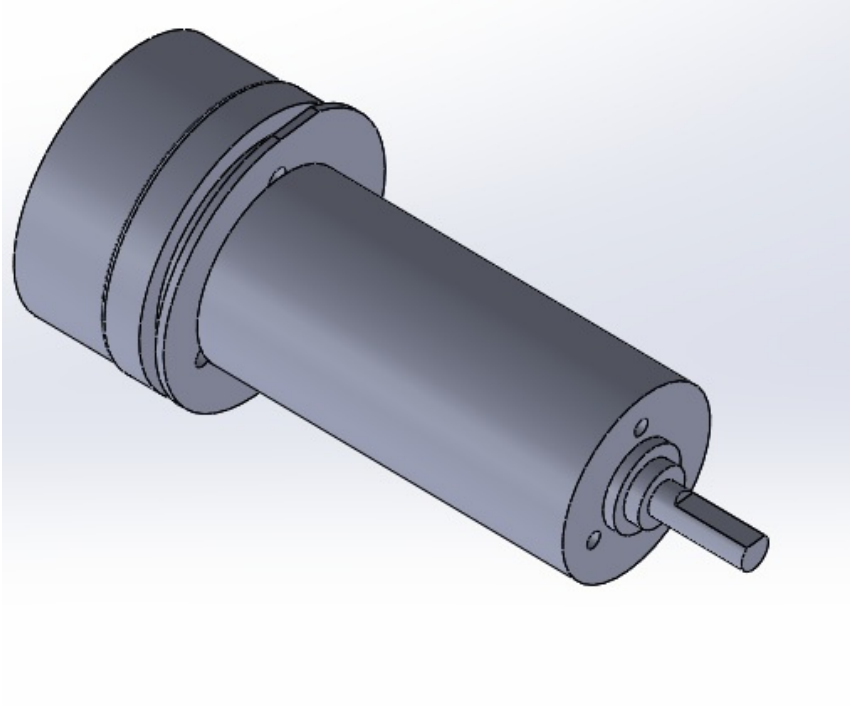

Figure 4.4: CAD of the prono-supination module.

Prototype and control of the prono-supination module

The components for the realization of the prono-supination module have been acquired from Maxon Motor and a prototype has been realized, creating

Tesi di dottorato in Bioingegneria industriale, di Roberto Barone,
discussa presso l'Università Campus Bio-Medico di Roma in data 04/03/2017.
La disseminazione e la riproduzione di questo documento sono consentite per scopi di didattica e ricerca,
a condizione che ne venga citata la fonte.

a shell for the interface with the socket and a threaded flange for the interface with the prosthetic hand (4.5).

Test-bed trials have been conducted in order to control the prototype and in

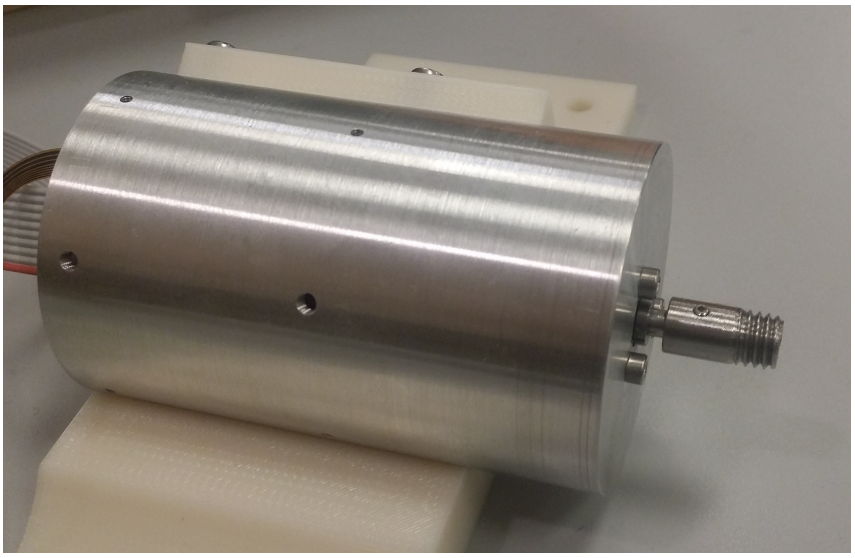

Figure 4.5: Shell and flange of the prono-supination module.

figure 4.6 it is possible to see the experimental setup realized. The experimen-

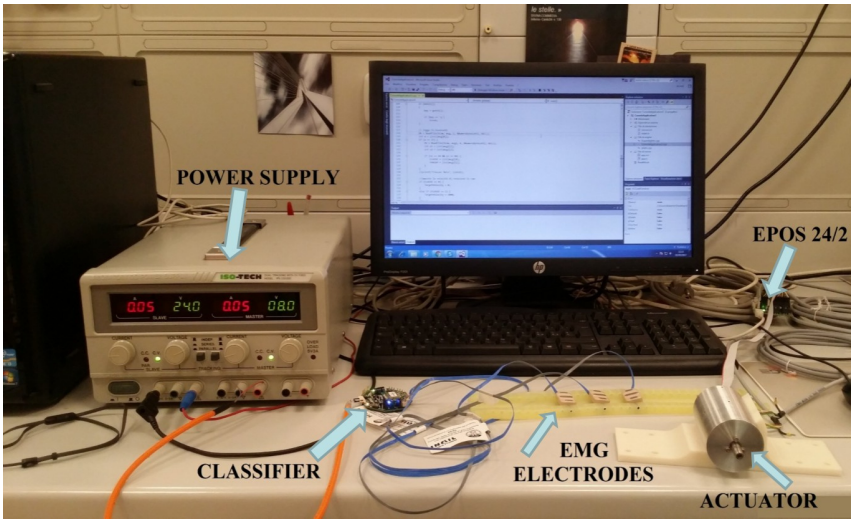

Figure 4.6: Experimental setup for the trials on the prono-supination module.

tal setup consists of a power supply that provides energy to the actuator, EMG electrodes for the motor intention detection and a non-linear logistic regression classifier, which classifies three classes: pronation, supination and rest condition. After the classification, the PCB with the classifier communicates the motor intention via bluetooth to the PC, which sends the actuation command to the Epos 24/2 controller that directly actuates the motor.

Tesi di dottorato in Bioingegneria industriale, di Roberto Barone,
discussa presso l'Università Campus Bio-Medico di Roma in data 04/03/2017.
La disseminazione e la riproduzione di questo documento sono consentite per scopi di didattica e ricerca,
a condizione che ne venga citata la fonte.

In figures 4.7-4.9 are reported the preliminary tests with a velocity control, by comparing the case of a constant velocity reference (taken as 2000 rpm) with a velocity profile.

For what concerns the velocity mode (Fig. 4.7), it is possible to see spikes

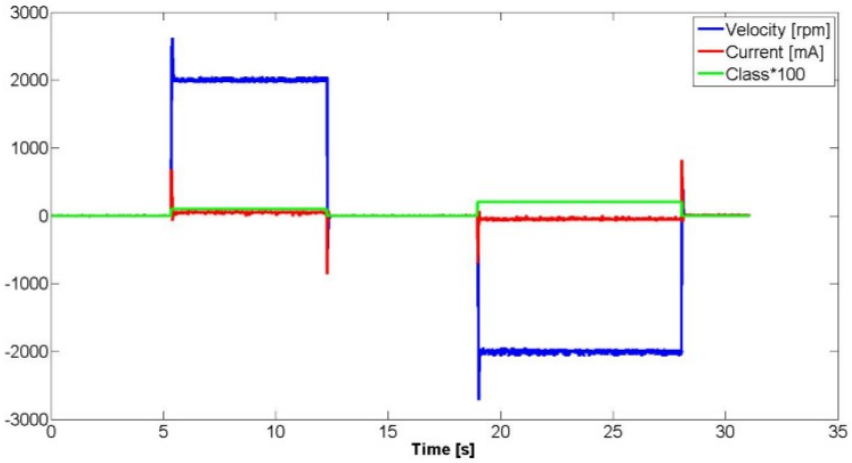

Figure 4.7: Speed control with the Epos 24/2 velocity mode.

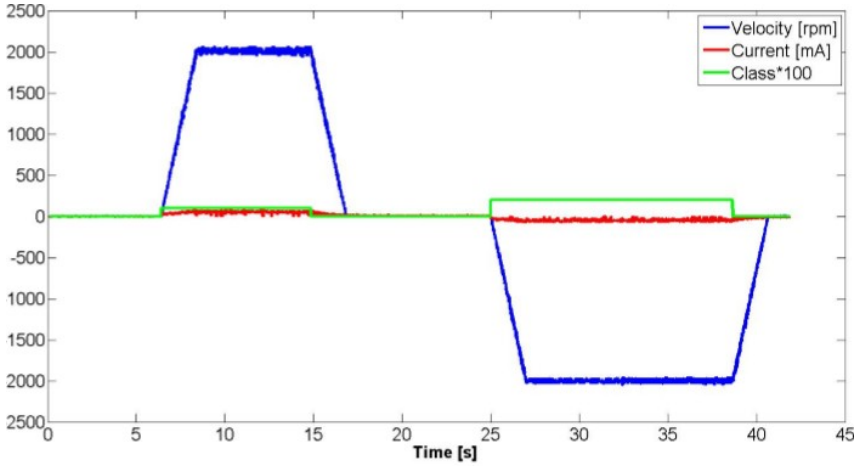

Figure 4.8: Speed control with the Epos 24/2 profile velocity mode (acc/dec 1000 rpm/s).

at the beginning and at the end of the prono-supination movements. These spikes vanish if the profile velocity mode (Fig. 4.8 and Fig. 4.9) is used at both 1000 rpm/s and 10000 rpm/s. These experimental trials have been useful to decide to use the profile velocity mode in order to avoid the spikes and to have a smoother behaviour of the actuator.

Tesi di dottorato in Bioingegneria industriale, di Roberto Barone,
discussa presso l'Università Campus Bio-Medico di Roma in data 04/03/2017.
La disseminazione e la riproduzione di questo documento sono consentite per scopi di didattica e ricerca,
a condizione che ne venga citata la fonte.

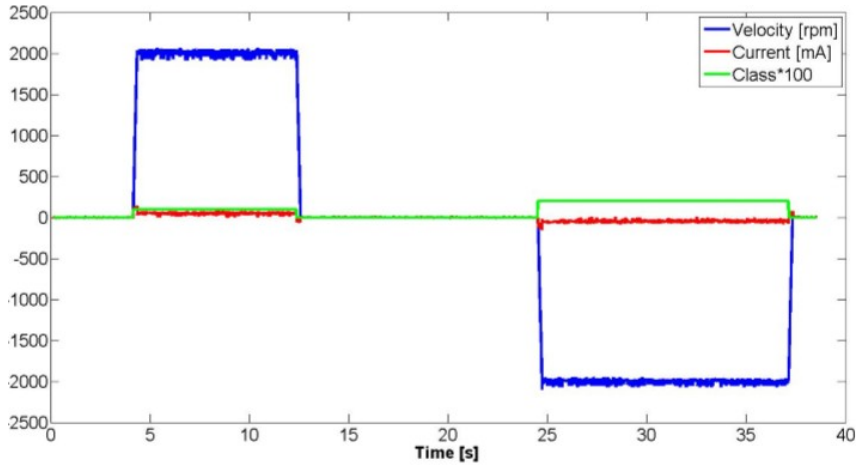

Figure 4.9: Speed control with the Epos 24/2 profile velocity mode (acc/dec 10000 rpm/s).

4.2.2 Design of a module for the passive flexion-extension

The conception and design phases are based on requisites that need to be respected and satisfied. Design choices and final decisions are conditioned by constraints imposed by the technical specifications defined in this section.
Requirements that during the development of an innovative prosthesis need to be taken into account are: low weight, reliability, robustness and low costs. Solutions adopted must be the results of a good compromise between dexterity, simplicity and reliability [85]. Another important aspect is the respect of the anthropometric dimensions, in fact an anthropomorphic prosthesis promotes the process of acceptance of the device from the amputee, helping him making it through psychological injuries consequent to the traumatic event of the amputation.
The module that has been designed has to implement the passive flexion-extension. The prosthesis has to be flexible, in order to furnish dexterity avoiding compensatory movements, but also rigid, in order to stably grasp objects. To this end, there is the need of ratchet positions where the prosthesis can be blocked; these positions are defined thanks to motion analysis studies of the wrist during some activities of daily living (ADLs).
A bibliographic research on biomechanical and anthropometric studies of the human wrist joint and an investigation between wrist modules produced by leader companies in the prosthetic field supported the definition of the technical specification with the aim of realizing a prototype able to meet the user needs and at the same time that has competitive characteristics in comparison to prosthetic wrists on the market.

Tesi di dottorato in Bioingegneria industriale, di Roberto Barone,
discussa presso l'Università Campus Bio-Medico di Roma in data 04/03/2017.
La disseminazione e la riproduzione di questo documento sono consentite per scopi di didattica e ricerca,
a condizione che ne venga citata la fonte.

Technical specification

Dimensions and weight A prosthesis with an appearance similar, almost unmistakable with the human articulation helps the amputee to accept the device, because when other people don't see its presence this is satisfying for the subject and helps the integration of the amputee in the society [86]. This survey suggests to design an anthropomorphic device.

It is possible to find in literature the anthropomorphic data of the perimeter

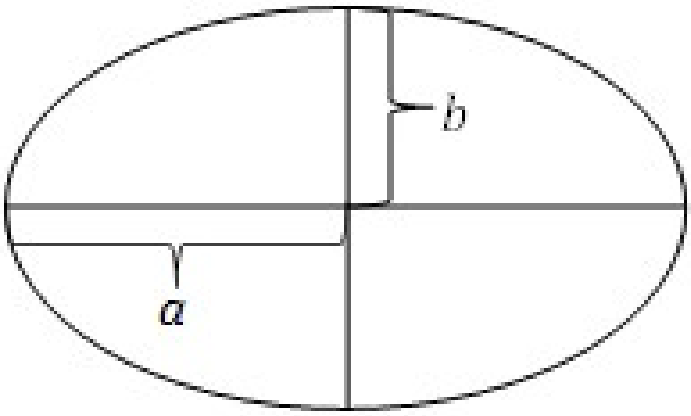

Figure 4.10: Ellipse: a= major semi-axis b= minor semi-axis.

and the width of a wrist, this is considered the major axis of the ellipse (2a) (Figure 4.10) [87] [88]. Minor axis (2b) can be found inverting the following:

$$P = \pi\sqrt{2(a^2 + b^2)} \tag{4.1}$$

Elliptical section of the wrist should have the minor axis equal to 40 mm and the major axis equal to 67.8 mm.

Extreme values where to choice the height of the module are chosen looking at prosthetic wrist available on the market: minimum height is 25 mm while maximum height is 27 mm [89].

Minimum value for the weight is 55 g, maximum is 89 g: data are taken from flexion-extension module available on the market.

Range of motion and ratchet positions Range of motion of a prosthetic wrist which implements flexion-extension needs to have an amplitude able to restore the complete movements of the human articulation.

Tesi di dottorato in Bioingegneria industriale, di Roberto Barone,
discussa presso l'Università Campus Bio-Medico di Roma in data 04/03/2017.
La disseminazione e la riproduzione di questo documento sono consentite per scopi di didattica e ricerca,
a condizione che ne venga citata la fonte.

The amplitude of the flexion-extension of a human wrist is 170°. Maximum reachable angle from the neutral position of the hand in both flexion-extension is 85°.
Passive module has to consider two modalities: flexible and rigid. In the first case the prosthetic articulation has to be flexible in order to simulate the wrist when it is not contract. The prosthetic wrist is moved by the contralateral sound hand from the neutral position to flexion-extension positions and the module has to be able to return to neutral position. This modality allows to have an adaptive module which favors the interaction with the external environment. Rigid modality is necessary in order to fix the wrist in different positions and guarantee firm grasps. To implement this modality some ratchet positions need to be put; the determination of the ratchet position is the result of an accurate analysis of the commercial prostheses and between bibliographic studies on the wrist biomechanics.
Minimum number of angles blocked are 5, referring to prosthetic wrists produced by leader companies [89] [90].

Michelangelo hand-wrist system implements the AxonWrist: it is a wrist with two degrees of freedom, both passive. Recently an active wrist is available for the Michelangelo hand. The system allows 75° of flexion, with 4 ratchet positions and 45° of extension with 3 ratchet positions. Maximum angle allowed by "Flexion Wrist", produced by Touch bionics company, is 40° both in flexion and extension directions. Angles possible to fix are: $-40°$, $-20°$, 0°, $+20°$, $+40°$ [90]. To define the blocking angles, data from commercial products have been integrated with results from bibliographic studies that have as objective to measure the angles of the upper arm, in particular of the wrist, during different ADLs. In the study presented in [91], angles of shoulder, elbow and wrist of 20 subjects have been measured during 16 activities utilizing the Polhemus Fastrak capture motion system. Angles obtained are shown in Fig. 4.11. Analyzing the medium values for the wrist it can be seen that the maximum flexion angle is 75° while the maximum extension is 29°. In [92] authors have utilized an electrogoniometer to measure flexion-extension and adduction-abduction angles of the wrist during 31 activities. Results show that with only 40° in flexion-extension, it is possible to complete most of the 24 activities selected.
Evaluating bibliographic results and commercial devices, ratchet position selected for flexion are 75°, 45°, 15° and 45°, 30° 15° for extension. The neutral position (0°) has to be added.

Tesi di dottorato in Bioingegneria industriale, di Roberto Barone,
discussa presso l'Università Campus Bio-Medico di Roma in data 04/03/2017.
La disseminazione e la riproduzione di questo documento sono consentite per scopi di didattica e ricerca,
a condizione che ne venga citata la fonte.

Tasks	Shoulder (thoracohumeral) joint																			
	Elevation					Plane of elevation					ISBAR axial rotation					NSAR axial rotation				
	Mean	SD	5th	Median	95th	Mean	SD	5th	Median	95th	Mean	SD	5th	Median	95th	Mean	SD	5th	Median	95th
Touching the ipsilateral axilla	51	18	22	58	72	−27	24	−59	−28	8	53	40	2	52	95	31	36	−19	38	73
Touching the opposite axilla	42	13	26	40	58	109	12	91	109	124	−11	24	−43	−11	33	65	27	31	64	116
Touching the mouth	40	10	27	39	61	102	15	87	99	131	−49	24	−79	−52	−17	25	26	−9	19	55
Touching the ipsilateral ear	70	12	54	69	84	86	14	72	85	107	−67	21	−93	−72	−37	−40	32	−74	−44	0
Touching the opposite ear	64	11	52	61	78	120	10	109	118	138	−39	21	−72	−41	−12	9	31	−43	11	48
Touching the forehead	59	10	49	55	80	108	13	90	107	131	−57	26	−95	−59	−28	−7	29	−65	−7	28
Touching the perineum	41	8	30	40	53	−86	18	−120	−87	−58	135	17	113	135	151	66	15	43	65	89
Touching the back	52	12	31	50	67	−59	10	−76	−60	−45	150	29	111	157	191	110	24	77	110	144
Fastening a button at neck level	29	11	15	29	45	76	24	48	72	105	−28	26	−64	−28	2	34	22	5	28	69
Fastening a button at navel level	19	6	12	20	26	−13	35	−64	−13	44	66	31	10	69	100	50	25	16	45	100
Washing the face	44	10	30	40	60	111	19	91	108	143	−57	24	−99	−57	−25	17	23	−32	25	42
Putting on a necklace	106	19	82	106	129	65	17	42	69	87	−58	23	−97	−61	−24	−77	31	−132	−81	−30
Combing hair	110	14	93	107	130	60	16	28	61	79	−57	18	−81	−55	−32	−79	21	−110	−78	−46
Eating with a spoon	56	11	43	55	73	74	13	50	76	92	−49	20	−76	−50	−20	−12	25	−53	−13	29
Pouring water into a glass	64	20	39	66	90	46	10	34	44	62	−17	20	−46	−14	13	−1	25	−42	−1	26
Drinking with a glass	87	12	68	88	106	80	14	63	75	101	−62	17	−83	−66	−39	−60	22	−88	−64	−24

Tasks	Elbow joint										Wrist joint									
	Flexion					Forearm rotation					Flexion					Deviation				
	Mean	SD	5th	Median	95th	Mean	SD	5th	Median	95th	Mean	SD	5th	Median	95th	Mean	SD	5th	Median	95th
Touching the ipsilateral axilla	137	7	130	138	149	−1	24	−27	−6	43	76	12	58	73	94	33	17	9	35	56
Touching the opposite axilla	100	10	89	99	112	27	25	−8	27	69	32	19	8	33	69	18	9	7	15	31
Touching the mouth	130	5	122	128	138	35	27	−6	36	72	−2	14	−25	1	16	2	11	−11	0	18
Touching the ipsilateral ear	132	5	125	132	140	109	31	60	111	141	−25	13	−42	−24	−7	1	9	−10	0	15
Touching the opposite ear	116	8	106	117	130	7	34	−27	−3	77	0	17	−36	4	18	1	8	−15	3	11
Touching the forehead	124	7	117	122	136	60	29	22	62	110	−24	10	−37	−22	−10	−8	10	−24	−7	3
Touching the perineum	56	22	27	55	96	12	28	−30	9	54	−1	17	−22	1	20	−5	8	−14	−5	9
Touching the back	115	9	105	114	128	4	46	−49	2	58	45	29	2	53	79	20	14	−9	24	36
Fastening a button at neck level	134	7	127	133	145	56	28	20	59	92	18	8	8	17	31	5	9	−9	5	16
Fastening a button at navel level	69	19	35	72	94	89	23	51	89	122	17	10	5	13	35	4	8	−10	5	15
Washing the face	128	6	123	127	142	69	27	30	72	116	−29	11	−41	−29	−7	−7	10	−25	−5	7
Putting on a necklace	138	6	132	137	148	87	32	57	93	117	−5	13	−24	−2	12	−2	14	−22	−2	15
Combing hair	119	8	108	119	131	75	21	53	76	108	−3	12	−18	−3	15	9	11	−4	6	28
Eating with a spoon	123	8	114	122	136	1	29	−28	−6	55	−21	8	−30	−21	−11	11	10	−6	13	24
Pouring water into a glass	93	7	83	94	103	146	20	121	142	178	−10	12	−28	−10	10	3	8	−10	3	15
Drinking with a glass	115	5	108	114	124	110	20	80	110	146	−15	13	−29	−16	−1	−3	12	−22	−2	9

Figure 4.11: Joint angles of the upper arm at the end of the daily living activities showed on the left [91].

Functioning principle of the module and blocking mechanism

Passive module for the flexion-extension is made of an upper base with elliptical section, mobile and hinged at half height of the prosthesis to a fixed lower base. There are two identical compression springs equidistant from the center of rotation of the mechanism. Rotating the upper base around the two hinges, it happens the flexion-extension. Springs are essential in order to have a flexible mechanism which return to the starting position autonomously.
A piston is integrated in each spring and connected to the 2 bases thanks to hinges. Springs during the flexion-extension movement, rotate around the hinges and the presence of the pistons guarantees the solicitation of the elastic element only in the main axis.
In Figure 4.12 it is shown a preliminary CAD of the device. Module is symmetric and also its functioning: both in flexion and extension maximum angle reached is the same; what happens in a direction is the same for the other direction.

We could image to rotate the device in counterclockwise direction. Left spring is compressed, while the right spring is extended. The two springs need to be precompressed in order to avoid problems during the rotation for the right spring. The two springs, during the functioning of the module, rotate around the inner hinges and made an angle respect to the vertical. Elastic elements remain parallel between them.

Tesi di dottorato in Bioingegneria industriale, di Roberto Barone,
discussa presso l'Università Campus Bio-Medico di Roma in data 04/03/2017.
La disseminazione e la riproduzione di questo documento sono consentite per scopi di didattica e ricerca,
a condizione che ne venga citata la fonte.

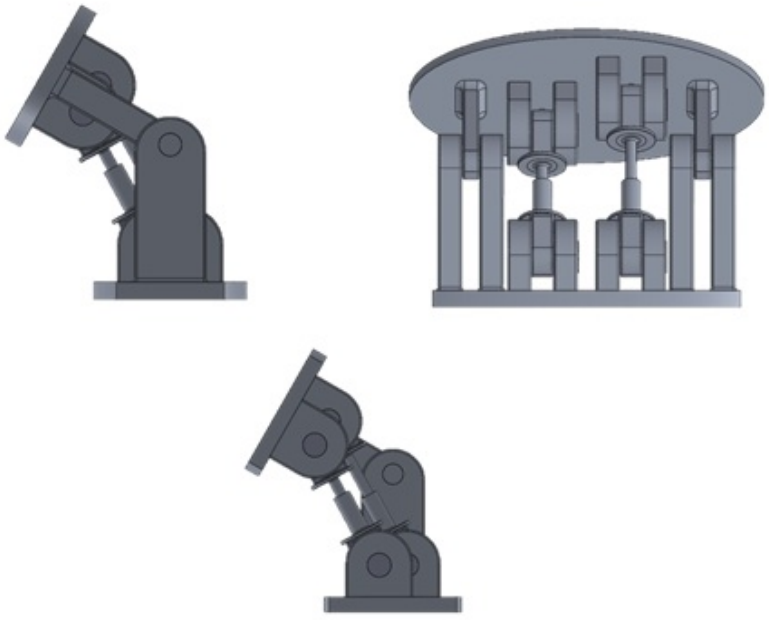

Figure 4.12: Preliminary CAD of the prosthetic wrist. On the left it is shown a lateral view, on the right a frontal view. Beneath it is shown a section view in which it is possible to see the variation of the pistons and consequently the variation of the springs.

Blocking mechanism needs to stop the rotation of the upper base and is made of 3 elements: a wheel, a little piston and a compression spring (Fig. 4.13). There are holes to be engaged in order to implement the ratchet positions.

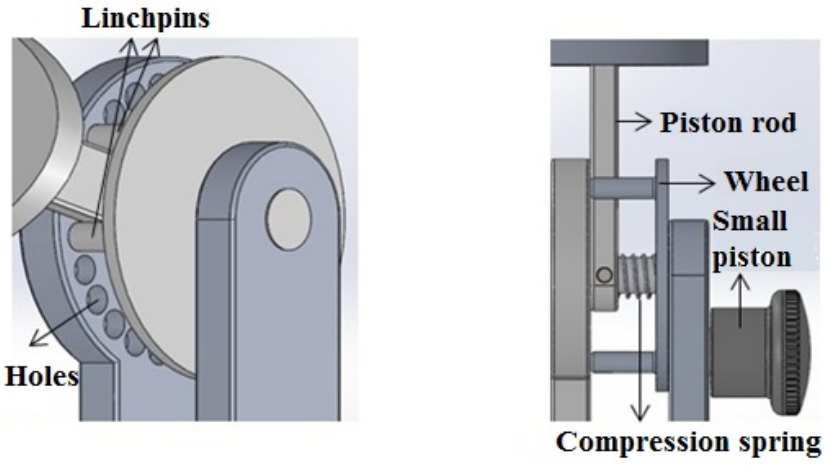

Figure 4.13: Blocking system.

Between the wheel and the piston rod of the upper base there is the spring; its function is to reactivate the flexible modality. Small piston has a pin which can be retracted or not thanks to an handle and allows to lock or unlock the

Tesi di dottorato in Bioingegneria industriale, di Roberto Barone,
discussa presso l'Università Campus Bio-Medico di Roma in data 04/03/2017.
La disseminazione e la riproduzione di questo documento sono consentite per scopi di didattica e ricerca,
a condizione che ne venga citata la fonte.

mechanism.

To explain the principle of functioning we can consider the module in the flexible modality: small piston has its pin retracted, the wheel is free to move together with the upper base and the spring is at its rest length. If we want to lock the wrist, we have to push the handle of the small piston so that the pin can exit and pins are translated towards the holes. The spring is compressed. To come back in flexible modality the user has to pull the handle of the small piston in order to retract the pin. The spring return to its initial length and linchpins exit the holes and the module is again flexible.

The dimensioning

The mechanism Kinematic analysis of the mechanism is useful to obtain the relationship between angles and segments, obtaining values for the free length and close-wound and the diameter of the springs necessary in the next phase of the design.

A kinematic study has been performed after the schematization of the entire mechanism as shown in Figure 4.14: the two springs are represented as extendable shaft hinged to two horizontal segments which represent the bases. Kinematic analysis has been done in the configuration of the wrist rotated

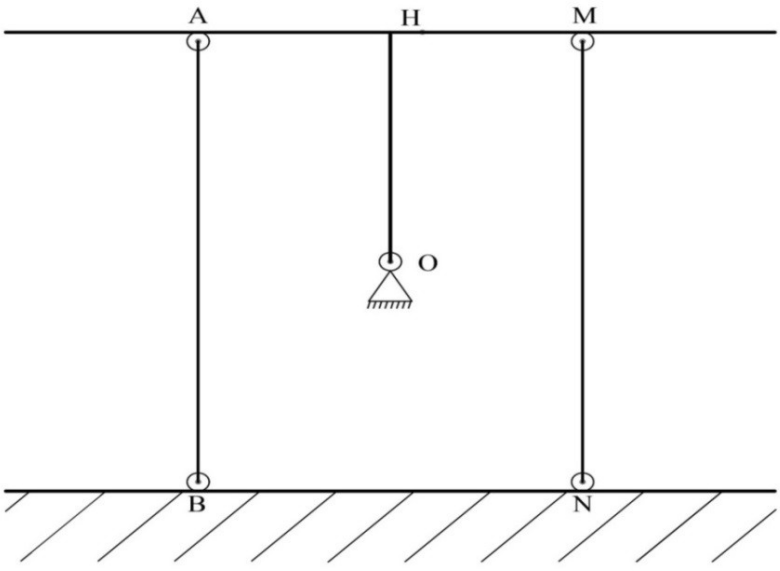

Figure 4.14: Schematization of the mechanism in neutral position.

counterclockwise of an angle α (Fig. 4.15 and Fig. 4.16). There are the same finding for a clockwise rotation because the module is symmetric.

To calculate the length of the segment $\overline{M'N}$ (Fig. 4.16) there is the following

Tesi di dottorato in Bioingegneria industriale, di Roberto Barone,
discussa presso l'Università Campus Bio-Medico di Roma in data 04/03/2017.
La disseminazione e la riproduzione di questo documento sono consentite per scopi di didattica e ricerca,
a condizione che ne venga citata la fonte.

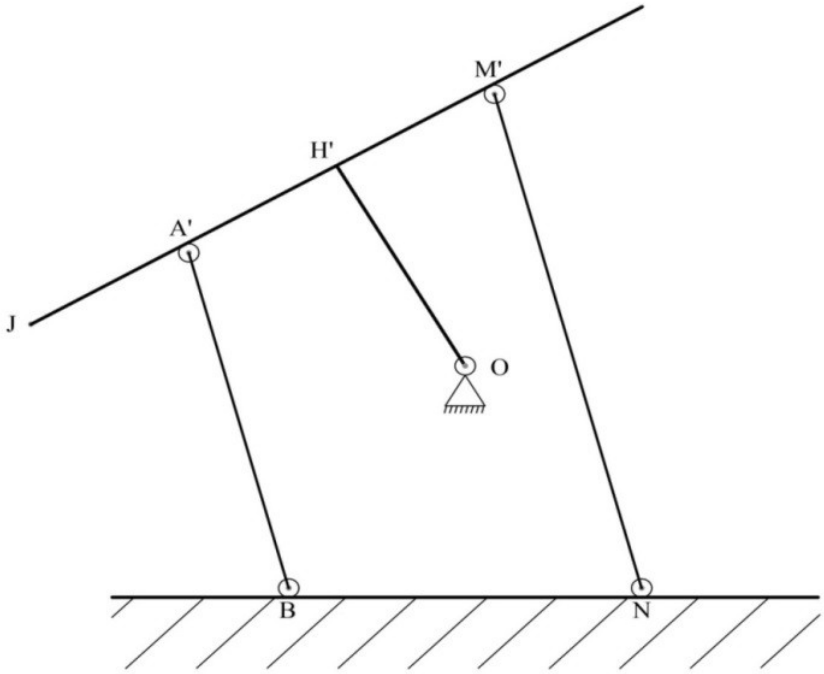

Figure 4.15: Schematization of the mechanism with the upper base counterclockwise rotated.

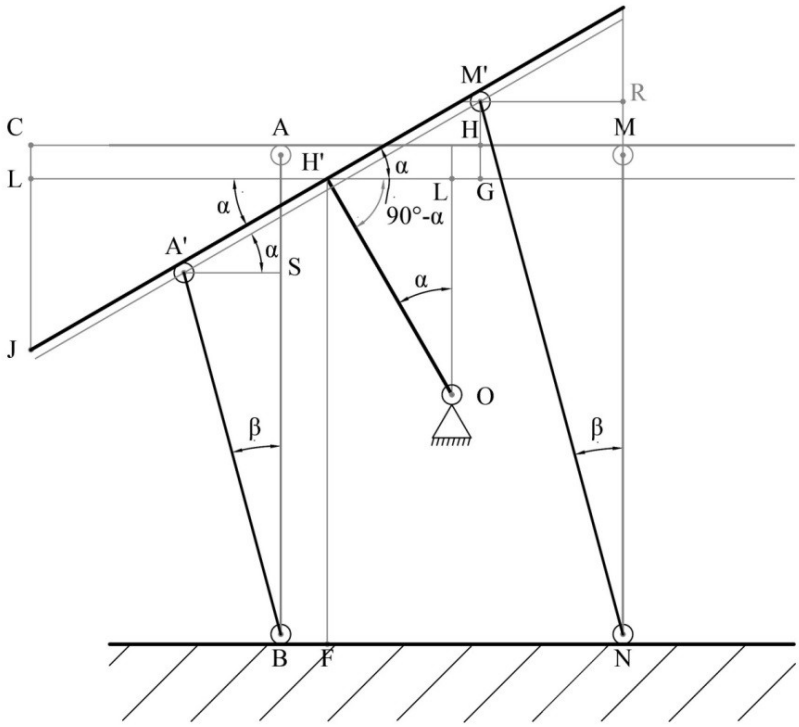

Figure 4.16: Schematization of the mechanism: the upper base is counterclockwise rotated of an angle α.

Tesi di dottorato in Bioingegneria industriale, di Roberto Barone,
discussa presso l'Università Campus Bio-Medico di Roma in data 04/03/2017.
La disseminazione e la riproduzione di questo documento sono consentite per scopi di didattica e ricerca,
a condizione che ne venga citata la fonte.

expression:

$$\overline{M'N} = \sqrt{\overline{M'R}^2 + \overline{NR}^2} \tag{4.2}$$

$$\overline{M'R} = \overline{OH}sin(\alpha) + \overline{AH} - \overline{AH}cos(\alpha) \tag{4.3}$$

$$\overline{NR} = \overline{AB} + (\overline{AH}sin(\alpha) - (\overline{OH} - \overline{OH}cos(\alpha))) \tag{4.4}$$

It is possible to calculate the rotation angle of the two shafts respect to the vertical:

$$\beta = tan^{-1}(\frac{\overline{M'R}}{\overline{NR}}) \tag{4.5}$$

The length of the segment $\overline{A'B}$ in Figure 4.16 is:

$$\overline{A'B} = \sqrt{\overline{BS}^2 + \overline{SA'}^2} \tag{4.6}$$

where $\overline{BS} = \overline{AB} - (\overline{AH}sin(\alpha) + (\overline{OH} - \overline{OH}cos(\alpha)))$ and $\overline{SA'} = \overline{BS}tan(\beta)$. The unknown design parameters are the distance $\overline{AH}$ between the point of attack of the spring and the center of rotation of the module and the height of the prosthetic wrist $\overline{AB}$. The kinematic equations are reported in Matlab. $\overline{AH}$ can vary between 1.5 and 20 mm. Minimum value for $\overline{AB}$ is 20 mm, the maximum is 27 mm. In Figure 4.17 are shown the graphs of $\overline{A'B}$ in function of angle α with $\overline{AB}$ constant and $\overline{AH}$ changing. The top subplot on the left is for $\overline{AB} = 20$ mm: graphs decrease if $\overline{AH}$ is included between 1.5 and 10.8 mm, for higher values there are increasing graphs over the minimum.
Minimum value of $\overline{AH}$ over which there are increasing graphs of $\overline{A'B}$ depends on the height of the module: if $\overline{BA}$ increases, it is possible to move the shafts away from the center of rotation without registering increasing trends. In Figure 4.18 are shown the trends of $\overline{A'B}$ in function of the angle α, varying $\overline{AB}$ and keeping constant $\overline{AH}$. The value of $\overline{AH}$ is different in each of the four subplots. Trends are decreasing when α varies. Increasing $\overline{AB}$ graphs are translated toward the top. Similarly, Figures 4.19 and 4.20 show the trends of $\overline{M'N}$ in function of the rotation angle α.

Tesi di dottorato in Bioingegneria industriale, di Roberto Barone,
discussa presso l'Università Campus Bio-Medico di Roma in data 04/03/2017.
La disseminazione e la riproduzione di questo documento sono consentite per scopi di didattica e ricerca,
a condizione che ne venga citata la fonte.

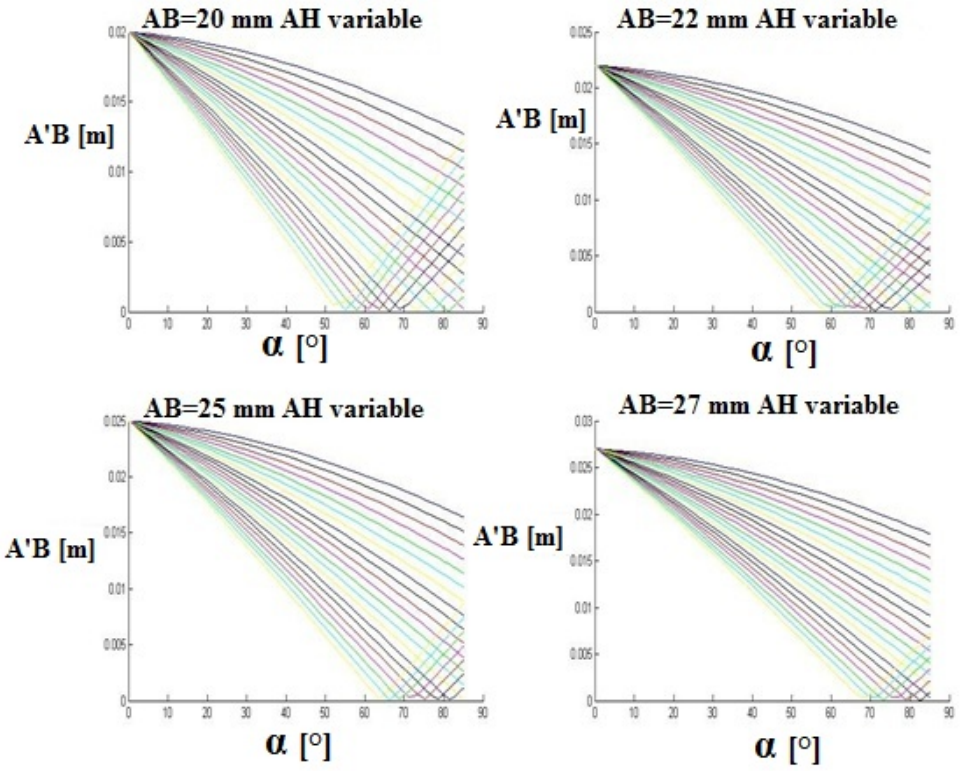

Figure 4.17: $\overline{A'B}$ trends in function of the rotation angle α. In every subplot $\overline{AH}$ is variable: upper graphic is for $\overline{AH} = 1.5$ mm, minimum value, while the lower graphic is for $\overline{AH} = 20$ mm, maximum value. In the four subplots $\overline{AB}$ is constant, but changes in the different images.

Tesi di dottorato in Bioingegneria industriale, di Roberto Barone,
discussa presso l'Università Campus Bio-Medico di Roma in data 04/03/2017.
La disseminazione e la riproduzione di questo documento sono consentite per scopi di didattica e ricerca,
a condizione che ne venga citata la fonte.

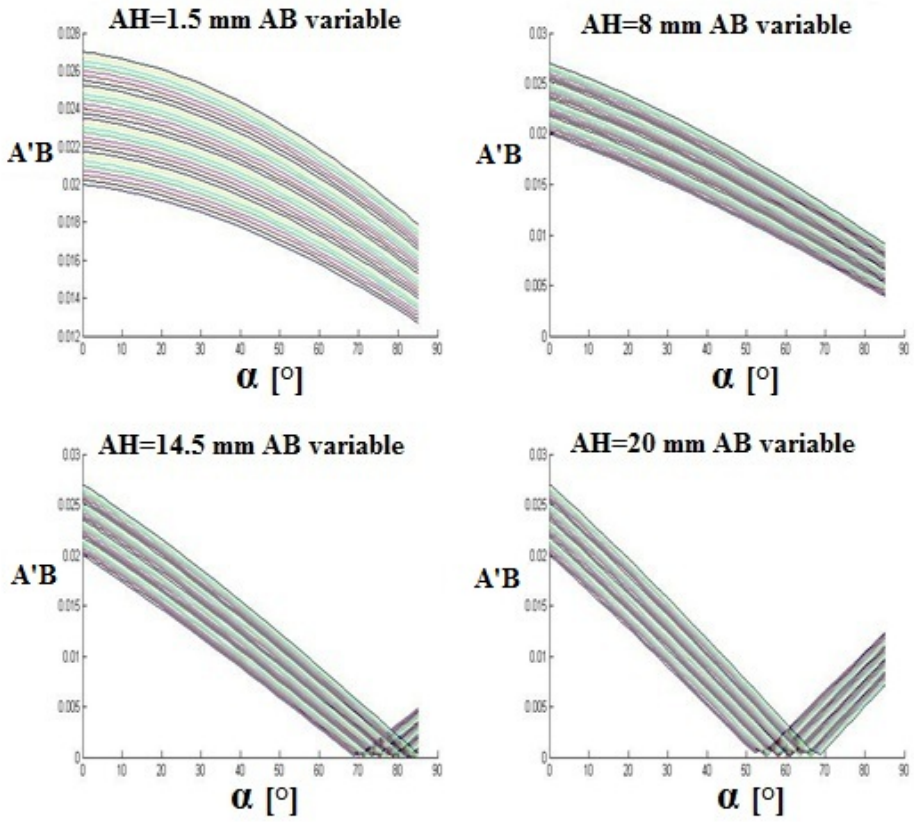

Figure 4.18: $\overline{A'B}$ trends in function of the rotation angle α. In every subplot the height of the module, $\overline{AB}$, is variable: lower graphic is for $\overline{AB} = 20$ mm, minimum value, while the upper graphic is for $\overline{AB} = 27$ mm, maximum value. In the four subplots $\overline{AH}$ is constant, but changes in the different images.

Tesi di dottorato in Bioingegneria industriale, di Roberto Barone,
discussa presso l'Università Campus Bio-Medico di Roma in data 04/03/2017.
La disseminazione e la riproduzione di questo documento sono consentite per scopi di didattica e ricerca,
a condizione che ne venga citata la fonte.

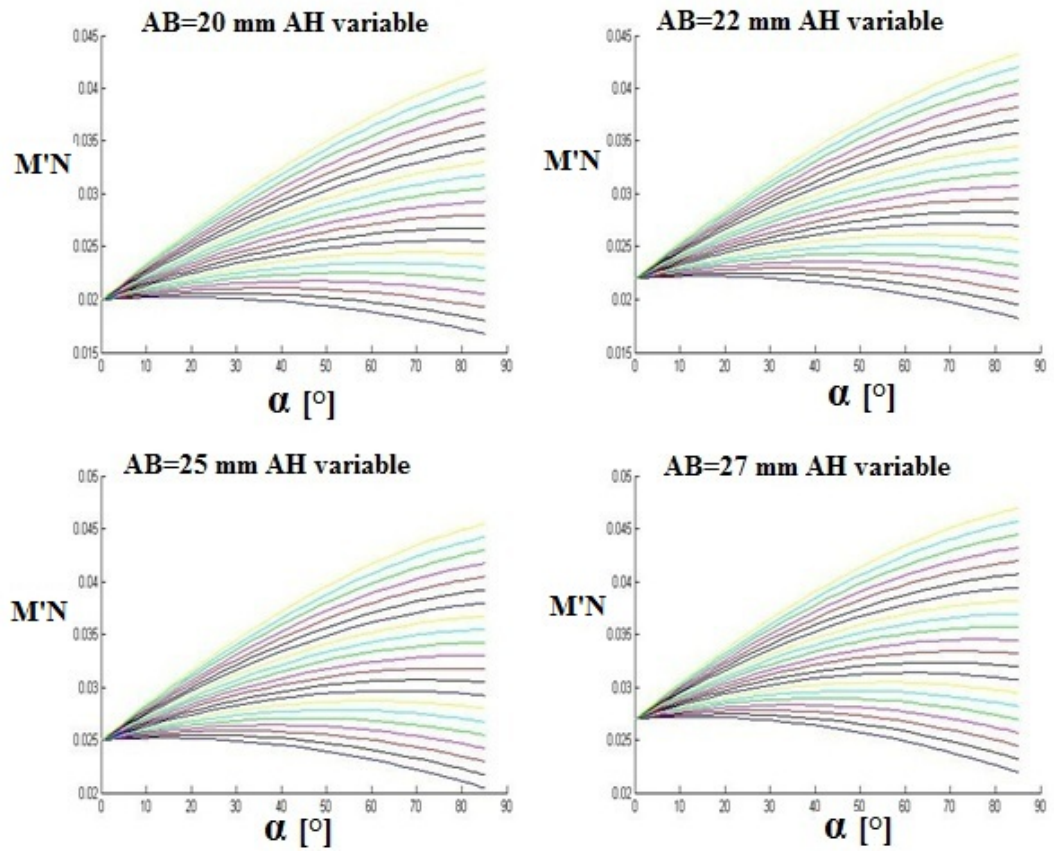

Figure 4.19: $\overline{M'N}$ trends in function of the rotation angle α. In every subplot $\overline{AH}$ is variable: lower graphic is for $\overline{AH} = 1.5$ mm, minimum value, while the upper graphic is for $\overline{AH} = 20$ mm, maximum value. In the four subplots $\overline{AB}$ is constant, but changes in the different images.

Tesi di dottorato in Bioingegneria industriale, di Roberto Barone,
discussa presso l'Università Campus Bio-Medico di Roma in data 04/03/2017.
La disseminazione e la riproduzione di questo documento sono consentite per scopi di didattica e ricerca,
a condizione che ne venga citata la fonte.

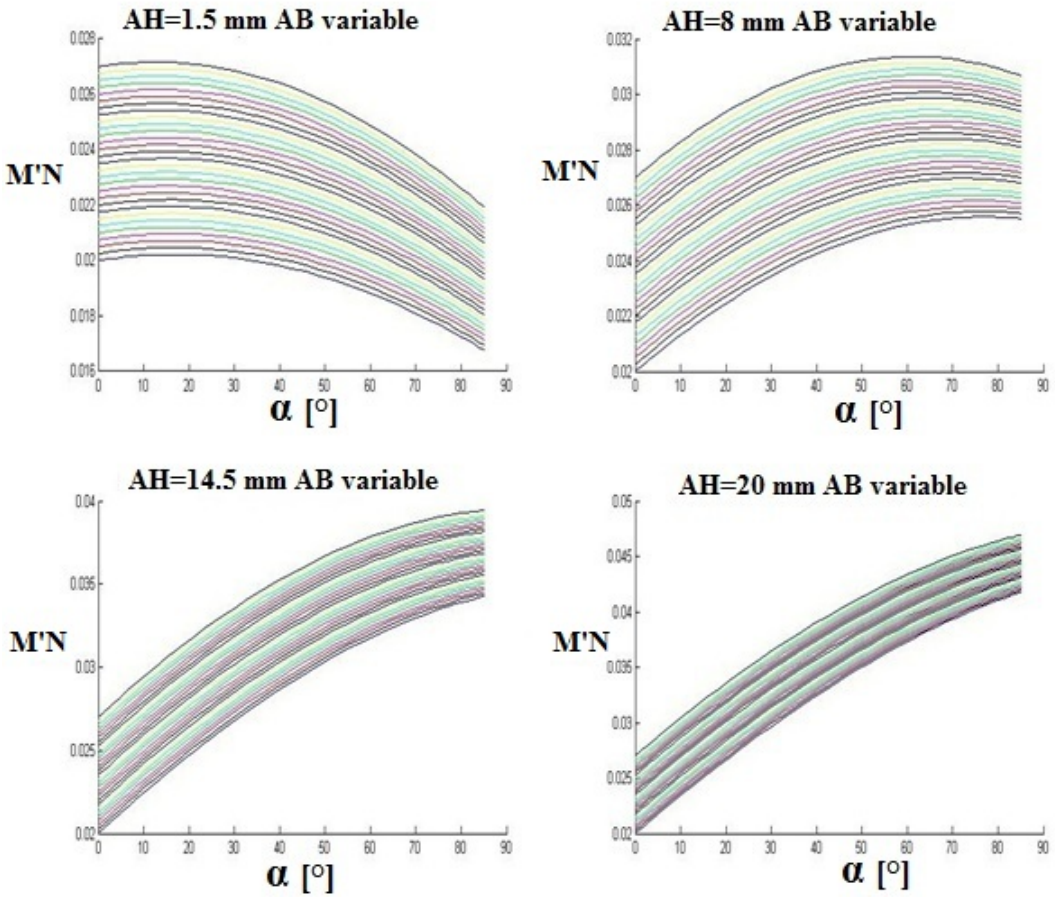

Figure 4.20: $\overline{M'N}$ trends in function of the rotation angle α. In every subplot $\overline{AB}$ is variable: lower graphic is for $\overline{AB} = 20$ mm, minimum value, while the upper graphic is for $\overline{AB} = 27$ mm, maximum value. In the four subplots $\overline{AH}$ is constant, but changes in the different images.

Tesi di dottorato in Bioingegneria industriale, di Roberto Barone,
discussa presso l'Università Campus Bio-Medico di Roma in data 04/03/2017.
La disseminazione e la riproduzione di questo documento sono consentite per scopi di didattica e ricerca,
a condizione che ne venga citata la fonte.

Design of the elastic elements Results of the kinematic analysis of the mechanism are the trends of the length of the extendable shafts in function of the rotation angle and varying the design parameters. In the bidimensional representation, elastic elements have been schematized like two shafts, so $\overline{A'B}$ and $\overline{M'N}$ (Figures 4.17-4.20) show the variation of the length of the springs. It was demonstrated that trends depend on the height of the module and the distance between springs and the center of rotation. To have a correct functioning of the module, in the design phase of the springs some requirements have to be respected: on the free length, on the diameter and on the stiffness coefficient. The definition of these requisites is the result of the study of the graphs obtained by the kinematic analysis and from the vision of a preliminary CAD.

First requisite During the flexion-extension of the module one spring is compressed and the other increase its length. In order to avoid to extend a compression spring, the free length of the spring should be greater or equal to the maximum length reached during movement, $l_{spring,max}$. Free length of the springs is greater than the height of the module, so the springs are precompressed in neutral position ($\alpha = 0$). During the flexion-extension one spring is compressed and the other increase its length returning to the free length.
Close-wound length of the springs should be less or equal to the minimum length reached by $\overline{A'H}$, $l_{spring,min}$ (Fig. 4.15).

Second requisite The external diameter of the springs is defined in relation to the distance between the connection point of the elastic elements and the center of rotation of the module:

$$r_{spring,ext} < \overline{AH} \tag{4.7}$$

To avoid the collision between the 2 springs, $2\overline{AH}$ should be greater than external diameter. During flexion-extension the two springs remain parallel so no collision is possible if the relation is verified.

Third requisite The stiffness of the springs, k, is calculated through the condition that the prosthetic wrist in neutral position ($\alpha = 0$), in the flexible modality and rotated of 90° could maintain the weight of a prosthetic hand (Figure 4.21 and Figure 4.22). The equilibrium of the momentum generated

Tesi di dottorato in Bioingegneria industriale, di Roberto Barone,
discussa presso l'Università Campus Bio-Medico di Roma in data 04/03/2017.
La disseminazione e la riproduzione di questo documento sono consentite per scopi di didattica e ricerca,
a condizione che ne venga citata la fonte.

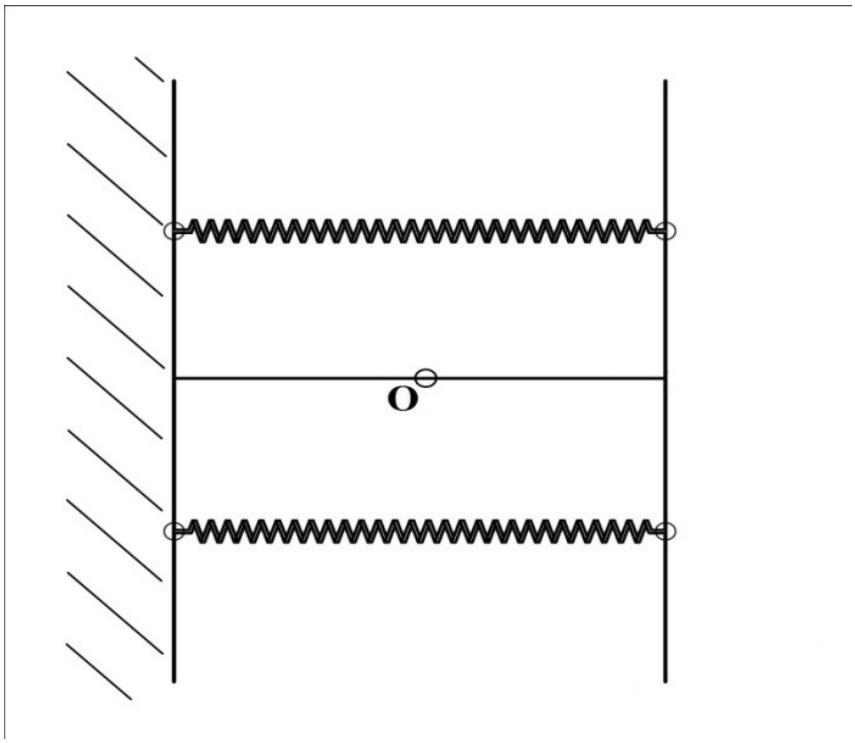

Figure 4.21: Schematization of the mechanism rotated of 90°.

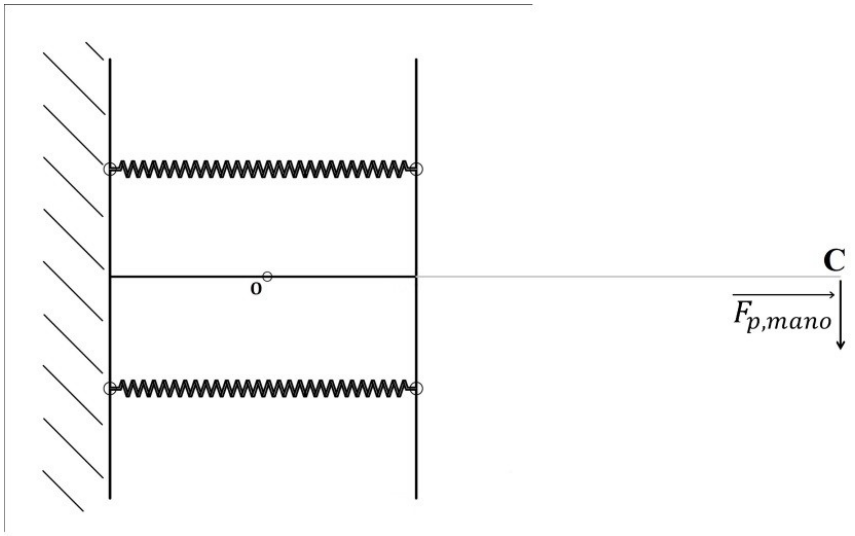

Figure 4.22: Schematization: C is the barycenter of the hand where is applied the force of the hand $\vec{F}_{p,hand}$.

Tesi di dottorato in Bioingegneria industriale, di Roberto Barone,
discussa presso l'Università Campus Bio-Medico di Roma in data 04/03/2017.
La disseminazione e la riproduzione di questo documento sono consentite per scopi di didattica e ricerca,
a condizione che ne venga citata la fonte.

by forces F_1 and F_{spring} acting on the upper base (Fig. 4.23) is:

$$-F_1\overline{OS} + k(l_{spring_{rest}} - \overline{BA})\overline{AH} = 0 \tag{4.8}$$

where $\overline{OS}$ is the arm of the momentum generated by the force F_1 and it is equal to the minor semiaxis of the elliptical section of the wrist and $l_{spring,rest}$ is the free length of the spring. Force F_1 is perpendicular to the upper base

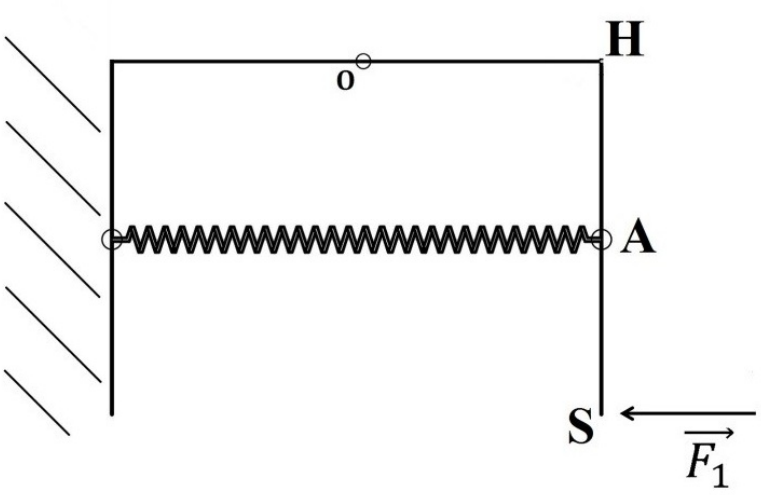

Figure 4.23: Schematization of half a module.

which value, multiplied by $\overline{OS}$, produces a momentum in "O" equal to the momentum produced by the F_p (Fig. 4.24):

$$F_1\overline{OS} = mg\overline{OC} \tag{4.9}$$

$$F_1 = \frac{mg\overline{OC}}{OS} \tag{4.10}$$

where $\overline{OC}$ is the distance between the center of rotation of the module and the center of gravity of the prosthetic hand. Stiffness is:

$$k = \frac{mg\overline{OC}}{(l_{free} - \overline{BA})\overline{AH}} \tag{4.11}$$

where m is the weight of the prosthetic hand and g the gravity acceleration. This equation is applied after determined the design parameters.

Tesi di dottorato in Bioingegneria industriale, di Roberto Barone,
discussa presso l'Università Campus Bio-Medico di Roma in data 04/03/2017.
La disseminazione e la riproduzione di questo documento sono consentite per scopi di didattica e ricerca,
a condizione che ne venga citata la fonte.

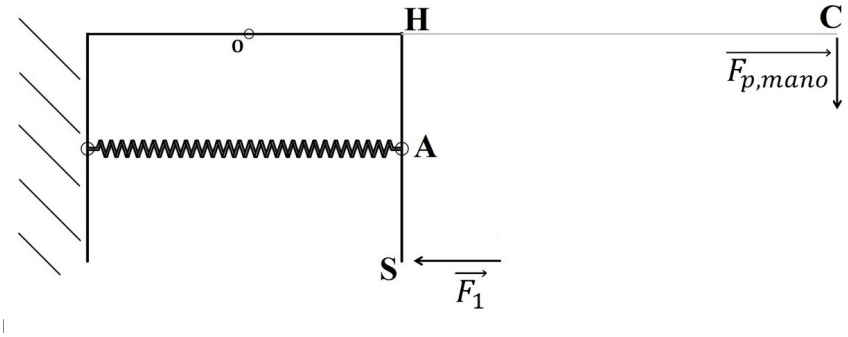

Figure 4.24: Schematization of half a module utilized to calculate the expression of the force $\vec{F}_1$.

The choice of the springs The choice of the commercial springs to utilize in the module has been done after restricted the spaces in which $\overline{AH}$ and $\overline{AB}$ can vary. The definition of these spaces required to consider the trends of the kinematic analysis. To restrict the spaces of values that can be attributed to $\overline{AH}$, $\overline{A'B}$ trends are analyzed. Minimum length is reached when the angle α is maximum. If the height increases, it increases also this minimum value and also when the springs are moved away from the center of rotation.
Minimum length determines a constraint for the close-wound length of the commercial spring. Values to exclude for $\overline{AH}$ are determined by the comparison between the minimum $\overline{A'B}$ with the close-wound lengths of commercial springs having free length greater than 20 mm. Values of $\overline{AH}$ greater than 10 mm are not considered because the kinematic model predicts a minimum length too little for $\alpha = 85°$. Are excluded also values included between 0.15 and 3 mm because there are no commercial springs with diameter lower than 3 mm that simultaneously respect the free and close-wound lengths conditions. The distance between the spring and the center of rotation should be a value between 4.5 and 9 mm.
To restrict the range of values to associate to the height of the module, $\overline{AB}$, $\overline{M'N}$ graphs are analyzed. These trends are not always increasing; for some combination of $\overline{AH}$ and $\overline{AB}$ the springs, after reached the maximum length, are compressed again. This behaviour should be avoided or limited. Maximum length reached by the spring determines the choice of the free length of the spring. Known minimum of $\overline{A'B}$, in relationship to the restricted range of $\overline{AH}$, and the maximum for $\overline{M'N}$, are obtained the approximate values for the free length. Looking at commercial catalogues, $\overline{BA}$ is chosen to vary between 25 and 27. Greater is the height of the module and greater should be both free length and close-wound length of the spring to choose.

Tesi di dottorato in Bioingegneria industriale, di Roberto Barone,
discussa presso l'Università Campus Bio-Medico di Roma in data 04/03/2017.
La disseminazione e la riproduzione di questo documento sono consentite per scopi di didattica e ricerca,
a condizione che ne venga citata la fonte.

By the comparison of the minimum values of $\overline{A'B}$ considered in the restricted spaces for the design parameters with the close-wound length of the commercial springs it results that is impossible to have elastic elements that produce 85° of rotation. Minimum length furnished by the model are smaller than the close-wound length of the commercial springs and this means that the springs reach the minimum length before the wrist can reach 85° of flexion-extension. Solution for this problem is restricting the range of motion of 10°. The commercial spring selected has the following characteristics: $l_{free} = 32mm$, $l_{close-wound} = 12.3mm$, $d_{ext} = 8.3mm$ and $k = 28.7N/mm$. Now the calculation of the stiffness required in theory will be done: to the equation of the stiffness, following values are substituted. $m = 640g$ is the weight of a commercial prosthesis, the IH2 hand; $\overline{AB} = 25mm$ and $\overline{AH} = 5mm$. $\overline{OC}$ is:

$$\overline{OC} = b_{hand} + h_{flange} + \frac{\overline{BA}}{2} \tag{4.12}$$

where b_{hand} is the center of gravity of the prosthetic hand (almost 30 mm). $\overline{OC} = 161.5mm$. k results to be 29.53, bigger than the stiffness of the selected spring but it is a good compromise respect to the other parameters.

The ball-bearings The ball-bearings are necessary to diminish the friction between two surfaces in rotation. They are inserted in the 6 hinges present in the mechanism: 2 link upper and lower base, the other 4 link the extremity of the pistons which are in the springs. The fork configuration has been chosen (Fig. 4.25). In Appendix A are reported the ball-bearings datasheets selected.

Mounting the ball-bearings The ball-bearings are inserted in suitable housings in the forks of the hinges. External rings are blocked with a seeger and with a shoulder. Housings have a slot where the elastic ring is inserted and after there is the housing for the ball-bearing: a hole with diameter and depth equal to the external diameter of the thickness of the ball-bearing (Fig. 4.26).

Elastic rings for holes The choice of the seegers has been done in function of the diameter of the hole. In the module are necessary two different elastic rings because there are two different type of ball-bearings. In the inner hinges are inserted seegers for a hole with diameter 17 mm (Appendix A-Seeger datasheet for hole of inner hinges), for outer hinges are chosen elastic rings for

Tesi di dottorato in Bioingegneria industriale, di Roberto Barone,
discussa presso l'Università Campus Bio-Medico di Roma in data 04/03/2017.
La disseminazione e la riproduzione di questo documento sono consentite per scopi di didattica e ricerca,
a condizione che ne venga citata la fonte.

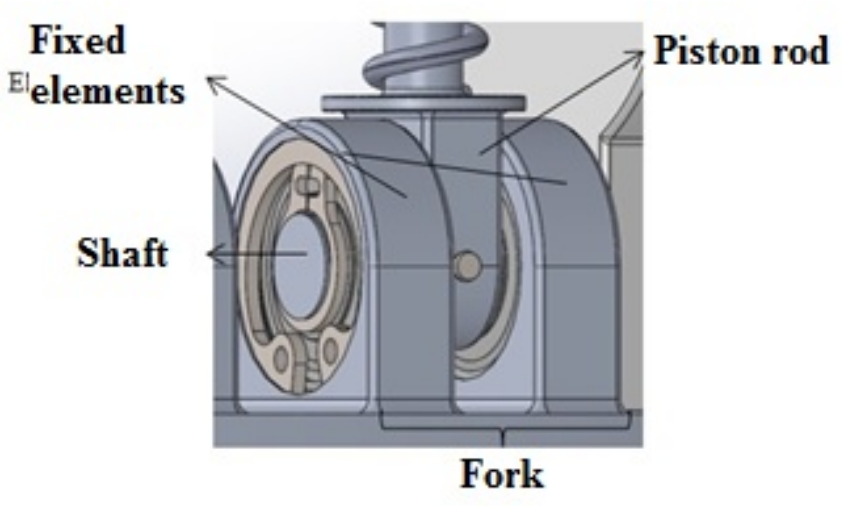

Figure 4.25: Particular of a fork hinge.

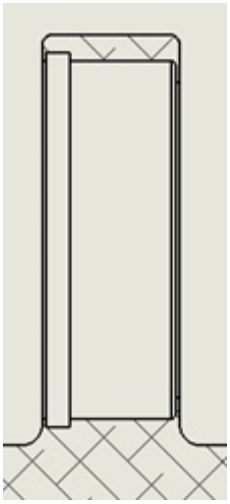

Figure 4.26: Section of a fix element of an hinge.

Tesi di dottorato in Bioingegneria industriale, di Roberto Barone,
discussa presso l'Università Campus Bio-Medico di Roma in data 04/03/2017.
La disseminazione e la riproduzione di questo documento sono consentite per scopi di didattica e ricerca,
a condizione che ne venga citata la fonte.

a hole of 15 mm (Appendix A-Seeger datasheet for hole of outer hinges).

Parts of the module For the design of the single parts which constitute the module are identified loads that mainly stress the pieces during flexion-extension. Single parts are represented utilizing the 3D CAD design software Solidworks. CAD of the part presents the variables to design which varies in spaces different for each case. Thanks to the software, forces acting on the parts are modeled, constraints are imposed and an iterated static analysis of the design study for each combination of values has been performed. Solidworks calculates Von Mises stress and defines a security factor reached in every point of the structure. Optimal dimensions are the ones that minimize the weight and that allow a minimum safety factor. In this way, a first design of the single parts necessary to realize a preliminary assembly of the module has been done. Final dimensions and materials are established in function of the Von Mises stresses resulting by the application of the momentum acting on the assembly of the prototype rotated of 75°.
Material chosen for the first prototype presented in this thesis is a metal. At the beginning parts are designed with an aluminum alloy with density 3 times lower than steel. If parts result to be too big or too much stresses are present a new design is done with steel. Aluminum alloy 6063 T6 with a yield strength of 215 MPa has been chosen. The second material is steel AISI 431, with a yield strength of 650 MPa.

Upper and lower bases These two elements are linked thanks to two hinges and the rotation of the upper base respect to the lower determines the movement of flexion-extension of the module. On the bases are collocated the forks of the inner hinges to design.

Width and thickness of the inner hinges In this part the thickness ($s_{hinges,inn}$) and the width ($l_{hinges,inn}$) of the forks of the hinges which connect the two bases with the extremity of the piston in the springs are designed (Fig. 4.27). The design is done for the lower base, but the same results are produced for the upper base because the loads are the same. Before starting the design it must be defined the distance between the center of rotation of the module where to put the two springs and so the center of the hinges. Springs must be aligned to the minor axis of the ellipse and must be at a distance of 5 mm from the center in order to avoid the close-wound of the elastic elements. External radius of the ball-bearings chosen is 8.5 mm, greater than 5 mm that is the

Tesi di dottorato in Bioingegneria industriale, di Roberto Barone,
discussa presso l'Università Campus Bio-Medico di Roma in data 04/03/2017.
La disseminazione e la riproduzione di questo documento sono consentite per scopi di didattica e ricerca,
a condizione che ne venga citata la fonte.

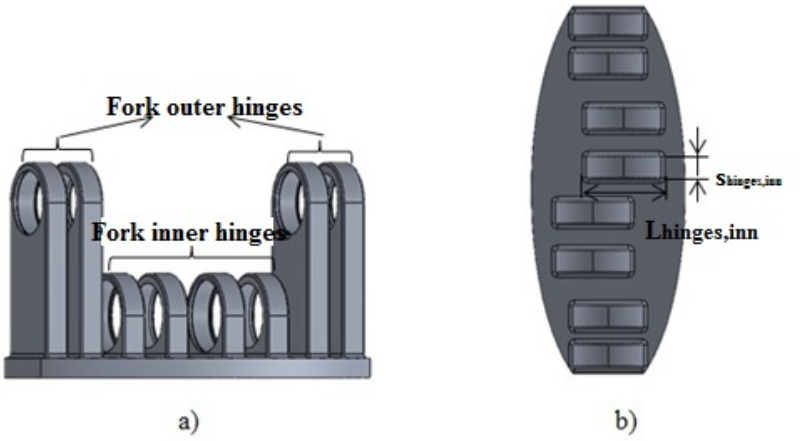

Figure 4.27: a) View of the lower base. b) View from the top of the lower base where there are highlighted the dimensions to design.

distance that permits to align the hinges. Forks are consequently misaligned (Fig. 4.28) The distance from the center, on the major axis of the ellipse, is the

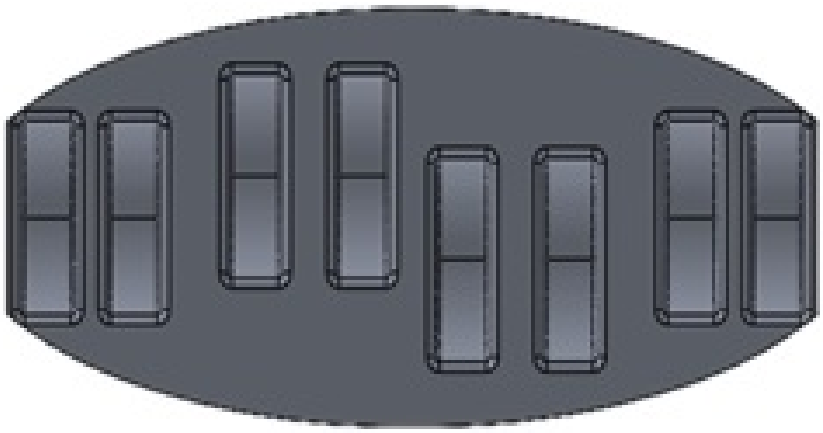

Figure 4.28: View from the bottom of the upper base.

same for the 2 forks, and is defined in function of the width of the ball-bearing because minimum spaces for their insertion has to be guaranteed. The distance from the center on the minor axis is the result of a good compromise between the minimum length reached by the elastic elements and the optimization of the trend of the non-compressed spring: to have a good functioning, it must be minimized the diminishing of the spring.
From the kinematic model it is possible to see that increasing $\overline{AH}$ the decreasing trend of $\overline{M'N}$ is less, but diminishes the length reached by the elastic elements. The height of the module is set to 28.5 mm. Utilizing Solidworks it is realized a preliminary CAD of the assembly of the module. The result

Tesi di dottorato in Bioingegneria industriale, di Roberto Barone,
discussa presso l'Università Campus Bio-Medico di Roma in data 04/03/2017.
La disseminazione e la riproduzione di questo documento sono consentite per scopi di didattica e ricerca,
a condizione che ne venga citata la fonte.

of the compromise is the choice to put the center of the hinges on the minor axis at 4 mm of distance from the center, registering a minimum length of the spring of 12.87 mm.
The CAD of the lower base is created, leaving parametric the dimensions to design. A static analysis is performed, constraining the lower surface and applying a load for the presence of the ball-bearings in the holes of the forks with module 283 N: half of the maximum force exerted from the spring on the hinge ($\frac{F_{el,max}}{2} = \frac{k(l_{free}-l_{block})}{2}$), supposing an equal distribution of the force between the fixed elements of a hinge (Fig. 4.29).

For the design optimization, study spaces where to vary variables to design

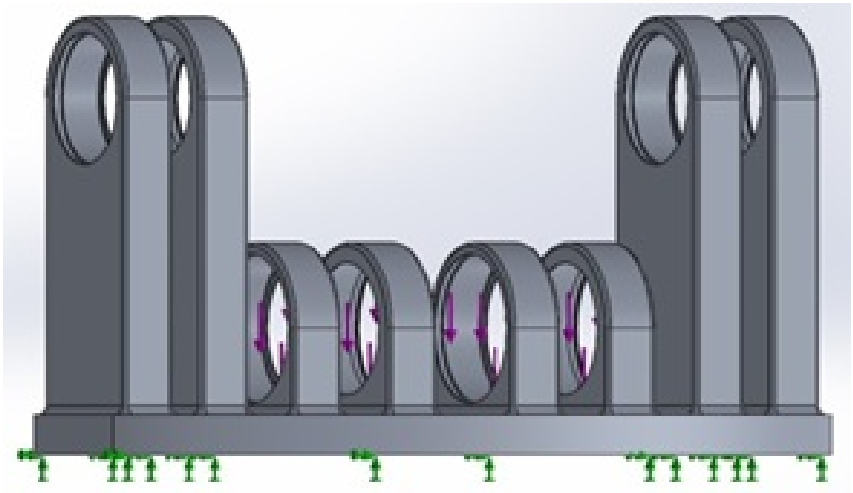

Figure 4.29: Static analysis of the part. Load are represented by violet arrows, the green ones represent the constraint.

are defined. Thickness can vary between 6.5 mm and 8 mm: minimum value is given by the sum of the ball-bearing, seeger and shoulder spaces:

$$s_{min} = s_{ball-bearing} + s_{seeger} + s_{shoulder} \tag{4.13}$$

where $s_{ball-bearing}$ is equal to 5 (Appendix A - datasheet ball-bearing 619/7-2Z), s_{seeger} is 1.3 mm and $s_{shoulder}$ is 0.2 mm. The upper extremity is defined thanks to the maximum obstruction possible.
Width can vary between 19.5 mm and 23 mm. This last value is given by the maximum obstruction possible. Minimum value is given by the Inglis formula, which quantifies the stress intensification when a cut is present. There are circular cuts because of holes for the ball-bearing and the seeger. Inglis formula for circular cut is:

$$\sigma_{max} = 3\sigma_n \tag{4.14}$$

Tesi di dottorato in Bioingegneria industriale, di Roberto Barone,
discussa presso l'Università Campus Bio-Medico di Roma in data 04/03/2017.
La disseminazione e la riproduzione di questo documento sono consentite per scopi di didattica e ricerca,
a condizione che ne venga citata la fonte.

with σ_n the nominal stress that in this case is:

$$\sigma_n = \frac{\frac{F_{el,max}}{2}}{s_{ball-bearing}(d_{hole} - L_{hinges,inn})} \tag{4.15}$$

where d_{hole} is the diameter of the greater cut (seeger) equal to 17.8 mm, while $L_{hinges,inn}$ is the width unknown of the fork. To calculate the minimum value of $L_{hinges,inn}$ the condition that the maximum stress must be lower than the ratio between the yield strength of the material and the safety factor, SF, equal to 2:

$$\sigma_{max} < \frac{\sigma_n}{SF} \tag{4.16}$$

$$L_{hinges,inn} > \frac{3F_{el,max}SF}{s_{ball-bearing}\sigma_y} + d_{hole} \tag{4.17}$$

The material used for this first design is aluminum, so $\sigma_y = 215MPa$.
The design study is imposed defining as a constraint a safety factor of minimum 2 and as objective the minimization of the weight. Values found are: $L_{hinges,inn} = 19.5mm$ and $s_{hinges,inn} = 6.5mm$.
In Figure 4.30 Von Mises stresses are reported and result to be less than the yield strength of the aluminum alloy selected. Minimum safety factor is 24 (Fig. 4.31). The height of the inner hinges, $h_{hinges,inn}$, is equal to the optimal

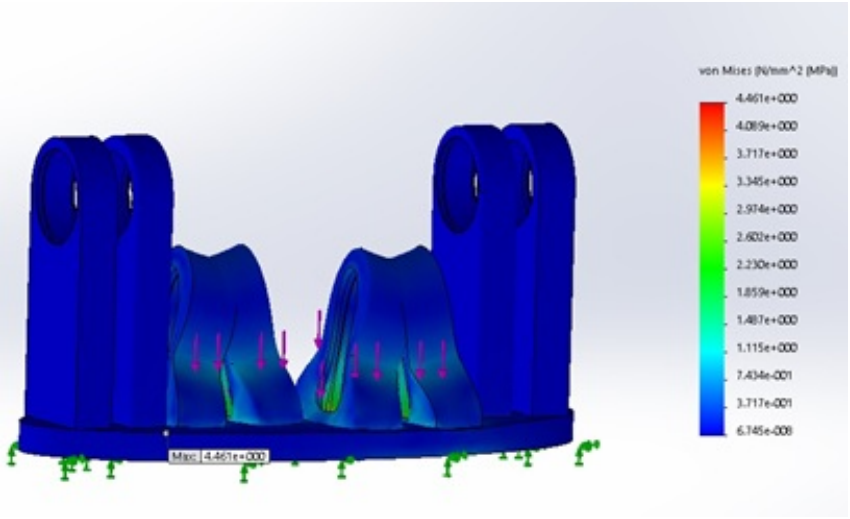

Figure 4.30: In the structure are reported Von Mises stresses: maximum value is 4.461 MPa and it is lower than the yield strength of the aluminum 6063 T6. The deformation scale is 34930.8.

Tesi di dottorato in Bioingegneria industriale, di Roberto Barone,
discussa presso l'Università Campus Bio-Medico di Roma in data 04/03/2017.
La disseminazione e la riproduzione di questo documento sono consentite per scopi di didattica e ricerca,
a condizione che ne venga citata la fonte.

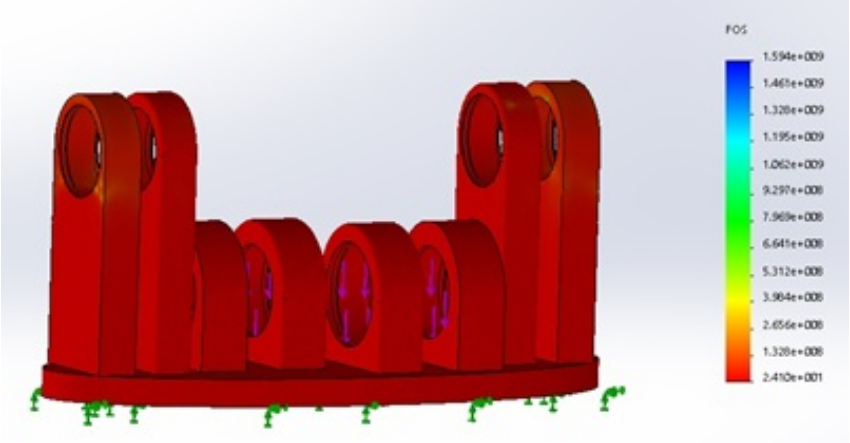

Figure 4.31: Graphic of the distribution of the safety factor.

value obtained for the width (Fig. 4.32)

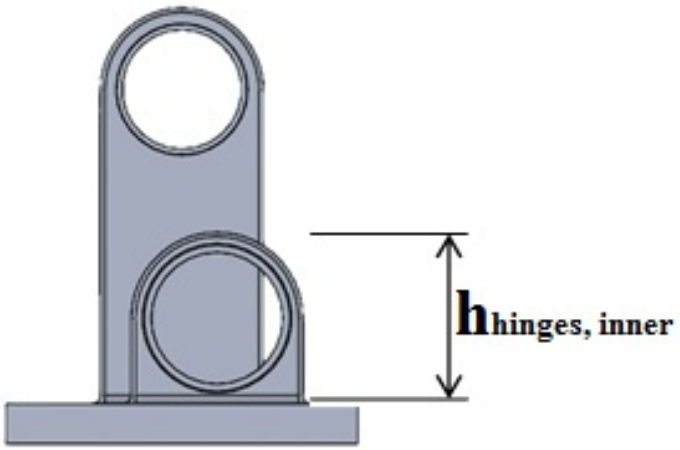

Figure 4.32: Section of the lower base.

Thickness of the upper and lower bases We start with the design of the upper base, $s_{base,upp}$. A static study is defined imposing two forces on an area of $4.15mm^2$ in the position corresponding of the two springs, and the cut on the piston rod are constrained (Fig. 4.33). The module of the two forces is equal to the maximum load registered when the module is rotated of 75°:

$$F_{el1} = k(l_{free} - l_{close-wound}) \tag{4.18}$$

$$F_{el2} = k(l_{free} - l_{75°}) \tag{4.19}$$

Tesi di dottorato in Bioingegneria industriale, di Roberto Barone,
discussa presso l'Università Campus Bio-Medico di Roma in data 04/03/2017.
La disseminazione e la riproduzione di questo documento sono consentite per scopi di didattica e ricerca,
a condizione che ne venga citata la fonte.

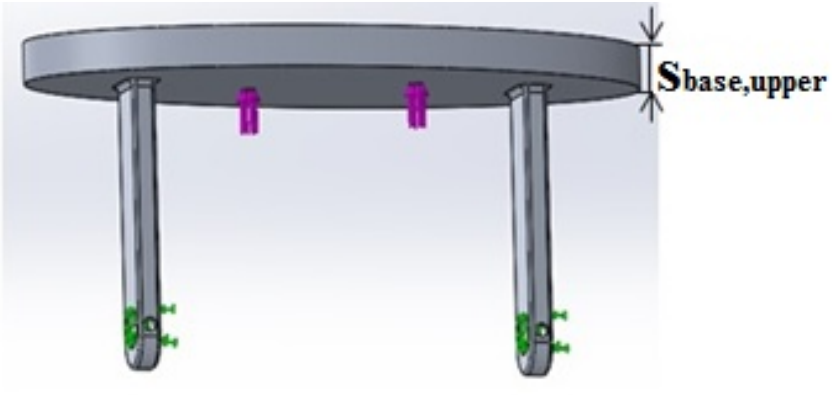

Figure 4.33: Loads and constraints for the static analysis needed to design the thickness of the upper base.

where $l_{75°}$ is the length of the non-compressed spring corresponding to a rotation of 75° of the module; this value is obtained by measures on a preliminary CAD of the assembly of the mechanism built thanks to the following steps.
Once defined the dimensions of the inner hinges of the bases and the length of the spring in the neutral position (28.5 mm), it is possible to calculate the height of the center of rotation dividing by two the distance between the two inner hinges (Fig. 4.34). Rotating the module of 75°, $l_{75°}$ results to be equal

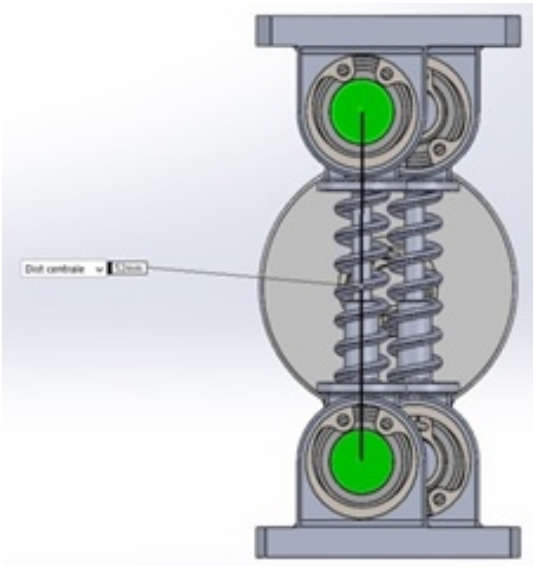

Figure 4.34: Section of the module. Length of the black line represents the distance between the centers of the hinges and it is 52 mm. Dividing by two this value we can obtain the height for the center of rotation.

to 22.6 mm.
For safety reasons $l_{75°} = 22mm$. Elastic force F_{el1} is 566 N and F_{el2} is 287

Tesi di dottorato in Bioingegneria industriale, di Roberto Barone,
discussa presso l'Università Campus Bio-Medico di Roma in data 04/03/2017.
La disseminazione e la riproduzione di questo documento sono consentite per scopi di didattica e ricerca,
a condizione che ne venga citata la fonte.

N. Material chosen is the aluminum alloy 6063 T6. The design study is set defining the thickness of the base a parametric variable which value can vary between 1 mm and 5 mm. The upper extremity is given by limits in weight and encumbrance. The optimal value for the upper base is 4.5 mm. Von Mises stresses are reported in Figure 4.35. The minimum safety factor is 1.65 (Fig. 4.36). This value is ok because in the real scenario the two elastic forces are distributed on a greater area and moreover is ignored the resistance of the material due to the presence of the hinges. The thickness of the lower base

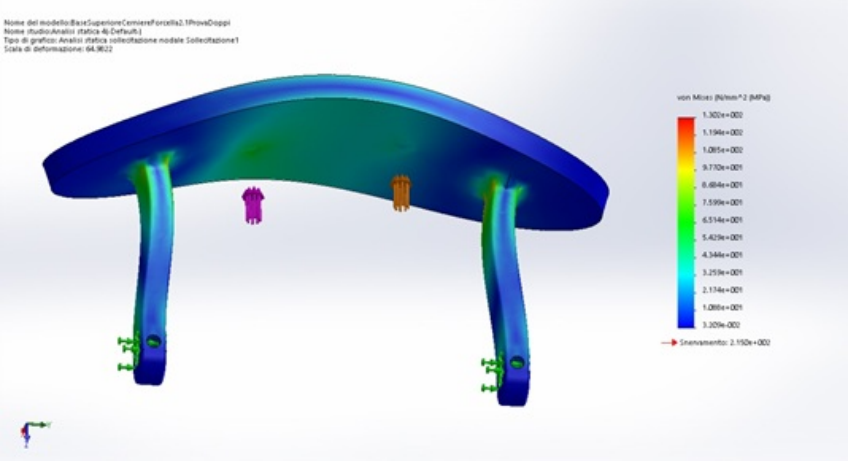

Figure 4.35: Von Mises stresses on the part with thickness 4.5 mm. Structure is represented with a deformation scale of 64.98.

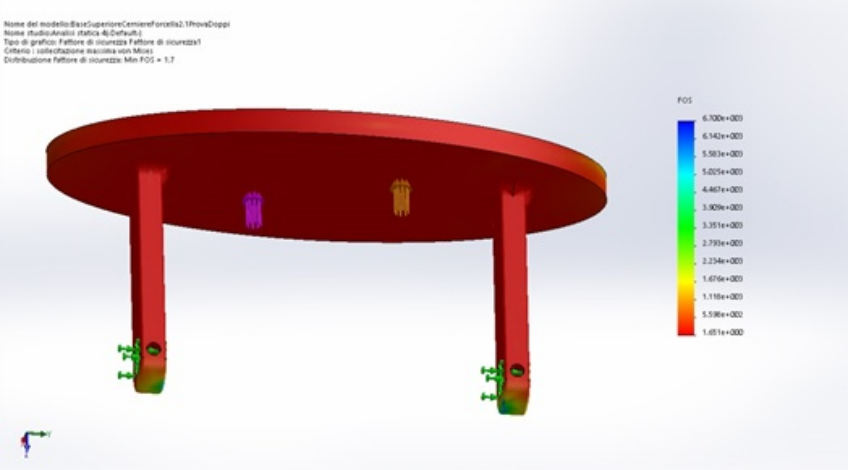

Figure 4.36: Distribution of the safety factor: minimum value is 1.65.

is calculated in the same way of the upper base. Graphs for a module with thickness 3 mm are reported in Figures 4.37-4.39.

Tesi di dottorato in Bioingegneria industriale, di Roberto Barone,
discussa presso l'Università Campus Bio-Medico di Roma in data 04/03/2017.
La disseminazione e la riproduzione di questo documento sono consentite per scopi di didattica e ricerca,
a condizione che ne venga citata la fonte.

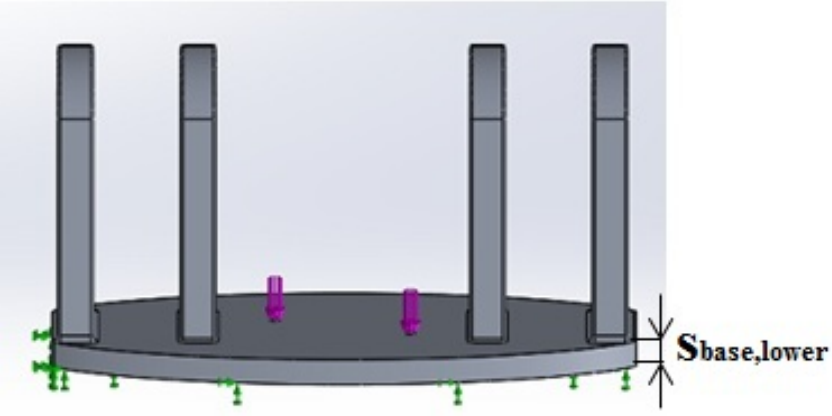

Figure 4.37: Loads and constraints for the static analysis needed to design the thickness of the lower base.

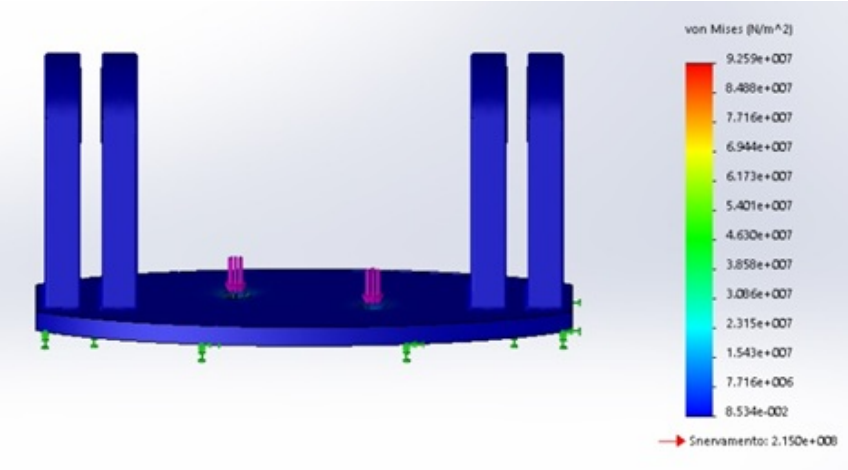

Figure 4.38: Von Mises stresses applied on the base with thickness 3 mm.

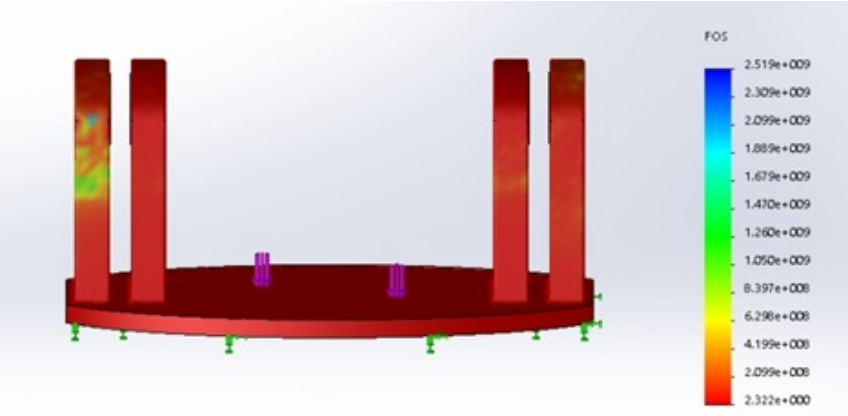

Figure 4.39: Distribution of the safety factor: minimum value is 2.32.

Tesi di dottorato in Bioingegneria industriale, di Roberto Barone,
discussa presso l'Università Campus Bio-Medico di Roma in data 04/03/2017.
La disseminazione e la riproduzione di questo documento sono consentite per scopi di didattica e ricerca,
a condizione che ne venga citata la fonte.

Forks of the outer hinges present on the lower base Width ($L_{hinges,out}$) and thickness ($s_{hinges,out}$) of the forks of the hinges that link the upper base with the lower base (Fig. 4.40). Forks are stressed with ball-bearing loads

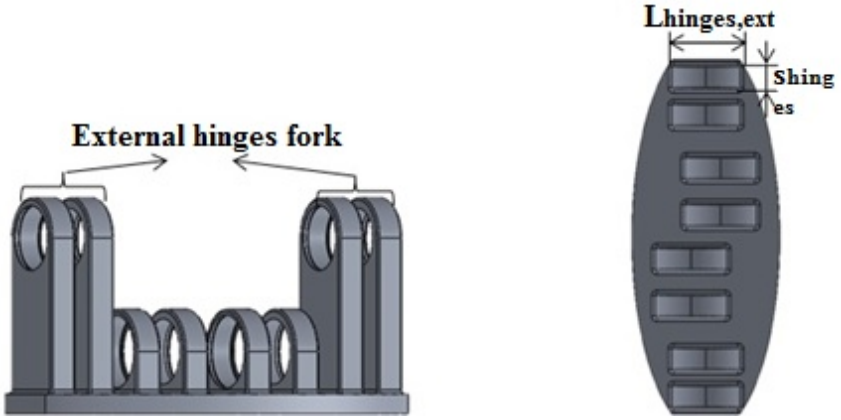

Figure 4.40: Lower base: in the left image are represented the forks design; in the right image it is represented a view from the top of the base and are indicated the variables to design.

with module 214 N.

Parametric variables are: thickness, which can vary between 6.5 and 8 mm, and width, which can vary between 17 and 20 mm. The same considerations of the inner hinges have been done.

Design study results are verified with a static analysis: maximum Von Mises stress is 89 MPa, less than 215 MPa that is the yield strength of the material (Fig. 4.42). Minimum safety factor is 2.43 (Fig. 4.43).

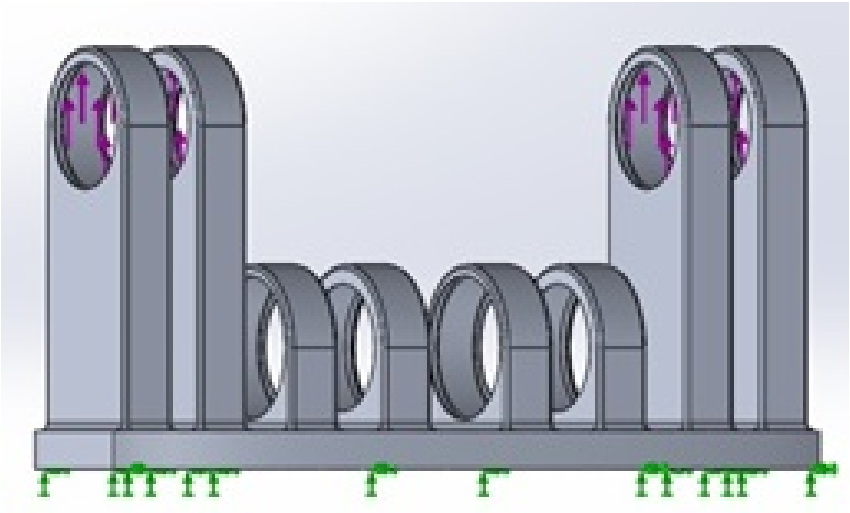

Figure 4.41: Loads and constraints imposed in the static analysis for the design of $L_{hinges,ext}$ and $s_{hinges,ext}$.

Tesi di dottorato in Bioingegneria industriale, di Roberto Barone,
discussa presso l'Università Campus Bio-Medico di Roma in data 04/03/2017.
La disseminazione e la riproduzione di questo documento sono consentite per scopi di didattica e ricerca,
a condizione che ne venga citata la fonte.

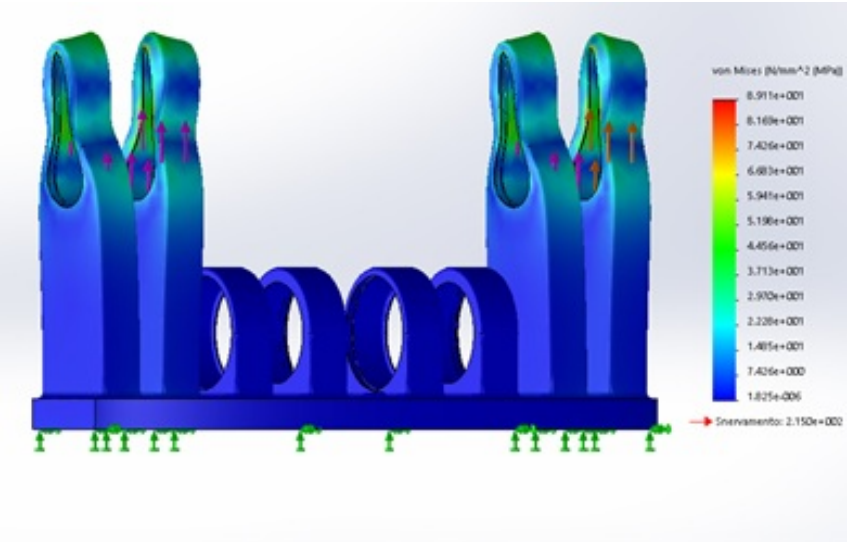

Figure 4.42: Von Mises stresses resulting from the static analysis on the part with 18.5 mm of width and 6.5 of thickness. The deformation scale is 540.56.

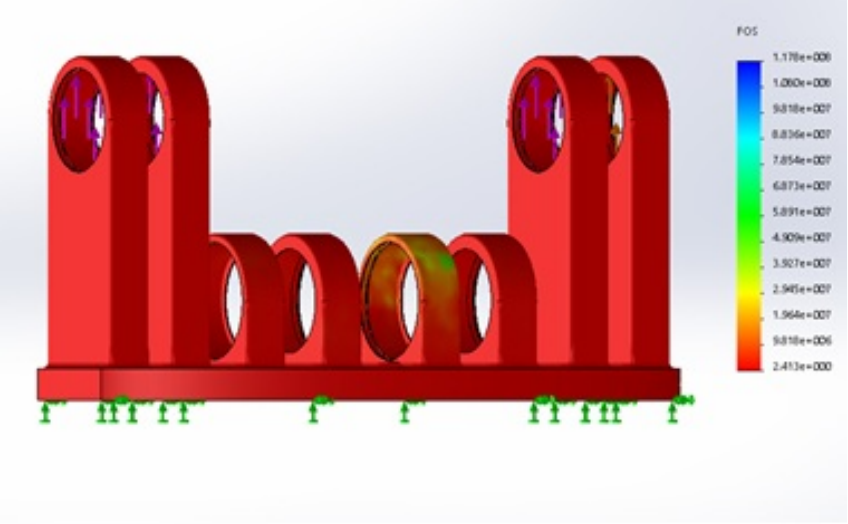

Figure 4.43: Graph of the distribution of the safety factor resulting from the design study that furnished the optimal value for the external forks width and thickness on the lower base.

Tesi di dottorato in Bioingegneria industriale, di Roberto Barone,
discussa presso l'Università Campus Bio-Medico di Roma in data 04/03/2017.
La disseminazione e la riproduzione di questo documento sono consentite per scopi di didattica e ricerca,
a condizione che ne venga citata la fonte.

Piston rods of the outer hinges on the upper base To complete the design of the upper base it must be defined the optimal values for the thickness and width of the two piston rods that connect the upper base with the lower base (Fig. 4.44). A static analysis is imposed as reported in Figure 4.45

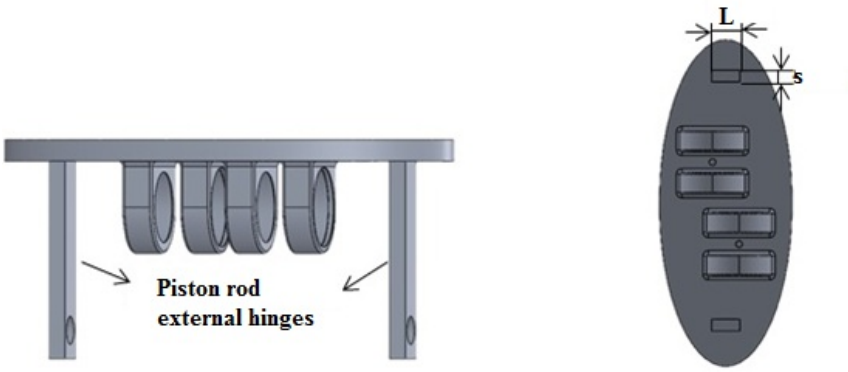

Figure 4.44: Upper base: in the left image are reported the piston rods of the external hinges; in the right image is represented the lower view of the base and the variables to design.

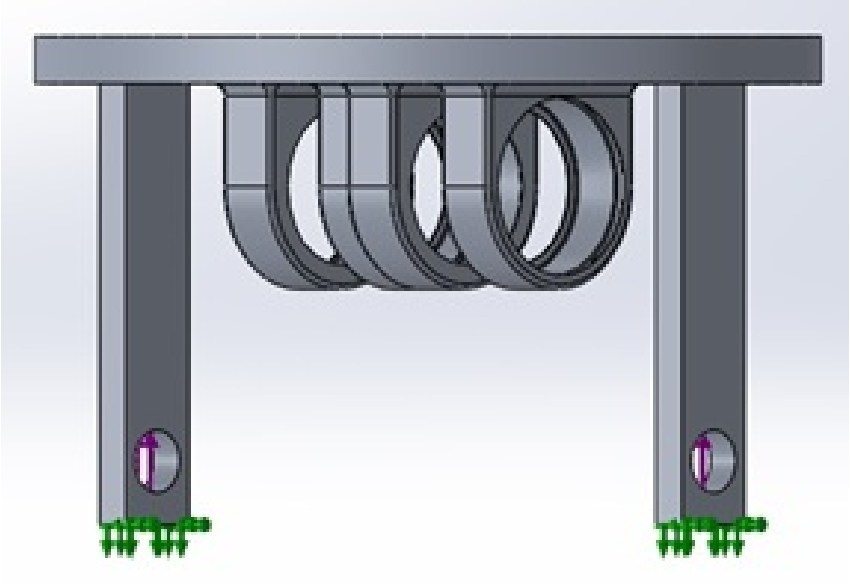

Figure 4.45: Loads and constraints set in the static analysis executed in the design study for the design of L_{hinge} and s_{hinge}.

applying on both the piston rods a distributed force of 430 N on a surface of 3.14 mm^2 in the hole. This force represents the force due to the two springs, its direction is the top and the module is the division by two of $F_{el,tot}$.
Variables to find are parametric: thickness can assume values between 3 mm and 5 mm while width between 8.4 and 14 mm. Minimum thickness is determined by the presence of a pin with diameter not less than 2 mm. Maximum

Tesi di dottorato in Bioingegneria industriale, di Roberto Barone,
discussa presso l'Università Campus Bio-Medico di Roma in data 04/03/2017.
La disseminazione e la riproduzione di questo documento sono consentite per scopi di didattica e ricerca,
a condizione che ne venga citata la fonte.

thickness is selected to minimize the encumbrance. To define the minimum width it has been applied the Inglis formula repeating passages executed for the design of the inner hinges.
Values that come from the design study are 3.5 mm for the thickness and 8.5 mm for the width. Von Mises stresses are reported in Figure 4.46; minimum safety factor is 1.92, as reported in Figure 4.47. It is less than 2 that is the constraint for the design study but it is acceptable.

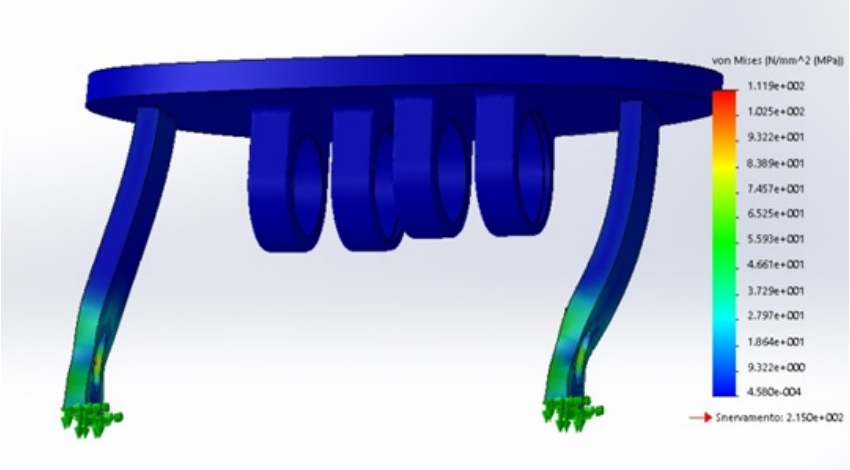

Figure 4.46: Von Mises stresses resulting from the static analysis on the upper base completely designed. Deformation scale is 493.7.

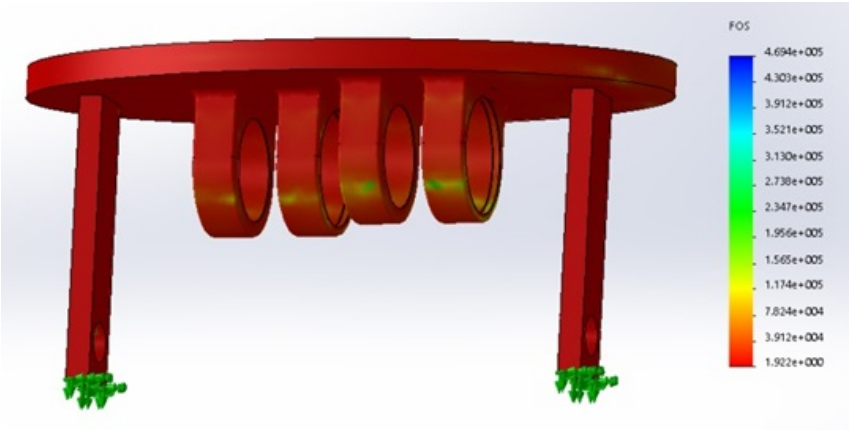

Figure 4.47: Graphic of the distribution of the safety factor resulting from the static analysis of the upper base totally designed.

Consideration for the assembly of the module With the aim of reducing the encumbrance, forks of the outer hinges are disposed at a distance of 1.10 mm from the inner hinges (Fig. 4.48). These spaces are not sufficient to mount ball-bearings and shafts in the hinges. The solution chosen is to make modular

Tesi di dottorato in Bioingegneria industriale, di Roberto Barone,
discussa presso l'Università Campus Bio-Medico di Roma in data 04/03/2017.
La disseminazione e la riproduzione di questo documento sono consentite per scopi di didattica e ricerca,
a condizione che ne venga citata la fonte.

one of the two fixed elements of the outer hinges and the two piston rods on the upper base (Fig. 4.49 and Fig. 4.50).

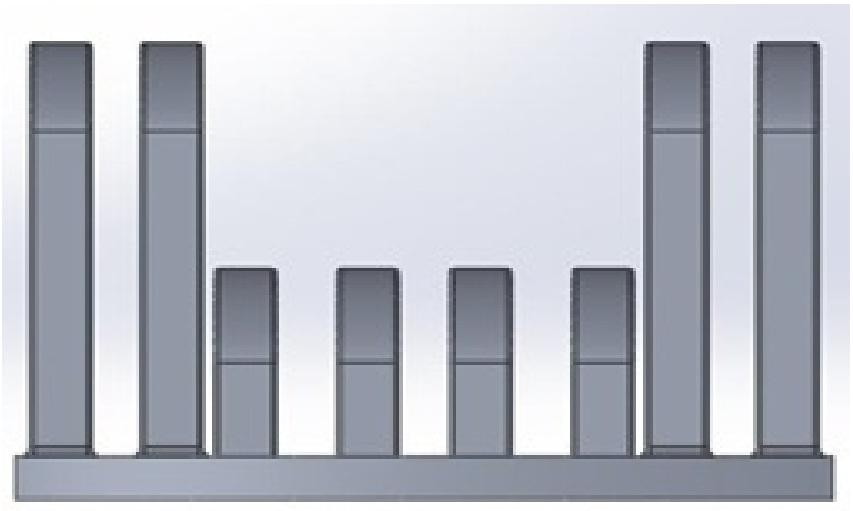

Figure 4.48: Lower base: in the image it is possible to see the position of the external forks.

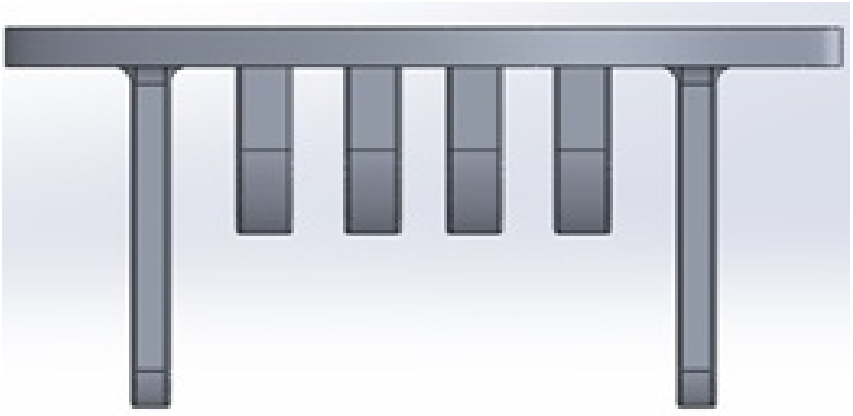

Figure 4.49: Upper base: in the image it is possible to see the position of the piston rods.

The piston in the springs The presence of a piston in the springs guarantees to stress the elastic elements only on its axis. The piston is constituted by two parts: the female and the male (Fig. 4.52).

Some dimensions are defined optimizing the weight, other are defined in function of the encumbrance of commercial elements like the axlebox and the spring.

To avoid the friction in the piston, in the extruded part of the female an axlebox in PTFE is put. Datasheet of the axlebox is in Appendix A.

Tesi di dottorato in Bioingegneria industriale, di Roberto Barone,
discussa presso l'Università Campus Bio-Medico di Roma in data 04/03/2017.
La disseminazione e la riproduzione di questo documento sono consentite per scopi di didattica e ricerca,
a condizione che ne venga citata la fonte.

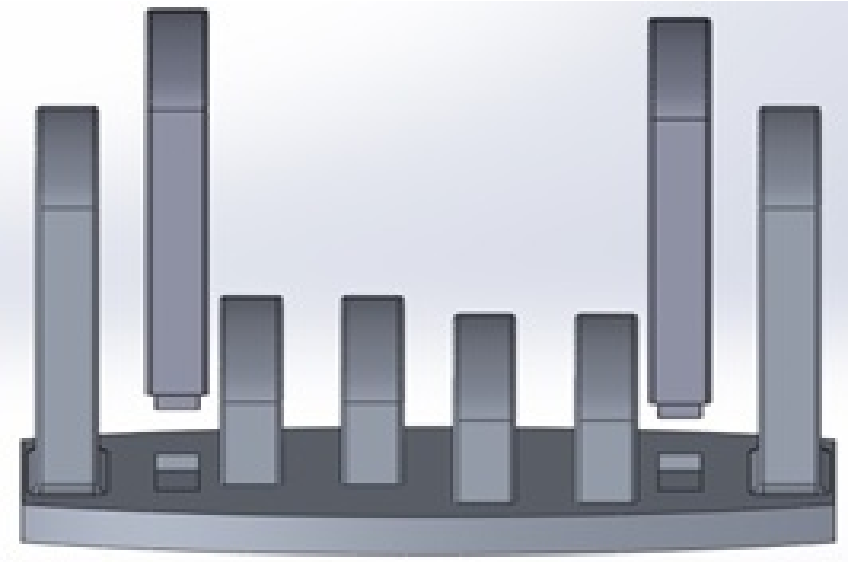

Figure 4.50: Lower base with the fixed elements of the hinges made modular.

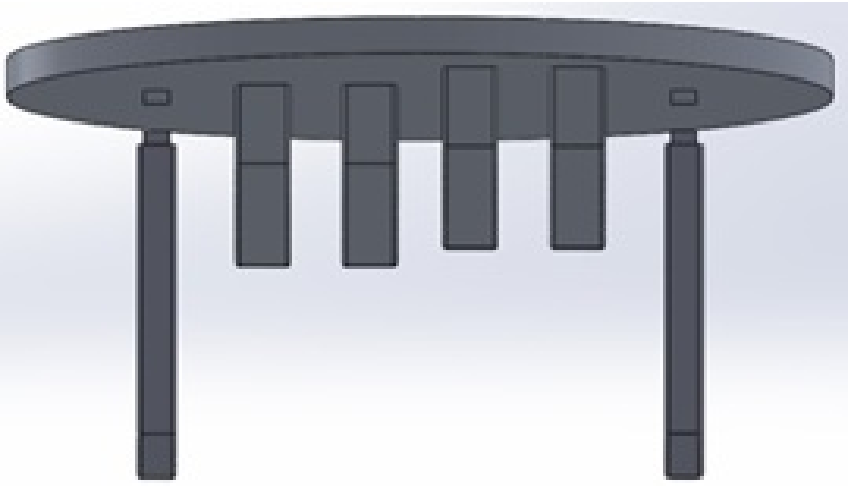

Figure 4.51: Upper base with the fixed elements of the hinges made modular.

Tesi di dottorato in Bioingegneria industriale, di Roberto Barone,
discussa presso l'Università Campus Bio-Medico di Roma in data 04/03/2017.
La disseminazione e la riproduzione di questo documento sono consentite per scopi di didattica e ricerca,
a condizione che ne venga citata la fonte.

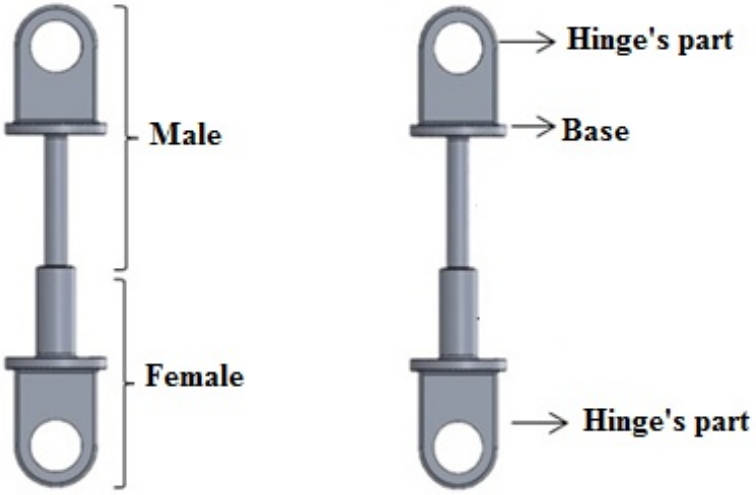

Figure 4.52: Piston inner to the springs.

The extruded part of the female is constituted by a cylinder with a hole and its external diameter is 5.2 mm, internal diameter is 4.50 mm and the height is 12 mm. This value is defined in relationship to the close-wound length of the spring. Piston has to support the decrease of the length of the spring so the minimum height, reached when the male is completely inserted in the female, must be equal to the close-wound length of the elastic element. Depth of the hole in the cylinder is 17.30. Maximum height reachable is 29.30 mm, equal to the sum of the height of the extruded part of the male and female. This value is less than the maximum height reached by the spring during the rotation of the module.
The part that has to be joined to the hinge has the same dimensions both for the female and for the male. The female part has been designed. To define the thickness, $s_{hinge,piston}$ and the width, $L_{hinge,piston}$, the piece is schematized as a parallelepiped with two holes: one of diameter 7 mm equal to the one of the shaft of the hinge, the other of 4.50 mm (Fig. 4.53). A static analysis is imposed, stressing the bigger hole with a ball-bearing load of 566 N, equal to the maximum elastic force. Part is constrained as illustrated in Figure 4.54.

Parametric variables are the thickness, the width and the height. In the design study the thickness varies between 5 mm and 7 mm: minimum value is because of the hole of 4.5 mm, the maximum is due to the maximum encumbrance possible. Width is between 9 mm and 11 mm: both the minimum and maximum values are obtained thanks to Inglis formula. The height of the

Tesi di dottorato in Bioingegneria industriale, di Roberto Barone,
discussa presso l'Università Campus Bio-Medico di Roma in data 04/03/2017.
La disseminazione e la riproduzione di questo documento sono consentite per scopi di didattica e ricerca,
a condizione che ne venga citata la fonte.

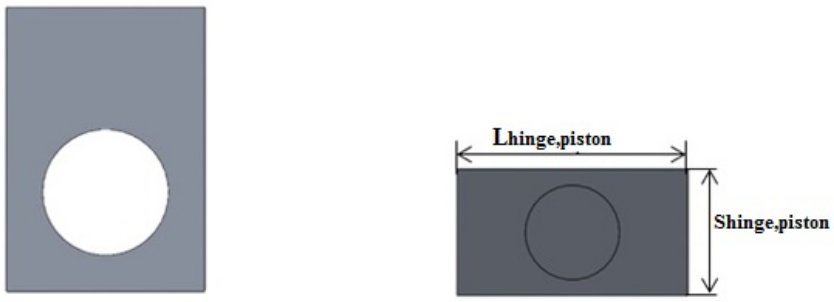

Figure 4.53: Parallelepiped utilized to schematize the part of the hinge of the piston in the design of the thickness and width.

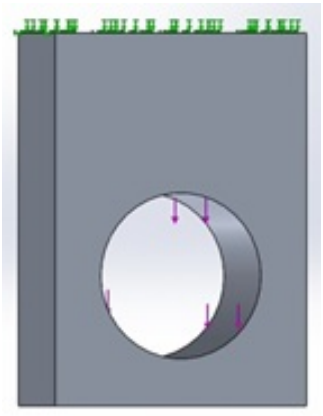

Figure 4.54: Loads and constraints imposed in the static analysis implemented in the design study thanks to which are obtained dimensions for $s_{hinge,piston}$ and $L_{hinge,piston}$.

Tesi di dottorato in Bioingegneria industriale, di Roberto Barone,
discussa presso l'Università Campus Bio-Medico di Roma in data 04/03/2017.
La disseminazione e la riproduzione di questo documento sono consentite per scopi di didattica e ricerca,
a condizione che ne venga citata la fonte.

parallelepiped is function of the width:

$$h_{hinge,piston} = \frac{h_{hinges,inn}}{2} + 0.50mm + \frac{L_{hinge,piston}}{2} \tag{4.20}$$

where 0.50 mm is the space between the forks of the two inner hinges and the basis of the piston. A design study is set up that minimize the weight and with a safety factor equal or greater than 2. Optimal values found for the thickness and the width are 6 mm and 11 mm, respectively. Von Mises stresses are reported in Figure 4.55. Minimum safety factor is 2.4 as reported in Figure 4.56.

The diameter, $d_{base,piston}$, and the thickness, $s_{base,piston}$, of the base of the

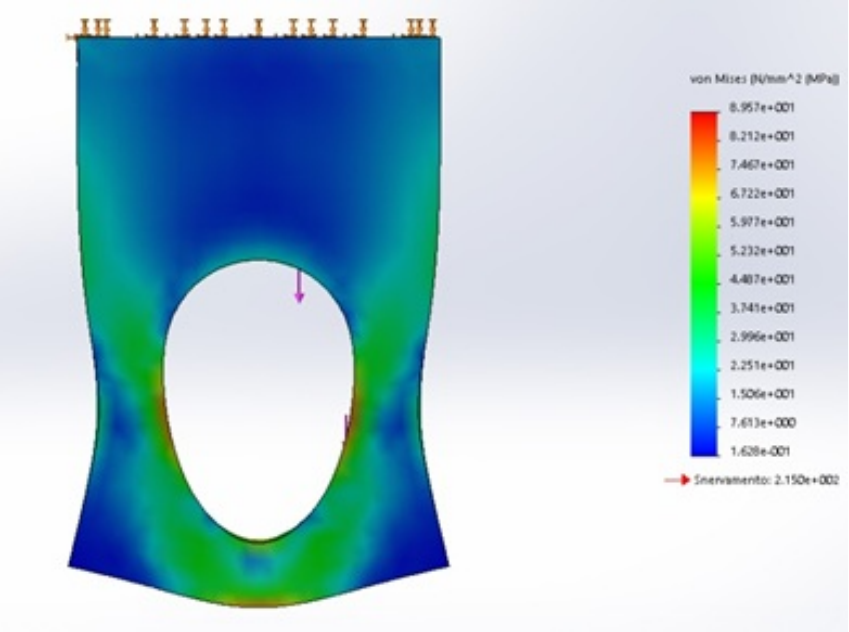

Figure 4.55: Von Mises stresses. Deformation scale is 145.

piston have the same values both for the male and for the female (Fig. 4.57). The value of the diameter of the circular section is defined by the necessity of inscribing in a circle a rectangle with the same dimensions of the just designed part. The diameter is 13.50.

To design the width of the base a static analysis of the male of the piston is set up. Load is the maximum elastic force, 566 N, distributed on an annular ring with the outer and inner diameters equal to the spring one. The hole where to insert the shaft is fixed (Fig. 4.58). In the design study, the thickness is parametric and can varies between 0.5 and 3.0 mm; safety factor must be greater than 2 and the objective is the minimization of the weight. Optimal value results to be 1 mm, with a minimum safety factor of 3.62.

Tesi di dottorato in Bioingegneria industriale, di Roberto Barone,
discussa presso l'Università Campus Bio-Medico di Roma in data 04/03/2017.
La disseminazione e la riproduzione di questo documento sono consentite per scopi di didattica e ricerca,
a condizione che ne venga citata la fonte.

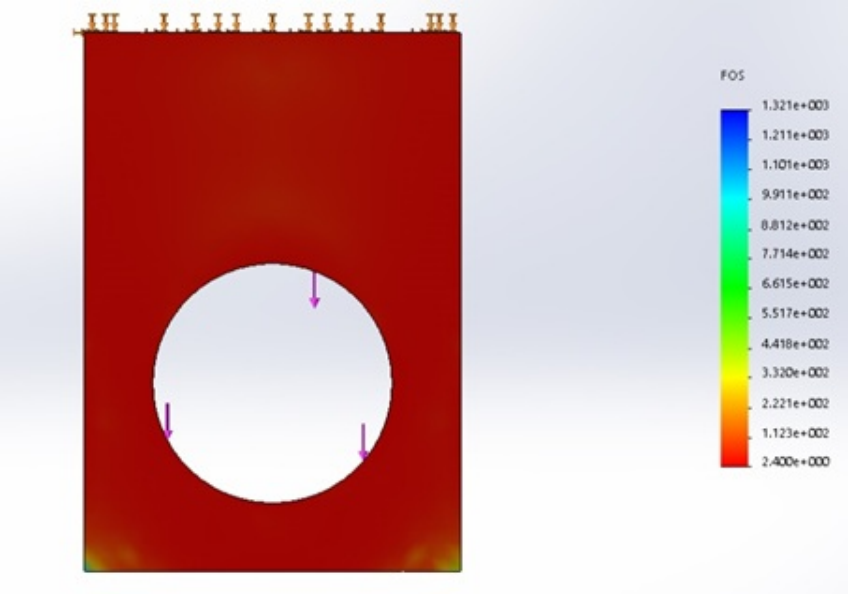

Figure 4.56: Distribution of the safety factor.

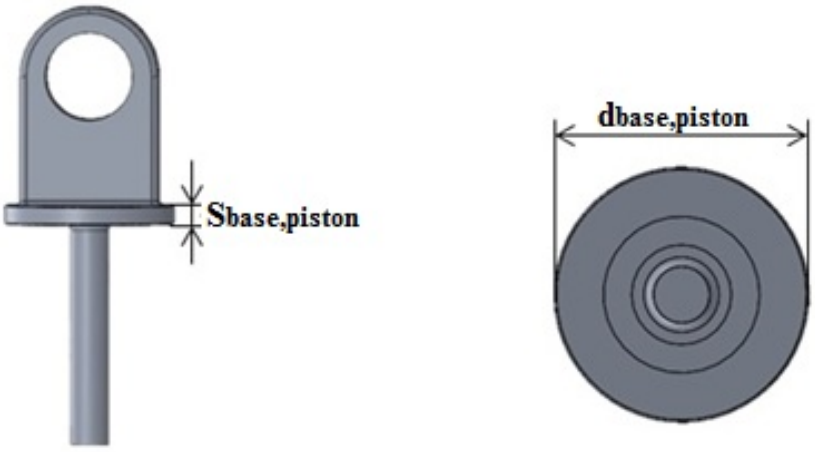

Figure 4.57: Male part of the piston: on the left a front view shows the thickness of the base; on the right a top view shows the diameter of the base.

Tesi di dottorato in Bioingegneria industriale, di Roberto Barone,
discussa presso l'Università Campus Bio-Medico di Roma in data 04/03/2017.
La disseminazione e la riproduzione di questo documento sono consentite per scopi di didattica e ricerca,
a condizione che ne venga citata la fonte.

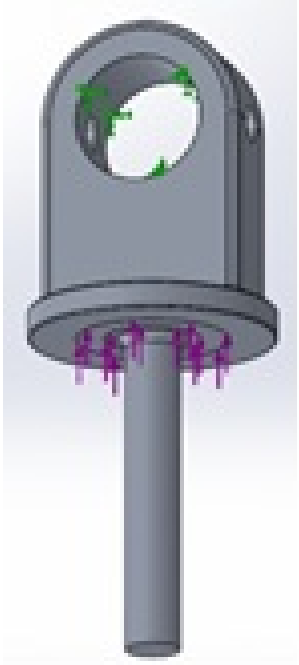

Figure 4.58: Loads and constraints imposed to execute the static analysis to obtain the best value for thickness of the male and female of the piston.

Components of the blocking system The elements that constitute the blocking system are: a wheel with pivots, a spring and a small piston as interface for the user. To complete the blocking mechanism the modular element of the outer hinges to be inserted on the lower base must be modified. On this part must be present the holes engaged by the pivots when the module is locked. Design choices are motivated by considering stresses and loads, which stress the parts. Blocking the structure, the mechanism must be able to stand the momentum generated by the elastic forces on the outer hinges. These stresses determined the choice to replicate the blocking mechanism on both the outer hinges. In the following are reported the motivations and the choices done to design the single elements.

The choice of the spring The spring has the function of restoring the position of the wheel and so of unlock the module. The choice of the commercial spring to insert in the blocking mechanism is based on minimum inner diameter and the stiffness. The elastic element must be inserted on the shaft of the outer hinge so the inner diameter must be greater than 6 mm.
Stiffness (k_{block}) is defined imposing the condition that the elastic force ($F_{el,block}$) must be greater than the weight of the wheel ($F_{p,wheel}$). Spring must be able to unlock the module also when it is rotated of 90°, so the elastic force must

Tesi di dottorato in Bioingegneria industriale, di Roberto Barone,
discussa presso l'Università Campus Bio-Medico di Roma in data 04/03/2017.
La disseminazione e la riproduzione di questo documento sono consentite per scopi di didattica e ricerca,
a condizione che ne venga citata la fonte.

win the weight of the wheel:

$$F_{el,block} > F_{p,wheel} \tag{4.21}$$

$$k_{block} > \frac{mg}{\delta l} \tag{4.22}$$

where m is the weight of the wheel equal to 21 g, g is the gravity and δl is the variation of length of the spring due to translation of the wheel on the shaft when the module is locked. The elastic element is compressed of 3.10 mm, equal to the sum of the depth of the holes and the distance between the piston rod and the inner fixed element of the outer hinge. Substituting the values in the equation 4.21 the stiffness must be greater than $0.06\frac{N}{mm}$.
The chosen spring has the inner diameter of 6.5 mm and stiffness equal to $0.94\frac{N}{mm}$ (Appendix A). Free length is 6.4 mm. It must be verified that the maximum compression force, $F_{el,max,block}$, is lower than the maximum load supported by the small piston, equal to 12 N:

$$F_{el,max,block} = k_{block}\delta l \tag{4.23}$$

$F_{el,max,block}$ results to be equal to 2.9 N, lower than the maximum load of the small piston. The close-wound length of the spring is 2.10 mm, lower than 3.3 that is the minimum length reached by the spring when the module is locked.

The small piston The small piston chosen is a mini positioning small piston with a spring which datasheet is in Appendix A. Its dimensions reduce the encumbrances and so it is possible to put it on thin metal sheets. Main components are an handle, a spring and a pin that can be retracted or not. The pin has a diameter of 4 mm and a length of 5 mm. Spring is pre-stressed with 4.5 N and the maximum load is 12N.
The small piston in the rest position has the pin not retracted and the spring is compressed; pulling and rotating the handle of 30° the pin is retracted and locked in that position. When the pin is retracted the spring is at its free length. The presence of the small piston allows the translation of the wheel on the shaft and to push the pins also when the two parts are not perfectly aligned.
When the module is in the flexible modality, the small piston is locked and the pin is retracted so that the spring is free to move solidly to the upper base. To

Tesi di dottorato in Bioingegneria industriale, di Roberto Barone,
discussa presso l'Università Campus Bio-Medico di Roma in data 04/03/2017.
La disseminazione e la riproduzione di questo documento sono consentite per scopi di didattica e ricerca,
a condizione che ne venga citata la fonte.

unlock the wrist, the user has to rotate the handle of 30° so that the pin can exit and the translation of the wheel towards the holes is permitted. To return in the flexible modality the user has to pull and rotate of 30° the handle.

The wheel and the modular parts of the upper and lower base The wheel is positioned on the shaft of the outer hinge between the piston rod and the fixed element more external of the fork (Fig. 4.59). It has two pivots which distance is 0.10 more than the width of the piston rod of the upper base so to allow the insertion of the piston rod and the translation of the wheel in order to lock the module in the desired position.

Are examined two different configurations: one with two and the other with

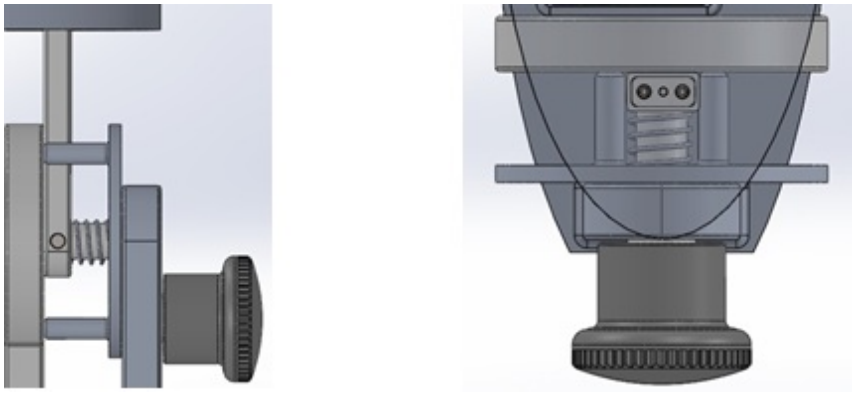

Figure 4.59: Blocking system: in the left image there is a frontal view, in the right image a top view with the upper base hidden.

four pivots. The choice of the number of pivots is the trade-off between the need for resistance and the minimization of the weight. The dimensions to define are the thickness of the wheel, s_{wheel}, and the diameters of the pins, d_{pivot} (Figure 4.60). The extrusion of the pivots are 10.90 mm, equal to the sum of the free length of the spring inserted in the blocking mechanism and the thickness of the piston rod. A static analysis is set up in a design study in order to find the optimal dimensions.

To simulate the worst load condition it is applied on a face of the pivot a force of 1200 N and the inner face of the central hole is constrained and also the surfaces of the pivots that are inserted in the holes when the module is locked (Fig. 4.61). This setting is needed to reproduce the applied forces on the wheel by the locked piston rod which tries to come back in the neutral position because of the elastic forces (Fig. 4.62). To estimate the force utilized in the static analysis the momentum generated by the elastic forces on the outer hinges is calculated. Maximum momentum, equal to 19 Nm, is

Tesi di dottorato in Bioingegneria industriale, di Roberto Barone,
discussa presso l'Università Campus Bio-Medico di Roma in data 04/03/2017.
La disseminazione e la riproduzione di questo documento sono consentite per scopi di didattica e ricerca,
a condizione che ne venga citata la fonte.

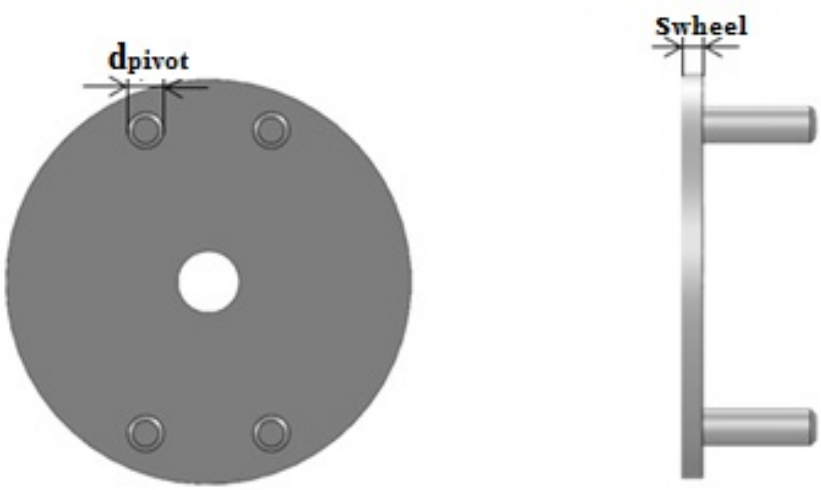

Figure 4.60: Wheel with four pivots: in the left image it is reported a frontal view; in the right image it is reported a left view.

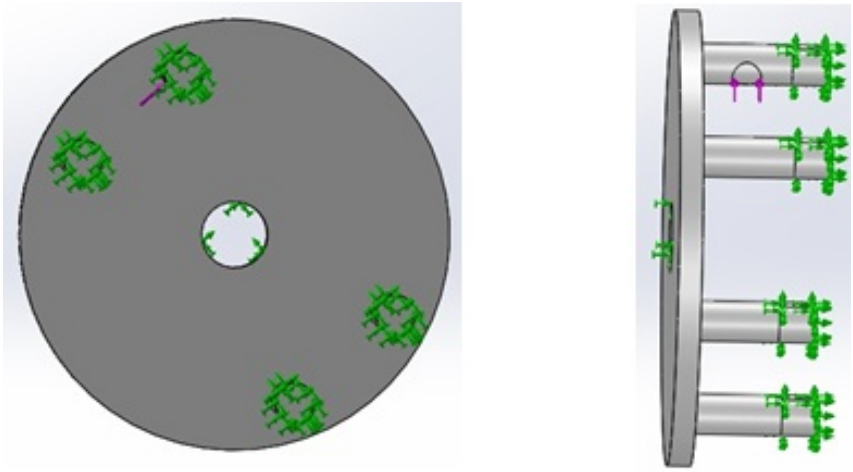

Figure 4.61: Loads and constraints set for the static analysis implemented in the design study that has as output optimal dimensions of s_{wheel} and d_{pivot}.

Tesi di dottorato in Bioingegneria industriale, di Roberto Barone,
discussa presso l'Università Campus Bio-Medico di Roma in data 04/03/2017.
La disseminazione e la riproduzione di questo documento sono consentite per scopi di didattica e ricerca,
a condizione che ne venga citata la fonte.

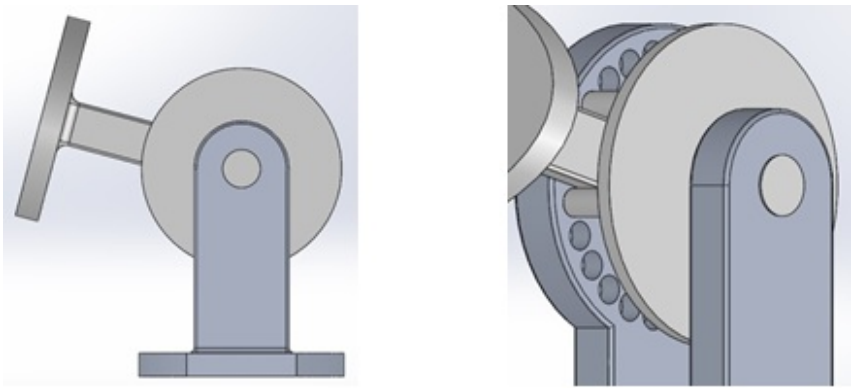

Figure 4.62: Simplified assembly of the wrist module with the blocking system. Left image represents a lateral view. In the right image is represented a particular of the wheel of the piston rod of the upper base. The piston rod exerts a force on the pivots in the holes because on the upper base there are the elastic forces which try to restore the neutral position of the module.

calculated as follows (Appendix B) (Fig. 4.63)

$$Mf_{el,1} = \vec{F_{el,1}} \times \vec{AO}$$

$$Mf_{el,2} = \vec{F_{el,2}} \times \vec{BO}$$

$$M_{tot} = Mf_{el,1} + Mf_{el,2} \tag{4.24}$$

The components of the vectors of the forces and arms are:

$$\vec{F_{el,1}} = \begin{bmatrix} -k \cdot (l_{free} - l_{block}) \cdot sin(\beta) \\ -k \cdot (l_{free} - l_{block}) \cdot cos(\beta) \end{bmatrix}$$

$$\vec{F_{el,2}} = \begin{bmatrix} -k \cdot (l_{free} - l_{75^{circ}}) \cdot sin(\beta) \\ -k \cdot (l_{free} - l_{75^{\circ}}) \cdot cos(\beta) \end{bmatrix}$$

$$\vec{A'O} = \begin{bmatrix} -A'O \cdot \cos(\theta - (\frac{\pi}{2} - \alpha)) \\ -A'O \cdot \sin(\theta - (\frac{\pi}{2} - \alpha)) \end{bmatrix}$$

$$\vec{M'O} = \begin{bmatrix} M'O \cdot \sin(\alpha - \theta) \\ -M'O \cdot \cos(\alpha - \theta) \end{bmatrix}$$

where M'O is equal to A'O because the distance from the center of rotation of the two springs is the same. $A'O = \sqrt{A'H^2 + OM'^2}$, where A'H is the distance of the springs from the center of rotation, 4 mm, and M'H is 35.25 mm, equal

Tesi di dottorato in Bioingegneria industriale, di Roberto Barone,
discussa presso l'Università Campus Bio-Medico di Roma in data 04/03/2017.
La disseminazione e la riproduzione di questo documento sono consentite per scopi di didattica e ricerca,
a condizione che ne venga citata la fonte.

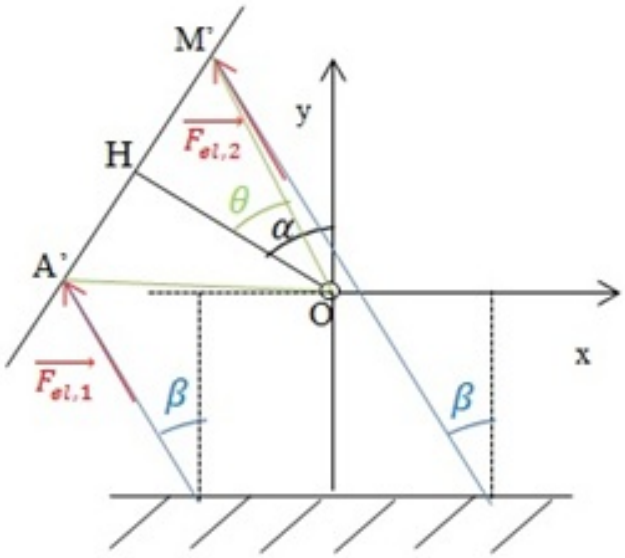

Figure 4.63: Schematization of the mechanism rotated of 75° utilized for the calculus of the momentum.

to half the distance between the centers of rotation of the two hinges which link one spring to the two basis.
It is set a total momentum equal to that generated by a force F perpendicular to the arm b (Fig. 4.64):

$$M_{tot} = F \cdot b \tag{4.25}$$

where b is the distance between the center of the hole on the wheel and the center of a pivot equal to 15.81. Inverting the equation 4.25 it is obtained the force to which is subject the wheel.
It is executed the design study setting up as objective the optimization of the weight and a safety factor greater than 2. Thickness can vary between 1 mm and 2 mm with a step of 0.5 mm; diameter of the pivots can vary between 1 mm and 3.5 mm with a step of 0.5 mm. Upper limits of the spaces are defined by the maximum allowed encumbrance.
At the beginning a design study is implemented on the CAD of the wheel with only two pivots choosing the Al 6063 T6 and after the AISI 431. With the aluminum alloy the safety factor is lower than 1 for every combination of values of thickness and diameter of the pivots. With the steel, minimum safety factor is 1.71 when thickness is 2 mm and diameter of the pivots is 3.5. The same study has been repeated on the CAD of the wheel with four pivots in aluminum and resulting dimensions are 2 mm and 3.5 for thickness and diam-

Tesi di dottorato in Bioingegneria industriale, di Roberto Barone,
discussa presso l'Università Campus Bio-Medico di Roma in data 04/03/2017.
La disseminazione e la riproduzione di questo documento sono consentite per scopi di didattica e ricerca,
a condizione che ne venga citata la fonte.

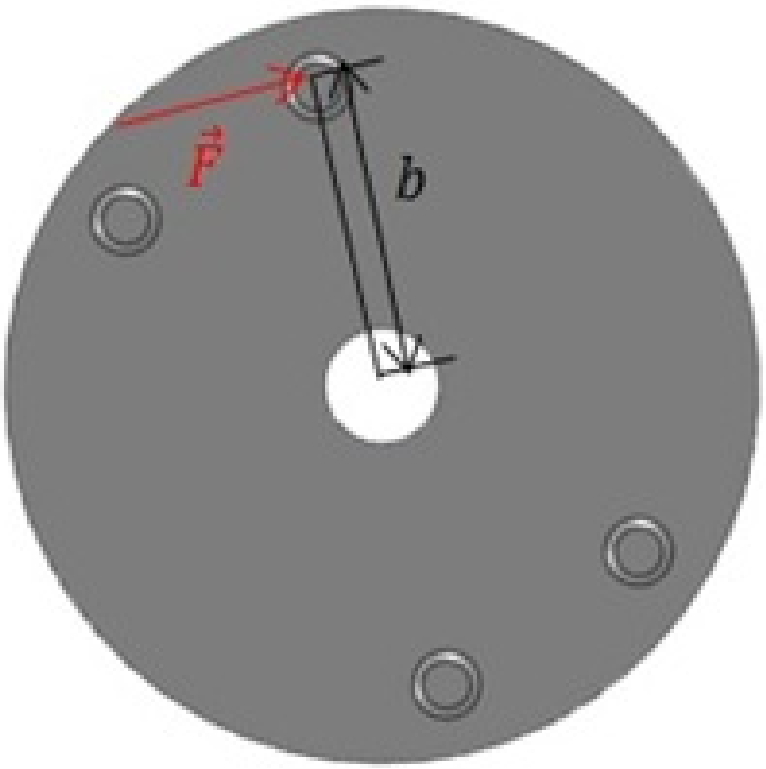

Figure 4.64: Schematization of the arm utilized to calculate the force exerted on the pivot.

Tesi di dottorato in Bioingegneria industriale, di Roberto Barone,
discussa presso l'Università Campus Bio-Medico di Roma in data 04/03/2017.
La disseminazione e la riproduzione di questo documento sono consentite per scopi di didattica e ricerca,
a condizione che ne venga citata la fonte.

eter, respectively. A steel structure with four pivots has not been considered to avoid a weight too high.

The definitive choice between the two configurations has been done after evaluating the stresses resulting from the static analysis of the module blocked at 75°. In fact, put two or four pivots determines a different distribution of the stresses in the holes. The configuration of the wheel chosen, determines a change in the material that can be used both for the wheel and for the fixed element of the outer hinge which has the holes for the blocking system. The consequence of the variation of the material is an increase or a decrease of the weight of the prototype. The version to choose is the one that minimize the weight. It must be defined and designed the modular part of the lower base which has the holes and simulate the stresses on the module at 75° and determine the ultimate configuration for the wheel.

Hole which are engaged by the pivots are positioned on a face of the modular fixed elements of the outer hinges (Fig. 4.65). Blocking angles, in addition to the neutral position (0°), are: 15°, 45°, 75° in flexion and 15°, 30°, 45° in extension. For each of the seven position it must be provided at least two holes with diameter 3.5 mm and with centers with a distance of 12.10 mm positioned on a circle with ray 15.81 mm. Depth of the holes is 3 mm. In Figure 4.65 is shown the simplified CAD of the lower base of the mechanism: in the right image there is a frontal view, in the left one a section view that shows the 22 holes. The diameter of the circular extrusion is 39 mm, less than the minor axis of the elliptical section of the prosthetic wrist.

A simplified assembly of the mechanism is created and is simulated a load

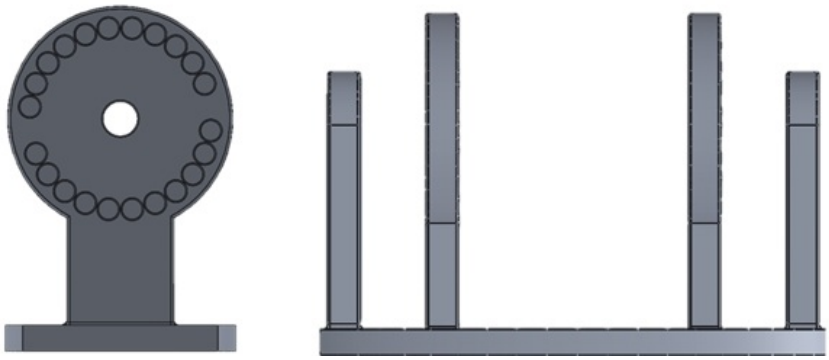

Figure 4.65: Lower base with the holes necessary to the blocking mechanism, put on a face of the fix elements of the hinges. In the left image it is reported a section view of the part, in the right image a frontal view.

condition equivalent to the momentum applied to the outer hinges generated by the elastic forces when the module is rotated of 75°: this is the worst load

Tesi di dottorato in Bioingegneria industriale, di Roberto Barone,
discussa presso l'Università Campus Bio-Medico di Roma in data 04/03/2017.
La disseminazione e la riproduzione di questo documento sono consentite per scopi di didattica e ricerca,
a condizione che ne venga citata la fonte.

condition. The CAD is composed of the upper and lower basis made of Al 6063 T6; the shafts for the outer hinges made of AISI 431; the two wheels for the blocking system and the pins. In the assembly, pivots engage the holes that lock the mechanism at 75°.
For the calculation of the stresses, a static analysis is set up constraining the lower base as in Figure 4.66 and applying a force F_1 of 540 N, perpendicular to each piston rod of the upper base. The value of the force is such that the momentum that it generates on the two outer hinges is equal to the one generated by the elastic forces:

$$M_{tot} = F_1 \cdot b_1$$

$$F_1 = \frac{M_{tot}}{b_1}$$

where M_{tot} is calculated applying the equation 4.24 and $b_1 = 32.55mm$ (Fig. 4.67).
The same static analysis is repeated for two different configurations of the module: the first with the wheel of the blocking mechanism made of steel with only two pivots, the second configuration with the wheel in aluminum with four pivots.
The stresses resulting in the configuration of the assembly with wheels with only two pivots impose to utilize the steel for the parts of the forks with the holes.
Results from the static analysis of the second configuration of the module are examined. Maximum Von Mises stress on the lower base is 188.4 MPa (Fig. 4.69) while the minimum safety factor is 1.14 (Fig. 4.68) less than the minimum safety factor for a safe design. Also for this configuration, steel must be chosen to realize the two modular parts of the lower base.
In order to minimize the weight, the configuration chosen is the one with the wheel in Al 6063 T6: weight with two pivots in steel is 19.58 g, while the one with four pivots is 7.43 g. In figure 4.70 are reported the stresses on the wheel resulting from the static analysis of the assembly.

The structure and the loads are symmetric so the stresses on one wheel are the same on the other one. Maximum stress is 76.6 MPa; from the Figure 4.71 is readable the minimum safety factor of the part. These results confirm the choice made for the wheel.

To choose the material with which realize the modular element of the upper base, Von Mises stresses on the part just set up are analyzed. The two piston

Tesi di dottorato in Bioingegneria industriale, di Roberto Barone,
discussa presso l'Università Campus Bio-Medico di Roma in data 04/03/2017.
La disseminazione e la riproduzione di questo documento sono consentite per scopi di didattica e ricerca,
a condizione che ne venga citata la fonte.

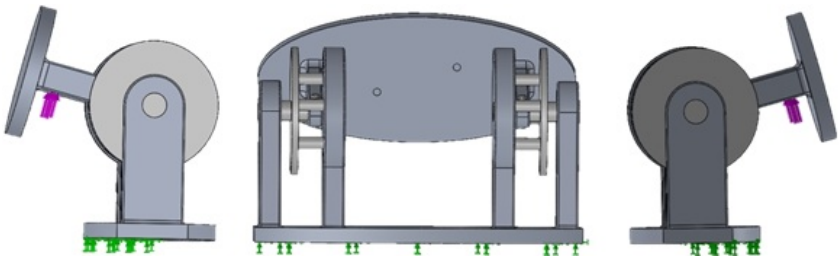

Figure 4.66: Loads and constraints imposed for the static analysis of a simplified assembly with the aim of calculating the stresses on the parts due to momentums generated by elastic forces on the outer hinges: violet arrows represents force F_1, green arrows the constraint. Three views are reported: one frontal and two lateral.

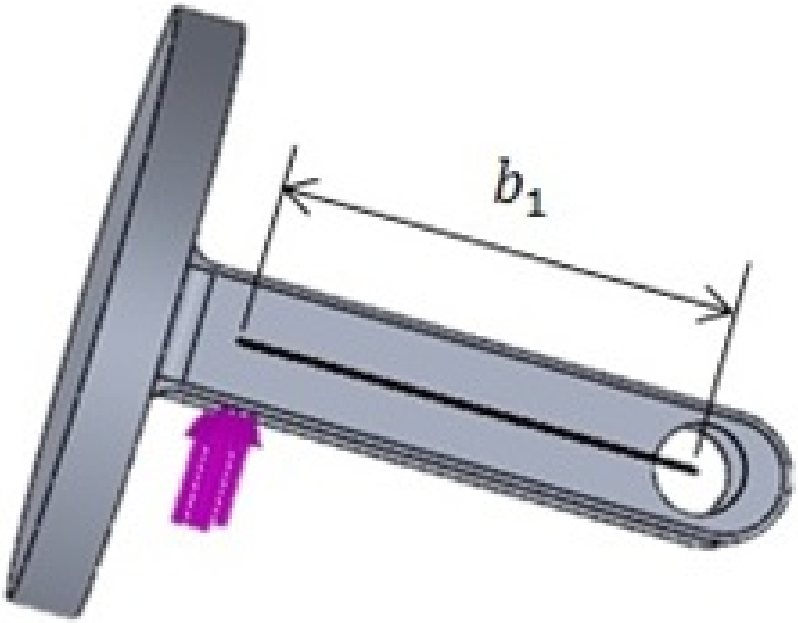

Figure 4.67: Particular of the upper base of the assembly in Fig. 4.66: it shows the arm b_1 utilized from the calculus of the module of the force F_1 represented with violet arrows.

Tesi di dottorato in Bioingegneria industriale, di Roberto Barone,
discussa presso l'Università Campus Bio-Medico di Roma in data 04/03/2017.
La disseminazione e la riproduzione di questo documento sono consentite per scopi di didattica e ricerca,
a condizione che ne venga citata la fonte.

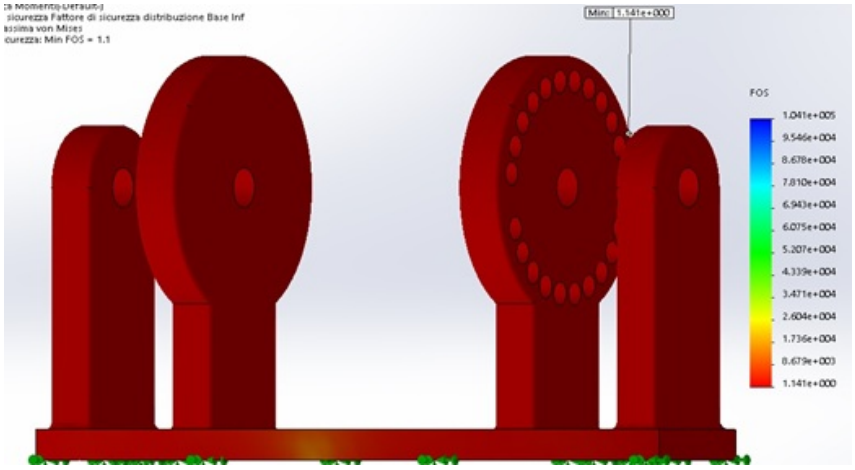

Figure 4.68: Distribution of the safety factor on the lower base resulting from the static analysis. Minimum safety factor is 1.14.

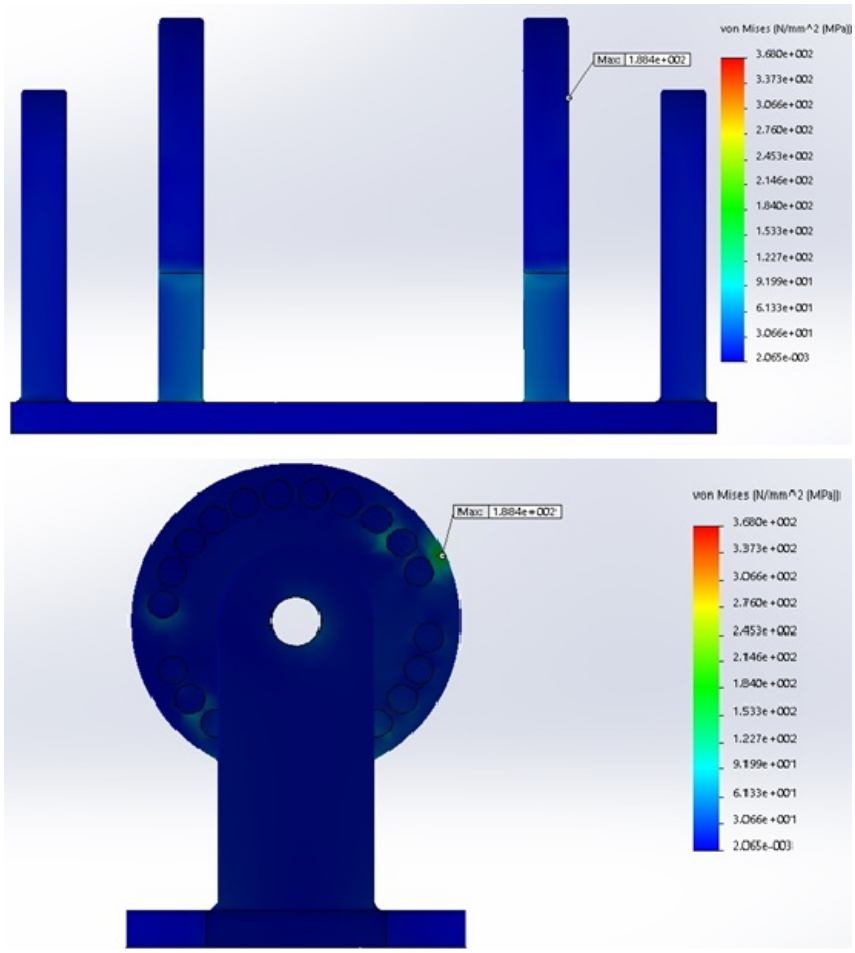

Figure 4.69: Von Mises stresses on the lower base resulting from the static analysis of the assembly. Maximum stress is 170 MPa. Stresses are simmetric respect to the center. Upper image shows the frontal view, the lower shows the right view.

Tesi di dottorato in Bioingegneria industriale, di Roberto Barone,
discussa presso l'Università Campus Bio-Medico di Roma in data 04/03/2017.
La disseminazione e la riproduzione di questo documento sono consentite per scopi di didattica e ricerca,
a condizione che ne venga citata la fonte.

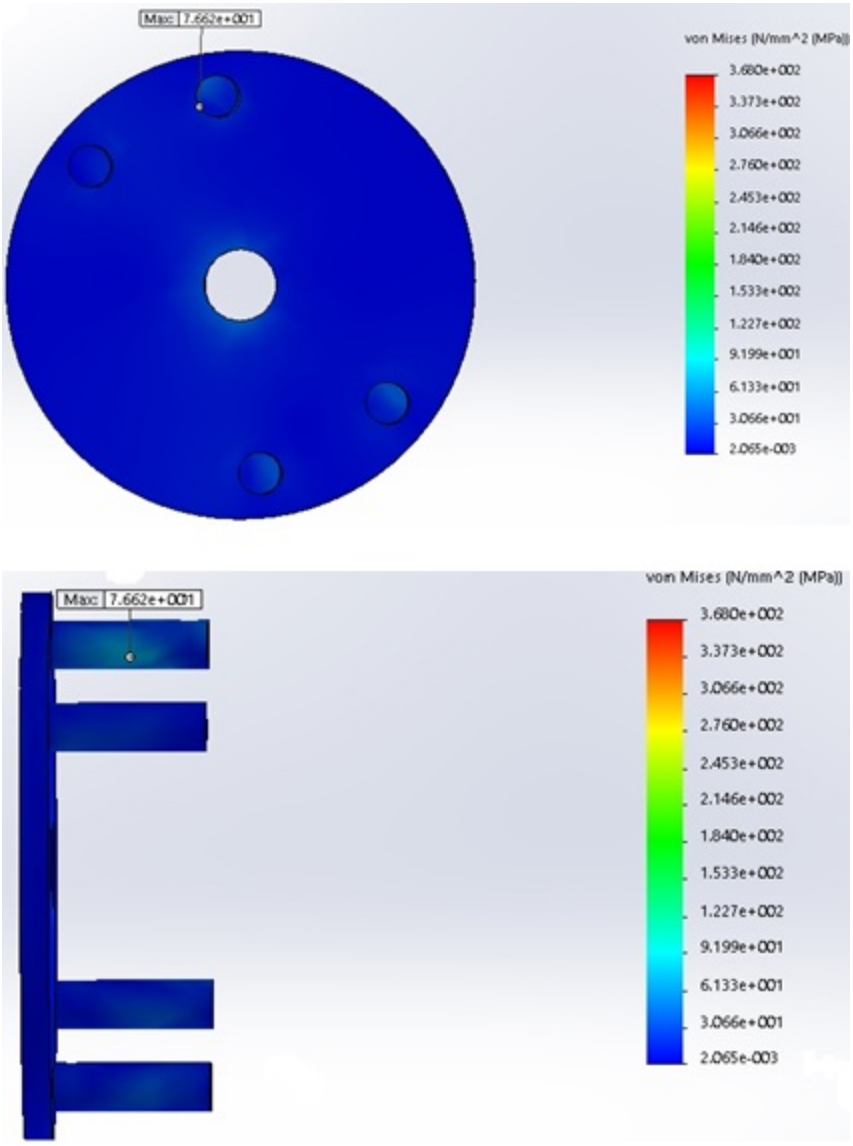

Figure 4.70: Von Mises stresses on the wheel resulting from the static analysis of the assembly.

Tesi di dottorato in Bioingegneria industriale, di Roberto Barone,
discussa presso l'Università Campus Bio-Medico di Roma in data 04/03/2017.
La disseminazione e la riproduzione di questo documento sono consentite per scopi di didattica e ricerca,
a condizione che ne venga citata la fonte.

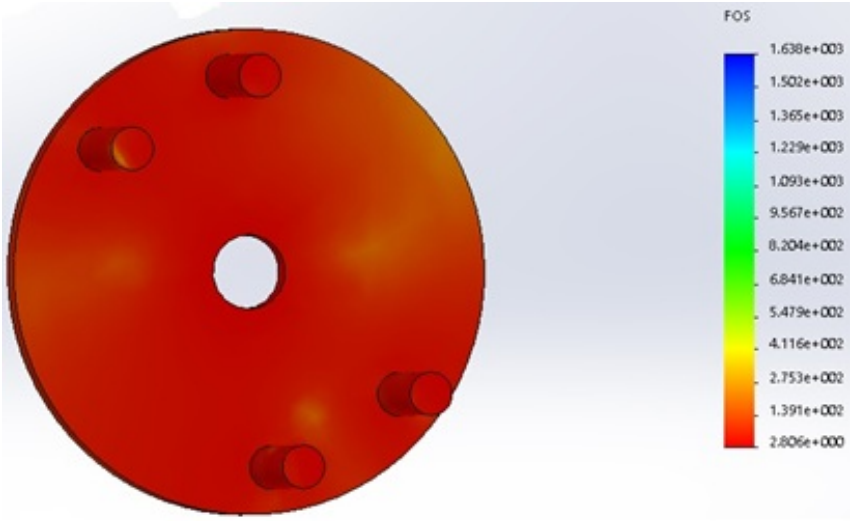

Figure 4.71: Distribution of the safety factor on the wheel resulting from the static analysis of the assembly.

rods have Von Mises stresses symmetric and are the more stressed elements of the base (248 MPa, Figure 4.72). This value exceeds the yield strength of the Al 6063 T6, so this material is substituted with the AISI 431.

4.3 The proposed wrist/hand combined control

Here it is presented a possible EMG wrist/hand combined control 4.73.

The system is in the rest position state if no activity from the EMG is registered. As soon as a muscle contraction pattern is detected, the non-linear logistic regression classifier decides if the control is for the hand or for the wrist and enters the relative state. Once entered a state, it is not possible to switch to the other state unless after an amount of time, to find empirically, of muscle inactivity. After this time, it is possible to decide again in which state enter.

4.4 Conclusions

The aim of this section has been the invention and the design of a new solution for an innovative flexion-extension module for a prosthetic passive wrist and an active prono-supination module.

The design of the prono-supination module has been done, based on requirements of torque, speed and maximum dimensions allowed. Trials on the prono-supination module have been conducted for the control with the EMGs signals.

A possible wrist/hand combined control has been proposed, which would allow

Tesi di dottorato in Bioingegneria industriale, di Roberto Barone,
discussa presso l'Università Campus Bio-Medico di Roma in data 04/03/2017.
La disseminazione e la riproduzione di questo documento sono consentite per scopi di didattica e ricerca,
a condizione che ne venga citata la fonte.

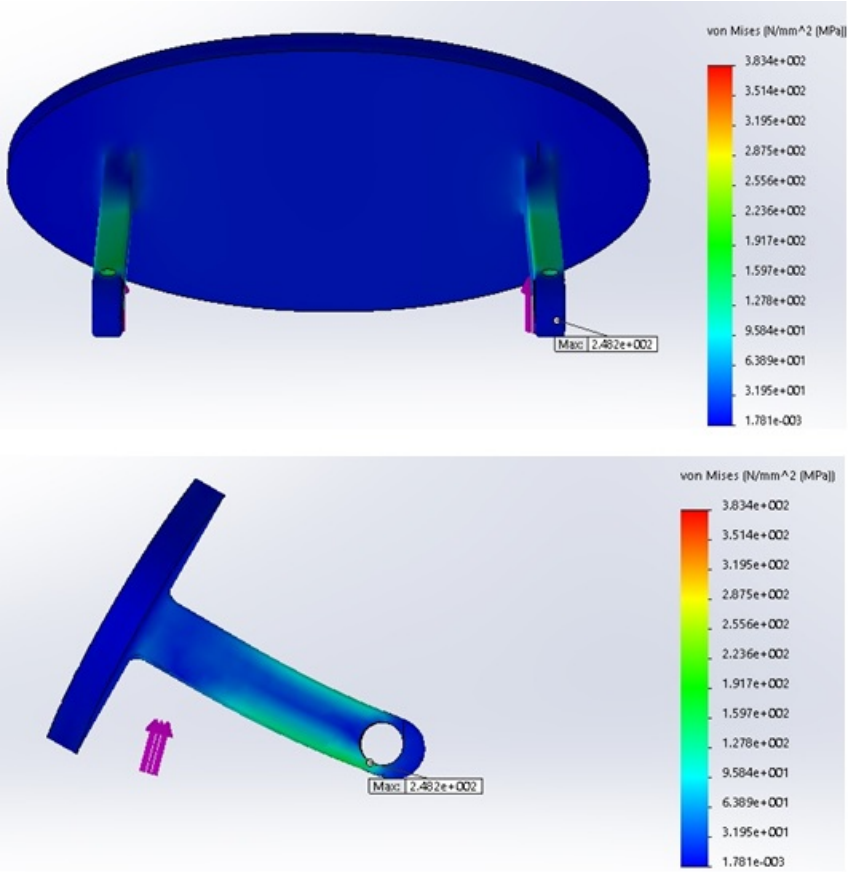

Figure 4.72: Von Mises stresses of the upper base. Deformation scale is 15.65. The upper image reports the frontal view, the lower reports the lateral view.

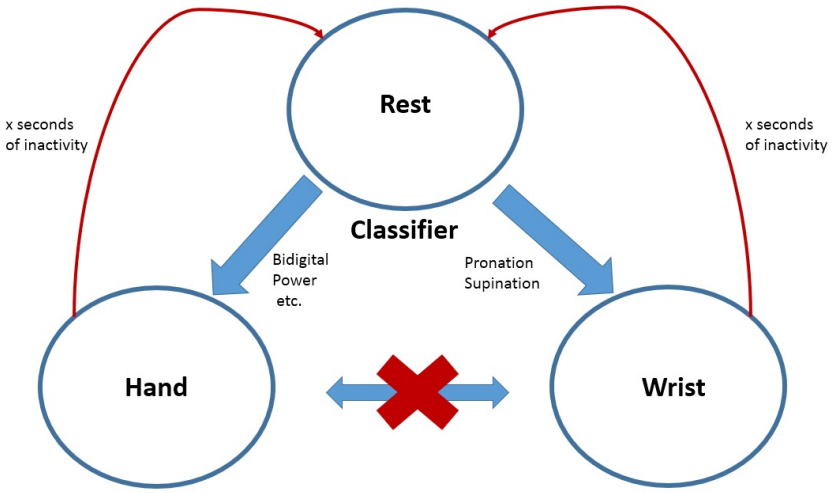

Figure 4.73: Wrist/hand combined control.

Tesi di dottorato in Bioingegneria industriale, di Roberto Barone,
discussa presso l'Università Campus Bio-Medico di Roma in data 04/03/2017.
La disseminazione e la riproduzione di questo documento sono consentite per scopi di didattica e ricerca,
a condizione che ne venga citata la fonte.

the amputee to easily control both the wrist and the hand movements.
A flexion-extension module has been designed. It has two modalities: flexible and rigid. The first simulates the wrist not contracted and allows a safe interaction with the around world; the second modality furnish stability to the system and it is important to execute different activities of daily living. The designed blocking system allows the user to implement the rigid modality fixing the module in the desired position.
The main critical issues found during the design involved weight and encumbrance and are common to the ones found during the design of a prosthesis. A following engineering phase will reduce the encumbrance trying to find a compromise between performance and compactness, and solutions for an easy and intuitive interface for the blocking system.
The prototype obtained by the design choices is shown in Figures 4.74-4.78.

The module has a symmetric range of movement: 75° is the maximum

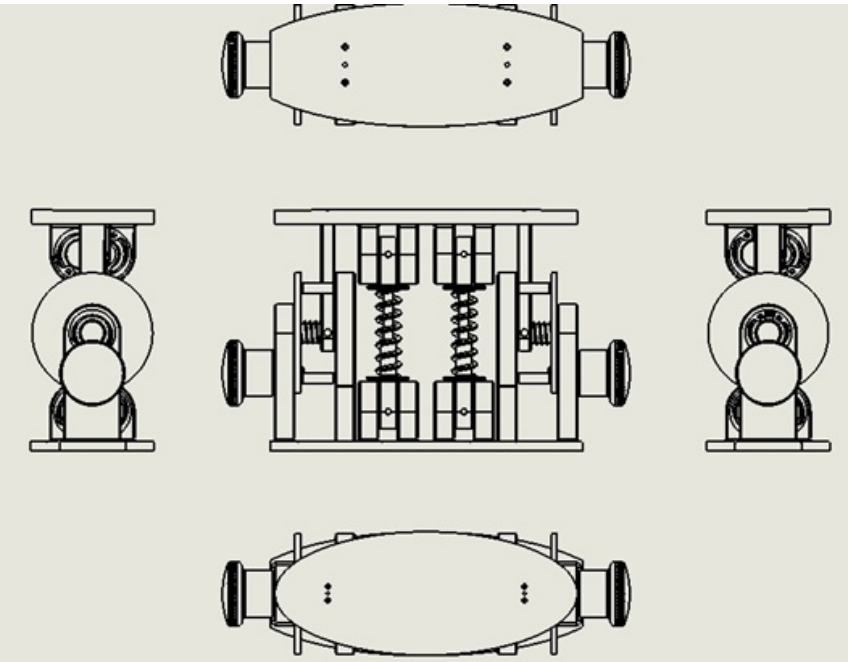

Figure 4.74: Drawing of the mechanism.

angle allowed both in flexion and extension. The system has seven blocking angles: 0°, 15°, 45°, 75° in flexion and 15°, 30°, 45° in extension. The choice of the fixed angles has been done integrating the results of human wrist biomechanical studies and the solutions adopted in the most advanced commercial prostheses.
Encumbrances are: width of 101.20 mm; height of 77.91 mm; depth of 40 mm. Resulting dimensions are almost two times the wanted ones. This over dimen-

Tesi di dottorato in Bioingegneria industriale, di Roberto Barone,
discussa presso l'Università Campus Bio-Medico di Roma in data 04/03/2017.
La disseminazione e la riproduzione di questo documento sono consentite per scopi di didattica e ricerca,
a condizione che ne venga citata la fonte.

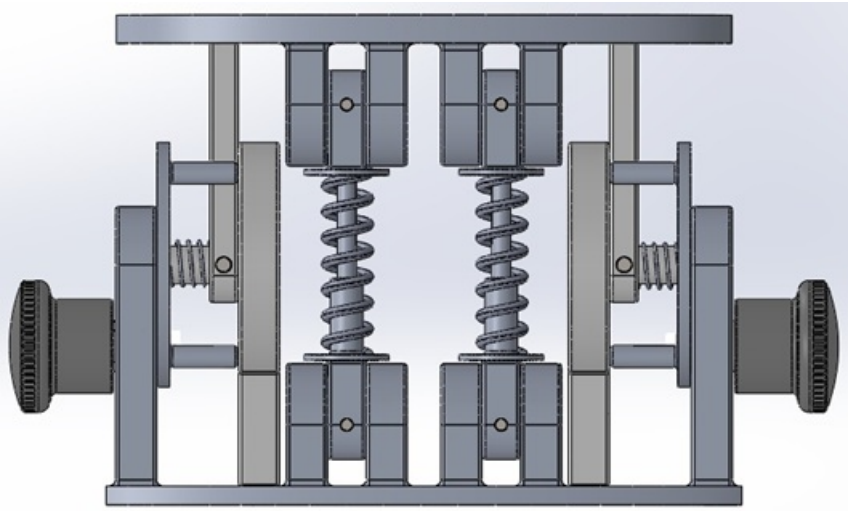

Figure 4.75: Frontal view of the module for the flexion-extension of a passive prosthetic wrist. Module is in the flexible modality: the wheel of the blocking mechanism can move togheter with the upper base.

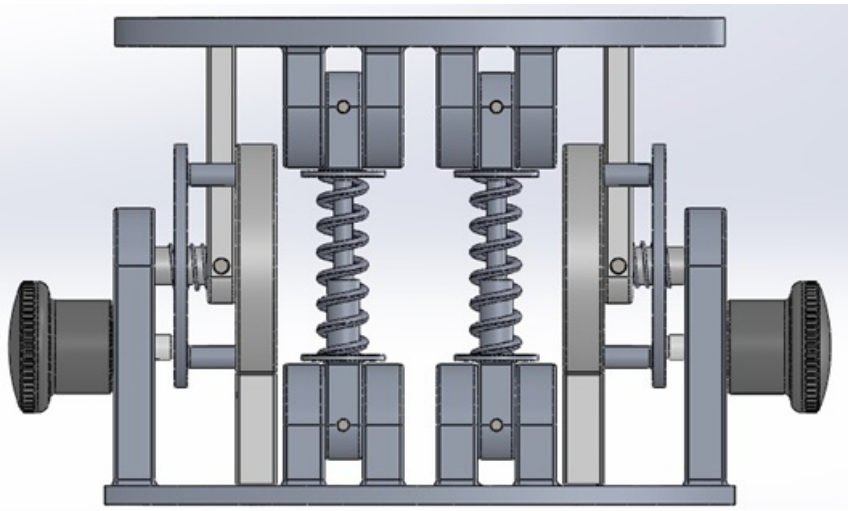

Figure 4.76: Frontal view of the module for the flexion-extension of a passive prosthetic wrist. The module is in rigid modality: small piston push the wheel towards the inner element of the external hinge and the pivots of the wheel are engaged in the holes.

Tesi di dottorato in Bioingegneria industriale, di Roberto Barone,
discussa presso l'Università Campus Bio-Medico di Roma in data 04/03/2017.
La disseminazione e la riproduzione di questo documento sono consentite per scopi di didattica e ricerca,
a condizione che ne venga citata la fonte.

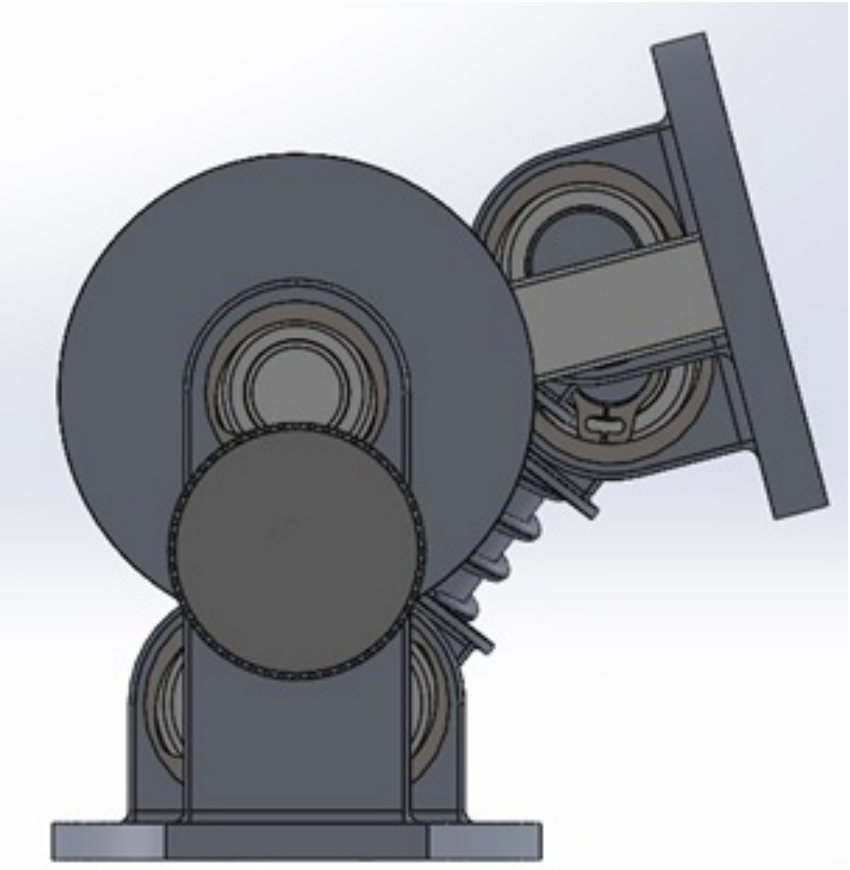

Figure 4.77: Module flexed at 75°.

Tesi di dottorato in Bioingegneria industriale, di Roberto Barone,
discussa presso l'Università Campus Bio-Medico di Roma in data 04/03/2017.
La disseminazione e la riproduzione di questo documento sono consentite per scopi di didattica e ricerca,
a condizione che ne venga citata la fonte.

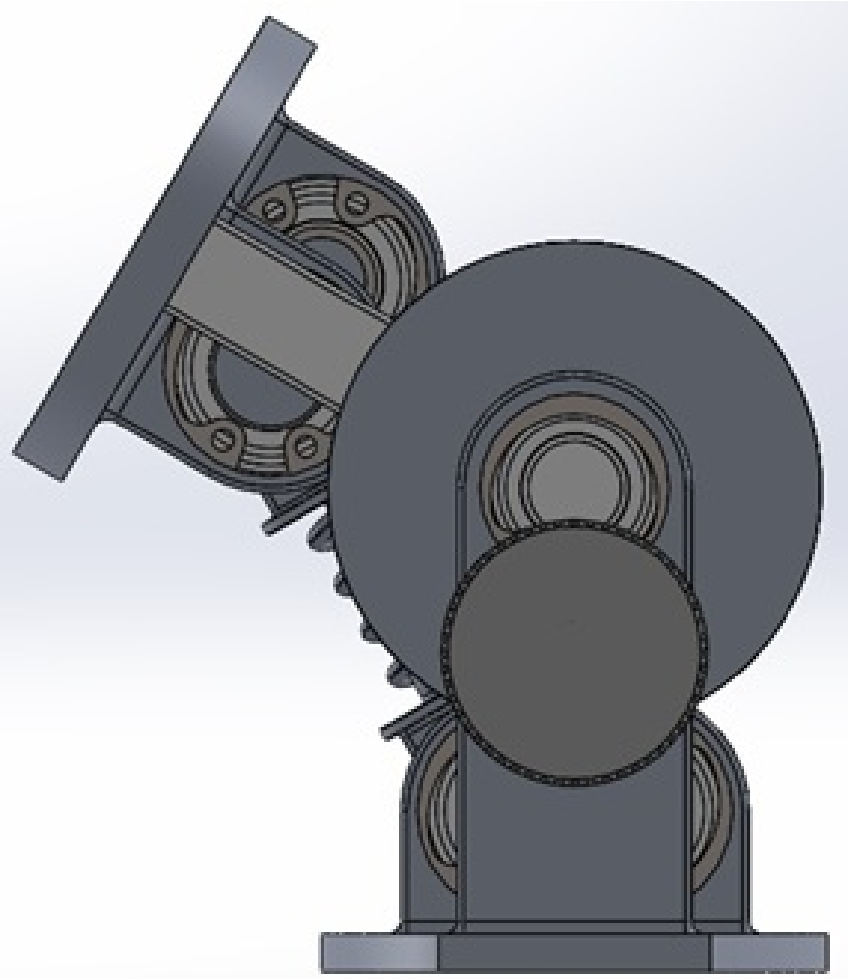

Figure 4.78: Module extended at 45°.

Tesi di dottorato in Bioingegneria industriale, di Roberto Barone,
discussa presso l'Università Campus Bio-Medico di Roma in data 04/03/2017.
La disseminazione e la riproduzione di questo documento sono consentite per scopi di didattica e ricerca,
a condizione che ne venga citata la fonte.

sioning is mainly due to the presence of the ball-bearings necessary to reduce the friction in the hinges. These elements maximize the performances but the encumbrances are high. Weight of the prototype is 304.42 g; the choice of the materials and of the dimensions is determined by the stresses in the structure and by a constraint on a minimum safety factor.

Tesi di dottorato in Bioingegneria industriale, di Roberto Barone,
discussa presso l'Università Campus Bio-Medico di Roma in data 04/03/2017.
La disseminazione e la riproduzione di questo documento sono consentite per scopi di didattica e ricerca,
a condizione che ne venga citata la fonte.

Chapter 5

Conclusions

This dissertation thesis presents the design of a new control technique based on two levels and the design of a wrist, which implements active prono-supination and passive flexion-extension.
The new control technique consists of two levels: the first is interfaced to the patient and gives as output the desired joint position for the hand, while the second level directly dialogues with the actuators of the prosthetic device to command them. The control demonstrated its capabilities to execute both grasp and cyclic tasks. For what concerns the grasp tasks, Kuka robot was used to induce slippage on different types of objects. The control has been able to prevent the fall of the objects thanks to the slippage feedback, measured by an analysis of the force sensor placed on the index fingertip. For what concerns the cyclic tasks, a neural network has been trained offline to learn how to rotate a wheel. The system has been able to rotate the ring-shaped object of 294 degrees, as shown in chapter 3. The experiments were repeated 5 times and the obtained performance are comparable (mean value 309 degrees and standard deviation 9 degrees), thus demonstrating a good level of repeatability of the manipulation task.
An innovative prosthetic wrist was also designed, with the aim of giving to the patients the ability of active prono-supination and passive flexion-extension. The module has a symmetric range of movement: 75° is the maximum angle allowed both in flexion and extension. Resulting dimensions are almost two times the wanted ones. This over dimensioning is mainly due to the presence of the ball-bearings necessary to reduce the friction in the hinges. These elements maximize the performances but the encumbrances are high. Weight of the prototype is 304.42 g; the choice of the materials and of the dimensions is determined by the stresses in the structure and by a constraint on a minimum

Tesi di dottorato in Bioingegneria industriale, di Roberto Barone,
discussa presso l'Università Campus Bio-Medico di Roma in data 04/03/2017.
La disseminazione e la riproduzione di questo documento sono consentite per scopi di didattica e ricerca,
a condizione che ne venga citata la fonte.

safety factor.

Future developments for the control will include the improvement of the setup reliability. More objects will be used and more trials will be performed. More FSR sensors should be added on the prosthetic hand in order to extend the approach to other grasping tasks and to manipulation. The EMG signal will be integrated and tests on amputees will be done. Will be implemented online learning on the prosthetic hand and possibly tested the developed architecture on different prosthetic hands. For what concerns the wrist, future development will include the optimization of the wrist design in order to have a lighter device and to improve the blocking system so to make it easier to use. The flexion-extension wrist prototype will be manufactured. An integration of wrist and hand will be done and a combined control will be developed.

Tesi di dottorato in Bioingegneria industriale, di Roberto Barone,
discussa presso l'Università Campus Bio-Medico di Roma in data 04/03/2017.
La disseminazione e la riproduzione di questo documento sono consentite per scopi di didattica e ricerca,
a condizione che ne venga citata la fonte.

List of publications

Published

International Journals

Barone R, Ciancio AL, Romeo RA, Davalli A, Sacchetti R, Guglielmelli E, Zollo L. Multilevel control of an anthropomorphic prosthetic hand for grasp and slip prevention. Advances in Mechanical Engineering. 2016 Aug;8(9):1687814016665082.

Ciancio AL, Cordella F, Barone R, Romeo RA, Bellingegni AD, Sacchetti R, Davalli A, Di Pino G, Ranieri F, Di Lazzaro V, Guglielmelli E. Control of prosthetic hands via the peripheral nervous system. Frontiers in neuroscience. 2016;10.

Peer-reviewd International Confererences

Cordella F, Gentile C, Zollo L, Barone R, Sacchetti R, Davalli A, Siciliano B, Guglielmelli E. A force-and-slippage control strategy for a poliarticulated prosthetic hand. InRobotics and Automation (ICRA), 2016 IEEE International Conference on 2016 May 16 (pp. 3524-3529). IEEE.

Ciancio AL, Barone R, Zollo L, Carpino G, Davalli A, Sacchetti R, Guglielmelli E. A bio-inspired force control for cyclic manipulation of prosthetic hands. InEngineering in Medicine and Biology Society (EMBC), 2015 37th Annual International Conference of the IEEE 2015 Aug 25 (pp. 4824-4827). IEEE.

Tesi di dottorato in Bioingegneria industriale, di Roberto Barone,
discussa presso l'Università Campus Bio-Medico di Roma in data 04/03/2017.
La disseminazione e la riproduzione di questo documento sono consentite per scopi di didattica e ricerca,
a condizione che ne venga citata la fonte.

Appendix A

SKF

Dimensioni principali			Coefficienti di carico base		Velocità di riferimento		Denominazione
			dinamico	statico	Velocità di riferimento	Velocità limite	
d	D	B	C	C0			* Cuscinetto della classe SKF Explorer
mm			kN		g/min		-
7	17	5	1,48	0,56	90000	45000	619/7-2Z

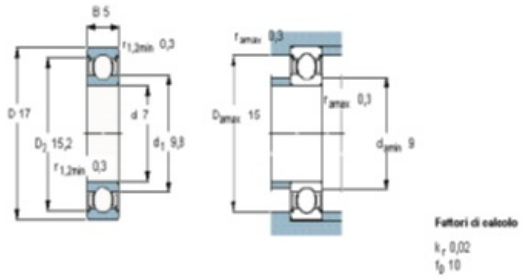

Figure A.1: Datasheet of the ball-bearing 619/7-2Z chosen for the inner hinges

SKF

Dimensioni principali			Coefficienti di carico base		Velocità di riferimento		Denominazione
			dinamico	statico	Velocità di riferimento	Velocità limite	
d	D	B	C	C0			* Cuscinetto della classe SKF Explorer
mm			kN		g/min		-
6	15	5	1,24	0,475	100000	50000	619/6-2Z

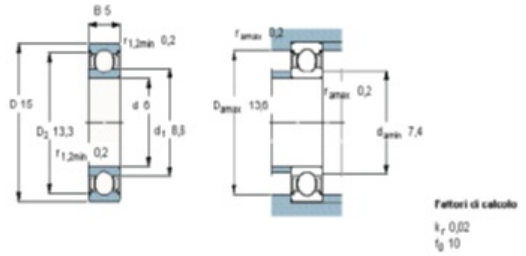

Figure A.2: Datasheet of the ball-bearing 619/6-2Z chosen for the outer hinges

Tesi di dottorato in Bioingegneria industriale, di Roberto Barone,
discussa presso l'Università Campus Bio-Medico di Roma in data 04/03/2017.
La disseminazione e la riproduzione di questo documento sono consentite per scopi di didattica e ricerca,
a condizione che ne venga citata la fonte.

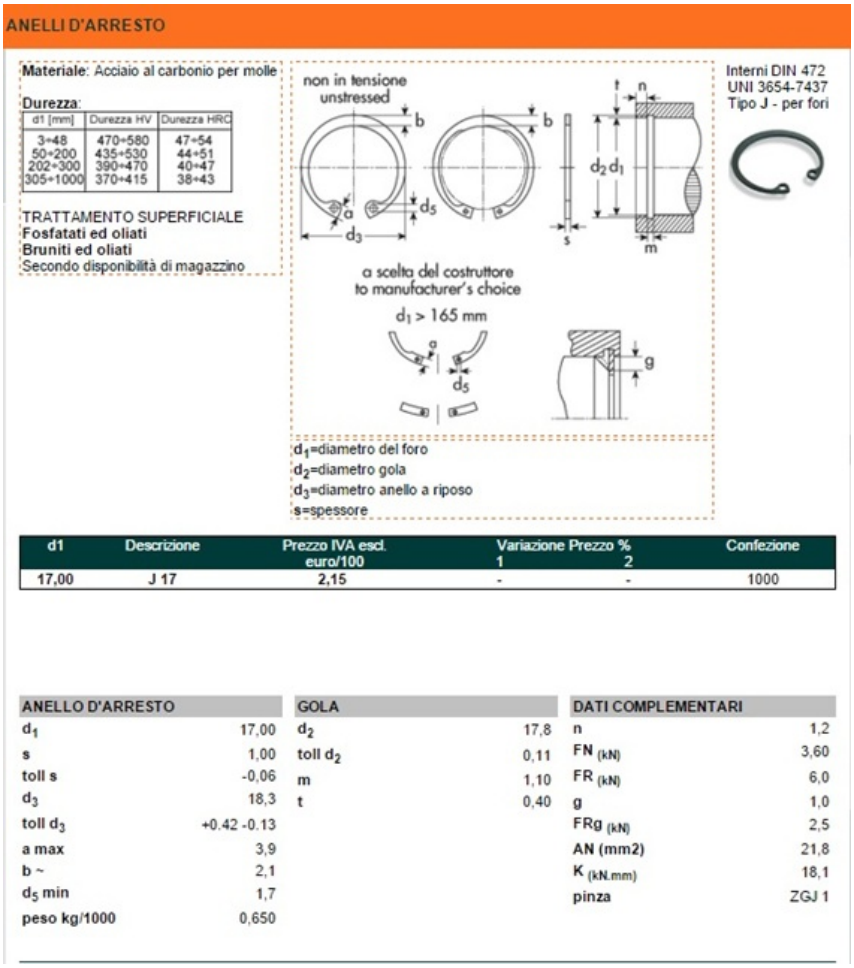

ANELLI D'ARRESTO

Materiale: Acciaio al carbonio per molle

Durezza:

d1 [mm]	Durezza HV	Durezza HRC
3÷48	470÷580	47÷54
50÷200	435÷530	44÷51
202÷300	390÷470	40÷47
305÷1000	370÷415	38÷43

TRATTAMENTO SUPERFICIALE
Fosfatati ed oliati
Bruniti ed oliati
Secondo disponibilità di magazzino

non in tensione
unstressed

a scelta del costruttore
to manufacturer's choice

$d_1 > 165$ mm

Interni DIN 472
UNI 3654-7437
Tipo J - per fori

d_1=diametro del foro
d_2=diametro gola
d_3=diametro anello a riposo
s=spessore

d1	Descrizione	Prezzo IVA escl. euro/100	Variazione Prezzo % 1	2	Confezione
17,00	J 17	2,15	-	-	1000

ANELLO D'ARRESTO		GOLA		DATI COMPLEMENTARI	
d_1	17,00	d_2	17,8	n	1,2
s	1,00	toll d_2	0,11	FN (kN)	3,60
toll s	-0,06	m	1,10	FR (kN)	6,0
d_3	18,3	t	0,40	g	1,0
toll d_3	+0.42 -0.13			FRg (kN)	2,5
a max	3,9			AN (mm2)	21,8
b ~	2,1			K (kN.mm)	18,1
d_5 min	1,7			pinza	ZGJ 1
peso kg/1000	0,650				

Figure A.3: Datasheet of the seeger for holes inserted in the inner hinges

Tesi di dottorato in Bioingegneria industriale, di Roberto Barone,
discussa presso l'Università Campus Bio-Medico di Roma in data 04/03/2017.
La disseminazione e la riproduzione di questo documento sono consentite per scopi di didattica e ricerca,
a condizione che ne venga citata la fonte.

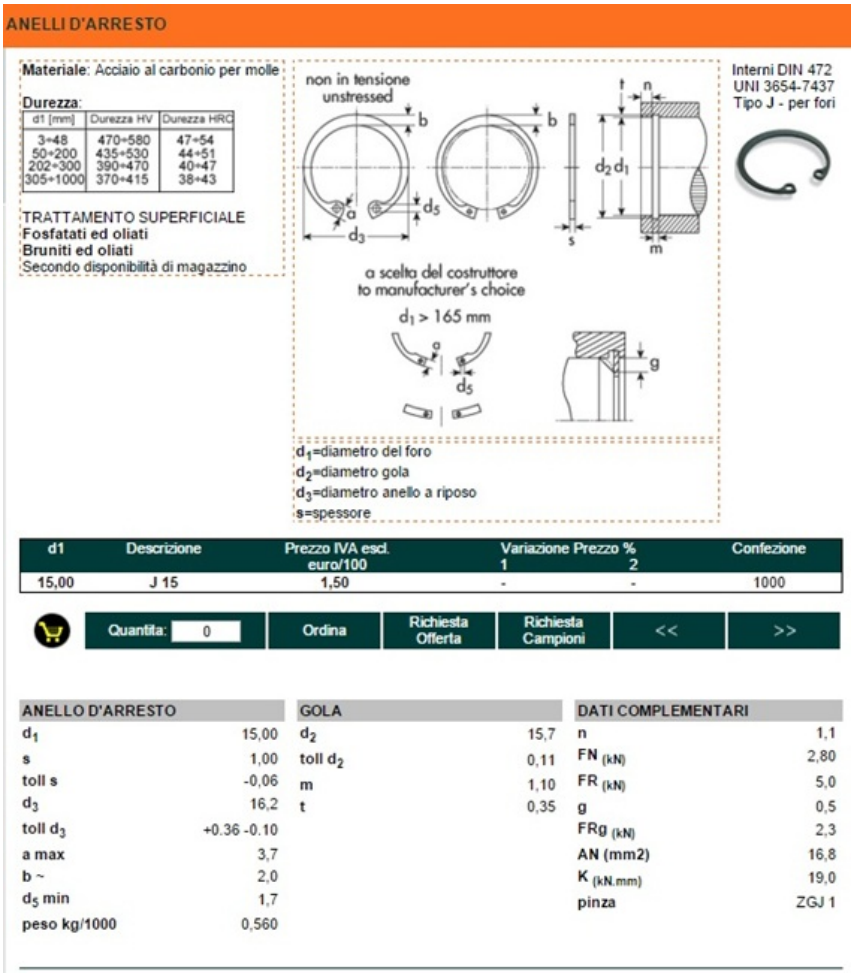

Figure A.4: Datasheet of the seeger for holes inserted in the outer hinges

Tesi di dottorato in Bioingegneria industriale, di Roberto Barone,
discussa presso l'Università Campus Bio-Medico di Roma in data 04/03/2017.
La disseminazione e la riproduzione di questo documento sono consentite per scopi di didattica e ricerca,
a condizione che ne venga citata la fonte.

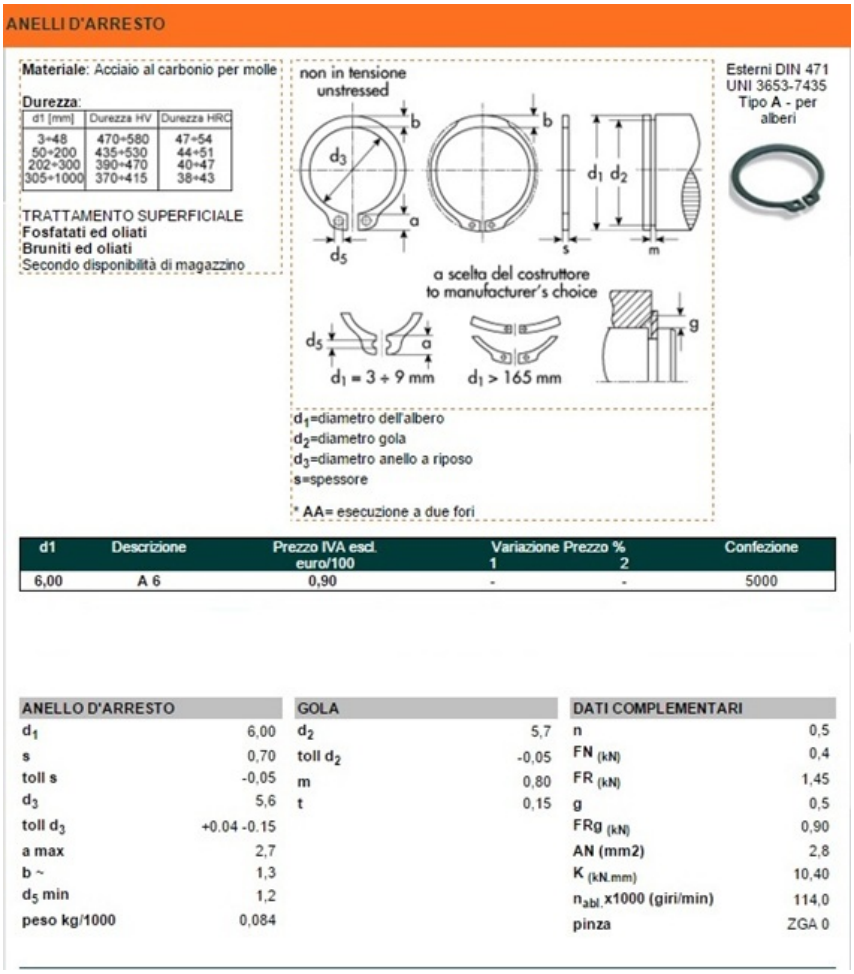

ANELLI D'ARRESTO

Materiale: Acciaio al carbonio per molle

Durezza:

d1 [mm]	Durezza HV	Durezza HRC
3÷48	470÷580	47÷54
50÷200	435÷530	44÷51
202÷300	390÷470	40÷47
305÷1000	370÷415	38÷43

TRATTAMENTO SUPERFICIALE
Fosfatati ed oliati
Bruniti ed oliati
Secondo disponibilità di magazzino

non in tensione
unstressed

a scelta del costruttore
to manufacturer's choice

$d_1 = 3 \div 9$ mm $d_1 > 165$ mm

Esterni DIN 471
UNI 3653-7435
Tipo A - per alberi

d_1=diametro dell'albero
d_2=diametro gola
d_3=diametro anello a riposo
s=spessore

* AA= esecuzione a due fori

d1	Descrizione	Prezzo IVA escl. euro/100	Variazione Prezzo % 1	2	Confezione
6,00	A 6	0,90	-	-	5000

ANELLO D'ARRESTO		GOLA		DATI COMPLEMENTARI	
d_1	6,00	d_2	5,7	n	0,5
s	0,70	toll d_2	-0,05	FN (kN)	0,4
toll s	-0,05	m	0,80	FR (kN)	1,45
d_3	5,6	t	0,15	g	0,5
toll d_3	+0.04 -0.15			FRg (kN)	0,90
a max	2,7			AN (mm2)	2,8
b ~	1,3			K (kN.mm)	10,40
d_5 min	1,2			n_{abl} x1000 (giri/min)	114,0
peso kg/1000	0,084			pinza	ZGA 0

Figure A.5: Datasheet of the seeger for shafts inserted in the outer hinges

Tesi di dottorato in Bioingegneria industriale, di Roberto Barone,
discussa presso l'Università Campus Bio-Medico di Roma in data 04/03/2017.
La disseminazione e la riproduzione di questo documento sono consentite per scopi di didattica e ricerca,
a condizione che ne venga citata la fonte.

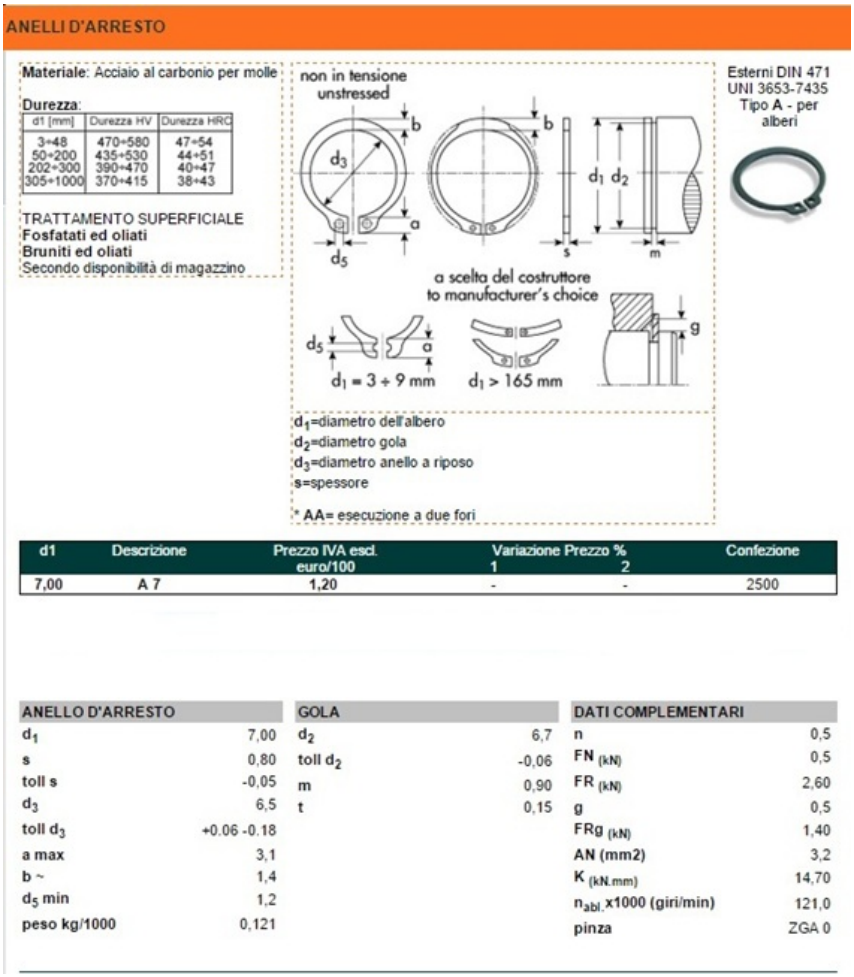

ANELLI D'ARRESTO

Materiale: Acciaio al carbonio per molle

Durezza:

d1 [mm]	Durezza HV	Durezza HRC
3÷48	470÷580	47÷54
50÷200	435÷530	44÷51
202÷300	390÷470	40÷47
305÷1000	370÷415	38÷43

TRATTAMENTO SUPERFICIALE
Fosfatati ed oliati
Bruniti ed oliati
Secondo disponibilità di magazzino

non in tensione
unstressed

Esterni DIN 471
UNI 3653-7435
Tipo A - per alberi

d_1=diametro dell'albero
d_2=diametro gola
d_3=diametro anello a riposo
s=spessore

* AA= esecuzione a due fori

d1	Descrizione	Prezzo IVA escl. euro/100	Variazione Prezzo % 1	2	Confezione
7,00	A 7	1,20	-	-	2500

ANELLO D'ARRESTO	
d_1	7,00
s	0,80
toll s	-0,05
d_3	6,5
toll d_3	+0.06 -0.18
a max	3,1
b ~	1,4
d_5 min	1,2
peso kg/1000	0,121

GOLA	
d_2	6,7
toll d_2	-0,06
m	0,90
t	0,15

DATI COMPLEMENTARI	
n	0,5
FN (kN)	0,5
FR (kN)	2,60
g	0,5
FRg (kN)	1,40
AN (mm2)	3,2
K (kN.mm)	14,70
n_{abl} x1000 (giri/min)	121,0
pinza	ZGA 0

Figure A.6: Datasheet of the seeger for shafts inserted in the inner hinges

Tesi di dottorato in Bioingegneria industriale, di Roberto Barone,
discussa presso l'Università Campus Bio-Medico di Roma in data 04/03/2017.
La disseminazione e la riproduzione di questo documento sono consentite per scopi di didattica e ricerca,
a condizione che ne venga citata la fonte.

› Specifiche sulle molle 'C.083.150.0320.A'

Numero di spire	7.7
Codice	C.083.150.0320.A
Diam. filo [mm]	1.5
Diam. est. [mm]	8.3
L. libera [mm]	32
Rigidità [daN/mm]	2.873563
Materiale	Filo armonico
Molatura	Si
Closed ends	Si
Diam. int. [mm]	5.3
Lc blocco [mm]	12.3
Peso [g]	2.329117
Alesaggio [mm]	8.466
Albero [mm]	5.194
Passo[mm]	5.08
Codice tariffa	4J
Flessione con lunghezza [mm]	nessun rischio
Lungh. max. [mm]	26.68

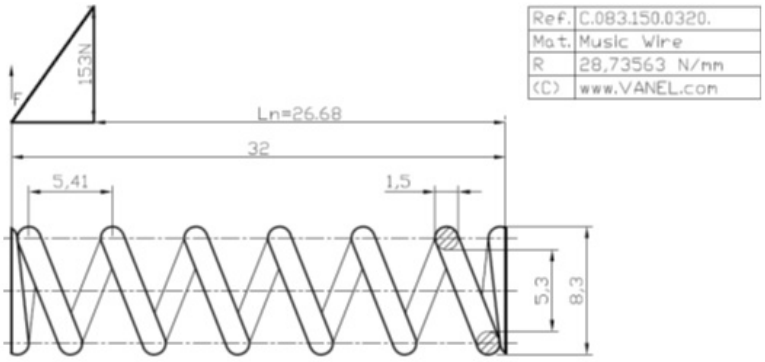

Figure A.7: Specification of the spring of the flexion-extension module

Tesi di dottorato in Bioingegneria industriale, di Roberto Barone,
discussa presso l'Università Campus Bio-Medico di Roma in data 04/03/2017.
La disseminazione e la riproduzione di questo documento sono consentite per scopi di didattica e ricerca,
a condizione che ne venga citata la fonte.

SKF

PCM 030406 E/VB055

Dimensions

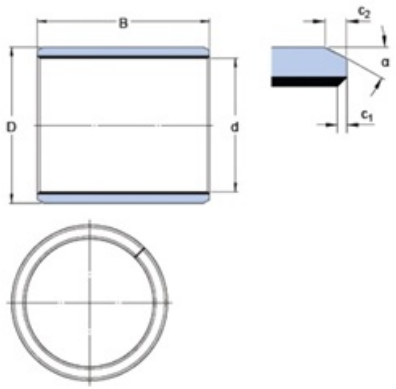

d		3	mm
D		4.5	mm
B		6	mm
c_1	min.	0.1	mm
c_1	max.	0.4	mm
c_2	min.	0.2	mm
c_2	max.	0.8	mm
α	±8	20	°

Recommended fits

Tolerance shaft	f7
Tolerance housing	H7

Calculation data

Basic dynamic load rating - radial direction	C		1.4	kN
Basic static load rating - radial direction	C_0		4.5	kN
Specific dynamic load factor	K		80	N/mm²
Specific static load factor	K_0		250	N/mm²
Factor depending on material and bearing type	K_M		480	
Permissible sliding velocity	v	min.	0	m/s
Permissible sliding velocity	v	max.	2	m/s
Coefficient of friction	μ	min.	0.03	
Coefficient of friction	μ	max.	0.25	

Mass

Mass bushing	0.0004	kg

Figure A.8: Datasheet axlebox

Tesi di dottorato in Bioingegneria industriale, di Roberto Barone,
discussa presso l'Università Campus Bio-Medico di Roma in data 04/03/2017.
La disseminazione e la riproduzione di questo documento sono consentite per scopi di didattica e ricerca,
a condizione che ne venga citata la fonte.

› Specifiche sulle molle 'C.075.050.0064.I'

Numero di spire	3.7
Codice	C.075.050.0064.I
Diam. filo [mm]	0.5
Diam. est. [mm]	7.5
L. libera [mm]	6.4
Rigidità [daN/mm]	0.094
Materiale	Inox
Molatura	Si
Closed ends	Si
Diam. int. [mm]	6.5
Lc blocco [mm]	2.1
Peso [g]	0.126816
Alesaggio [mm]	7.725
Albero [mm]	6.305
Passo[mm]	3.18
Codice tariffa	4D
Flessione con lunghezza [mm]	nessun rischio
Lungh. max. [mm]	2.43

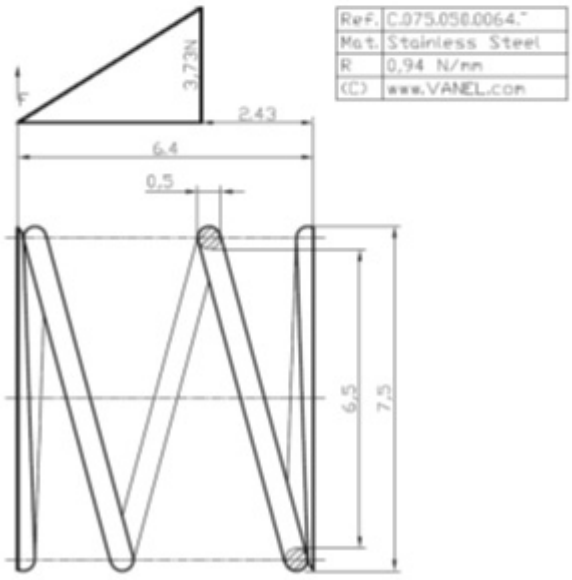

Figure A.9: Specification for the spring of the blocking mechanism

Tesi di dottorato in Bioingegneria industriale, di Roberto Barone,
discussa presso l'Università Campus Bio-Medico di Roma in data 04/03/2017.
La disseminazione e la riproduzione di questo documento sono consentite per scopi di didattica e ricerca,
a condizione che ne venga citata la fonte.

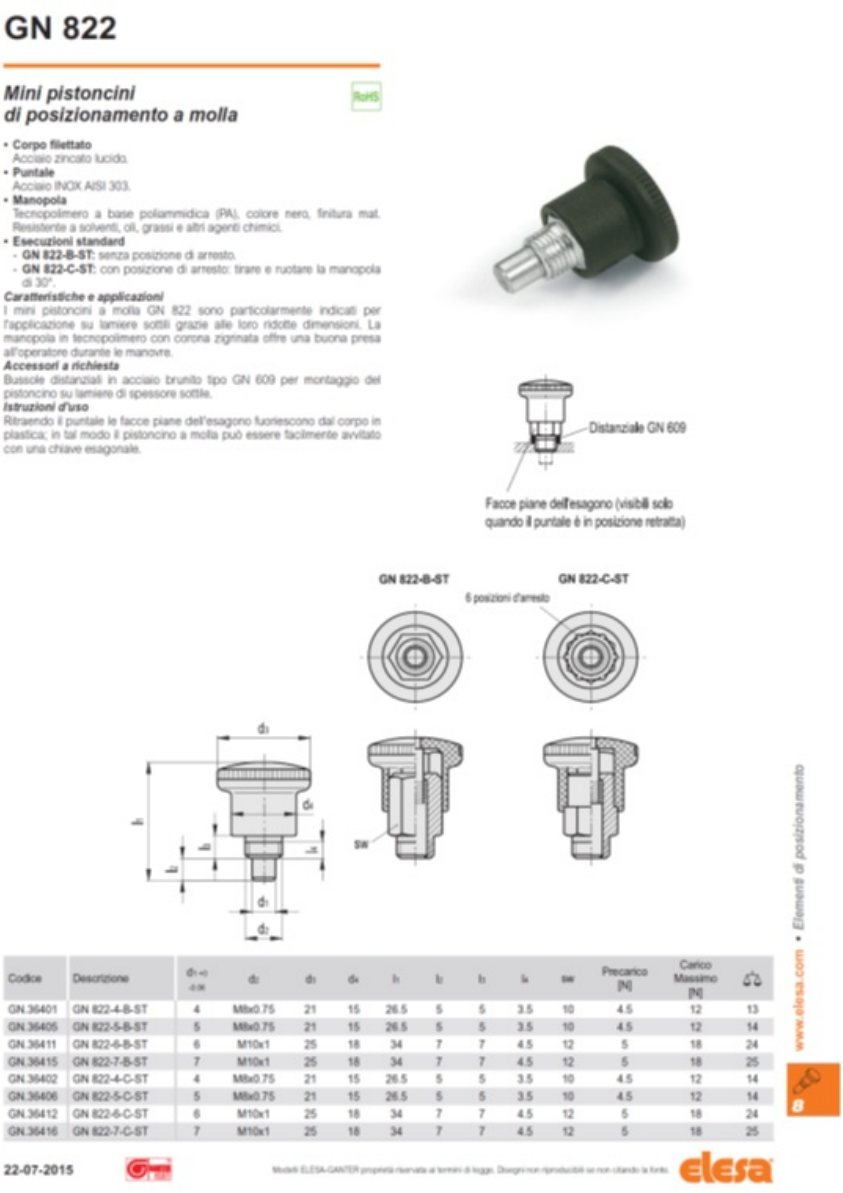

GN 822

Mini pistoncini di posizionamento a molla

RoHS

- **Corpo filettato**
  Acciaio zincato lucido.
- **Puntale**
  Acciaio INOX AISI 303.
- **Manopola**
  Tecnopolimero a base poliammidica (PA), colore nero, finitura mat. Resistente a solventi, oli, grassi e altri agenti chimici.
- **Esecuzioni standard**
  - **GN 822-B-ST:** senza posizione di arresto.
  - **GN 822-C-ST:** con posizione di arresto: tirare e ruotare la manopola di 30°.

Caratteristiche e applicazioni
I mini pistoncini a molla GN 822 sono particolarmente indicati per l'applicazione su lamiere sottili grazie alle loro ridotte dimensioni. La manopola in tecnopolimero con corona zigrinata offre una buona presa all'operatore durante le manovre.

Accessori a richiesta
Bussole distanziali in acciaio brunito tipo GN 609 per montaggio del pistoncino su lamiere di spessore sottile.

Istruzioni d'uso
Ritraendo il puntale le facce piane dell'esagono fuoriescono dal corpo in plastica; in tal modo il pistoncino a molla può essere facilmente avvitato con una chiave esagonale.

Codice	Descrizione	d_1	d_2	d_3	d_4	l_1	l_2	l_3	l_4	sw	Precarico [N]	Carico Massimo [N]	
GN.36401	GN 822-4-B-ST	4	M8x0.75	21	15	26.5	5	5	3.5	10	4.5	12	13
GN.36405	GN 822-5-B-ST	5	M8x0.75	21	15	26.5	5	5	3.5	10	4.5	12	14
GN.36411	GN 822-6-B-ST	6	M10x1	25	18	34	7	7	4.5	12	5	18	24
GN.36415	GN 822-7-B-ST	7	M10x1	25	18	34	7	7	4.5	12	5	18	25
GN.36402	GN 822-4-C-ST	4	M8x0.75	21	15	26.5	5	5	3.5	10	4.5	12	14
GN.36406	GN 822-5-C-ST	5	M8x0.75	21	15	26.5	5	5	3.5	10	4.5	12	14
GN.36412	GN 822-6-C-ST	6	M10x1	25	18	34	7	7	4.5	12	5	18	24
GN.36416	GN 822-7-C-ST	7	M10x1	25	18	34	7	7	4.5	12	5	18	25

22-07-2015

Modelli ELESA-GANTER proprietà riservata ai termini di legge. Disegni non riproducibili se non citando la fonte.

elesa

Figure A.10: Datasheet small piston for the blocking system

Tesi di dottorato in Bioingegneria industriale, di Roberto Barone,
discussa presso l'Università Campus Bio-Medico di Roma in data 04/03/2017.
La disseminazione e la riproduzione di questo documento sono consentite per scopi di didattica e ricerca,
a condizione che ne venga citata la fonte.

Appendix B

Script utilized to calculate the momentum generated by the elastic forces on the external hinges in the configuration of the module rotated of 75°

```
% CalcoloMomentiBlocco %
AH=4;            % [mm]
OH=35.25;        % [mm]
AO=sqrt(AH^2+OH^2);
BO=AO;
l_blocco=12.3;   % [mm]
l_lib=32;        % [mm]
l_75=22.3;         % [mm]
beta=deg2rad(37.5);
alpha=deg2rad(75);
theta=asin(AH/AO);
gamma=theta-((pi/2)-alpha);
k=28.7;          % [N/mm]
FelComp=[-k*(l_lib-l_blocco)*sin(beta);
        k*(l_lib-l_blocco)*cos(beta);
        0];
AObraccio=[-AO*cos(gamma);
            -AO*sin(gamma);
            0];
MFelComp=cross(FelComp,AObraccio);          % [Nmm]
FelEst75=[-k*(l_lib-l_75)*sin(beta);
        k*(l_lib-l_75)*cos(beta);
        0];
BObraccio=[-BO*sin(alpha-theta);
            BO*cos(alpha-theta);
            0];
```

Tesi di dottorato in Bioingegneria industriale, di Roberto Barone,
discussa presso l'Università Campus Bio-Medico di Roma in data 04/03/2017.
La disseminazione e la riproduzione di questo documento sono consentite per scopi di didattica e ricerca,
a condizione che ne venga citata la fonte.

```
MFelEst=cross(FelEst75,BObraccio);              % [Nmm]
Mtot=MFelEst(3)+MFelComp(3);
```

Kinematic

```
function [LMollaEstesa,LMollaComp,beta_tot,AHvet,AngoliAlphaPermessi]=
LunghezzaMollaMaxeMin(alpha_tot,BA_vet)
AHvet=0.0015:0.000925:0.020;
JHp=0.020;  % semiasse minore ellisse
for i=1:length(AHvet);
    AH=AHvet(i);
    for h=1:length(BA_vet);
        BA=BA_vet(h);
        OH=BA/2;
        for j=1:length(alpha_tot);
            alpha=alpha_tot(j);
            LJ=JHp*sin(alpha);
            BS=BA-(AH*sin(alpha)+(OH-OH*cos(alpha)));
            NR=BA+(AH*sin(alpha)-(OH-OH*cos(alpha)));
            FN=OH*sin(alpha)+AH;
            MpR=FN-AH*cos(alpha);
            MpN=sqrt(MpR^2+NR^2);
            beta=atan(MpR/NR);
      ApS=BS*tan(beta);
            ApB=sqrt(ApS^2+BS^2);
            beta_tot(j,h,i)=rad2deg(beta);
            LMollaComp(j,h,i)=ApB;
            LMollaEstesa(j,h,i)=MpN;
            AngoliAlphaPermessi(j,h,i)=rad2deg(alpha);
        end
    end
end
```

Tesi di dottorato in Bioingegneria industriale, di Roberto Barone,
discussa presso l'Università Campus Bio-Medico di Roma in data 04/03/2017.
La disseminazione e la riproduzione di questo documento sono consentite per scopi di didattica e ricerca,
a condizione che ne venga citata la fonte.

Bibliography

[1] Frontera WR and Silver JK. Fondamenti di Medicina Fisica e Riabilitativa. Verduci editore. 2004, 408-411.

[2] Brian MK et al. Upper limb prosthetics.

[3] Kyberd PJ and Chappell PH. The Southampton Hand: an intelligent myoelectric prosthesis. *Journal of rehabilitation Research and Development.* 1994, 31, 326.

[4] Pons JL, Rocon E, Ceres R, Reynaerts D, Saro B, Levin S and Van Moorleghem W. The MANUS-HAND dextrous robotics upper limb prosthesis: mechanical and manipulation aspects. *Autonomous Robots* 2004, 16, 143-163.

[5] Kyberd PJ, Holland OE, Chappell PH, Smith S, Tregidgo R, Bagwell PJ and Snaith M. MARCUS: A two degree of freedom hand prosthesis with hierarchical grip control. *IEEE Transactions on Rehabilitation Engineering.* 1995, 3, 70-76.

[6] Pylatiuk C, Mounier S, Kargov A, Schulz SASS, and Bretthauer G. Progress in the development of a multifunctional hand prosthesis. *In Engineering in Medicine and Biology Society* 2004. IEMBS'04. 26th Annual International Conference of the IEEE, 2, 4260-4263.

[7] Yang J, Pitarch EP, Abdel-Malek K, Patrick A, and Lindkvist L. A multifingered hand prosthesis. *Mechanism and Machine Theory* 2004, 39, 555-581.

[8] Karlik B, Tokhi MO, and Alci M. A fuzzy clustering neural network architecture for multifunction upper-limb prosthesis. *IEEE Transactions on Biomedical Engineering* 2003, 50, 1255-1261.

Tesi di dottorato in Bioingegneria industriale, di Roberto Barone,
discussa presso l'Università Campus Bio-Medico di Roma in data 04/03/2017.
La disseminazione e la riproduzione di questo documento sono consentite per scopi di didattica e ricerca,
a condizione che ne venga citata la fonte.

[9] Cipriani C, Antfolk C, Controzzi M, Lundborg G, Rosén B, Carrozza MC and Sebelius F. Online myoelectric control of a dexterous hand prosthesis by transradial amputees. *IEEE Transactions on Neural Systems and Rehabilitation Engineering.* 2011, 19, 260-70.

[10] http://www.ottobockus.com/prosthetics/upper-limb-prosthetics/solution-overview/michelangelo-prosthetic-hand/

[11] http://www.bebionic.com

[12] http://www.touchbionics.com/products/active-prostheses/i-limb-ultra

[13] Feix T, Romero J, Schmiedmayer HB et al. The GRASP taxonomy of human grasp types. *IEEE Transactions on Human-Machine Systems* 2016; 46: 66-77.

[14] http://hosmer.com/products/wrists/index.html

[15] http://bebionic.com/the_hand/system_components/bebionic3_wrist_options

[16] http://professionals.ottobockus.com/cps/rde/xchg/ob_us_en/hs.xsl/19015.html?id=42987#t42987

[17] http://www.liberatingtech.com/products/wrist/Lightweight_Wrist_System_for_Adults_-_Children.asp

[18] http://www.liberatingtech.com/products/wrist/Quick_Disconnect_Wrists_for_Adult_Electric_Hands.asp

[19] http://www.chemitec.co.il/images/stories/documents/orthopedia/Axon%20Bus%20Prosthethic%20System%20with%20Michelangelo%20hand.pdf

[20] Plettenburg DH. *The Wilmer 2-DOF Wrist Prosthesis for toddlers.* Proceedings of the 12th World Congress of the International Society of Prosthetics and Orthotics; 2007 Jul 29-Aug 3; Vancouver, Canada. p. 522.

[21] http://www.liberatingtech.com/products/wrist/OmniWrists_for_Adults_-_Children.asp

[22] http://www.utaharm.com/wrist-rotator.php

[23] http://www.liberatingtech.com/products/wrist/Wrist_Rotator_for_use_with_Adult_Hands.asp

Tesi di dottorato in Bioingegneria industriale, di Roberto Barone,
discussa presso l'Università Campus Bio-Medico di Roma in data 04/03/2017.
La disseminazione e la riproduzione di questo documento sono consentite per scopi di didattica e ricerca,
a condizione che ne venga citata la fonte.

[24] Kyberd PJ, Lemaire ED, Scheme E, MacPhail C, Goudreau L, Bush G, Brookeshaw M. Two-degree-of-freedom powered prosthetic wrist. *Journal of Rehabilitation Research And Development*, Volume 48, number 6, 2011.

[25] Ahmad S, Masood A, Khan US. Bowden Cable Based Powered Ball and Socket Wrist Actuator. *World Academy of Science, Engineering and Technology*, Issue 69, 2012. Tropea P, Stellin G, Carrozza MC, Dario P. Development of an innovative and compliant robotic wrist. *Proceedings of the 2nd Biennial IEEE/RAS-EMBS International Conference on Biomedical Robotics and Biomechatronics*, Scottsdale, AZ, USA, October 19-22, 2008.

[26] Tropea P, Stellin G, Carrozza MC, Dario P. Development of an innovative and compliant robotic wrist. *Proceedings of the 2nd Biennial IEEE/RAS-EMBS International Conference on Biomedical Robotics and Biomechatronics* Scottsdale, AZ, USA, October 19-22, 2008.

[27] Takeda H, Tsujiuchi N, Koizumi T, Kan H, Hirano M, Nakamura Y. Development of prosthetic arm with pneumatic prosthetic hand and tendon-driven wrist. *Engineering in Medicine and Biology Society*, 2009. EMBC 2009. Annual International Conference of the IEEE , pp.5048,5051, 3-6 Sept. 2009

[28] Scott RN and Parker PA. Myoelectric prostheses: state of the art. *J. Med. Eng. Technol.* 1988, 12, 143-151.

[29] Battyeet CK, Nightingale A and Whillis J. The use of myo-electric currents in the operation of prostheses. *J.Bone Joint Surg.* 1995, 37, 506-510.

[30] Popov B (1965). The bio-electrically controlled prosthesis. *J. Bone Joint Surg.* (British) 1965; 47B,421-424.

[31] Fougner A, Stavdahl O, Kyberd PJ, Losier YG and Parker P. Control of upper limb prostheses: terminology and proportional myoelectric control: a review. *IEEE Transac. Neural Syst. Rehabil. Eng.* 2012; 20,663-677.

[32] Jiang N and Farina D. Myoelectric control of upper limb prosthesis: current status, challenges and recent advances. *Front.Neuroeng.Conference* 2014.

[33] Hijjawi JB, Kuiken TA, Lipschutz RD, Miller LA, Stubblefield KA, and Dumanian GA. Improved myoelectric prosthesis control accomplished using multiple nerve transfers. *Plast.Reconstr.Surg.* 2006, 118, 1573-1578.

Tesi di dottorato in Bioingegneria industriale, di Roberto Barone,
discussa presso l'Università Campus Bio-Medico di Roma in data 04/03/2017.
La disseminazione e la riproduzione di questo documento sono consentite per scopi di didattica e ricerca,
a condizione che ne venga citata la fonte.

[34] Aszmann OC, Roche AD, Salminger S, Paternostro-Sluga T, Herceg M, Malvina H, et al. Bionic reconstruction to restore hand function after brachial plexus injury: a case series of three patients. *Lancet* 2015, 385, 2183-2189.

[35] Miller LA, Stubblefield KA, Lipschutz RD, Lock BA, and Kuiken TA. Improved myoelectric prosthesis control using targeted reinnervation surgery: a case series. *IEEE Trans. Neural Syst. Rehabil. Eng.* 2008, 16, 46-50.

[36] Roche AD, Rehbaum H, Farina D and Aszmann OC. Prosthetic myoelectric control strategies: a clinical perspective. *Curr. Surg. Reports* 2014, 2, 1-11.

[37] Zecca M, Micera S, Carrozza MC, and Dario P. Control of multi functional prosthetic hands by processing the electromyographic signal. *Crit. Rev. Biomed. Eng.* 2002, 30, 4-6.

[38] Ninu A, Dosen S, Muceli S, et al. Closed-loop control of grasping with a myoelectric hand prosthesis: Which are the relevant feedback variables for force control?. *IEEE Trans. Neural Systems and Rehabilitation Engineering* 2014; 22: 1041-1052.

[39] Ciancio AL, Cordella F, Barone R, et al. Control of prosthetic hands via the peripheral nervous system. *Frontiers in neuroscience.* 2016;10.

[40] Kappassov Z, Corrales JA, Perdereau V. Tactile sensing in dexterous robot hands-Review. *Robotics and Autonomous Systems* 2015; 74: 195-220.

[41] Huang HP, Liu YH, Lee WC, et al. Rehabilitation Robotic Prostheses for Upper Extremity. In: Zhou M, Li HX and Weijnen M (eds) *Contemporary Issues in Systems Science and Engineering.* USA: Wiley, 2015, pp.661-697.

[42] Naidu DS and Chen CH. Control strategies for smart prosthetic hand technology: An overview. In: *IEEE Int. Conf. Engineering in Medicine and Biology Society*, Vancouver, British Columbia, Canada, August 20-24, 2008, pp.4314-4317.

[43] Wettels N, Parnandi AR, Moon JH, et al. Grip control using biomimetic tactile sensing systems. *IEEE/ASME Trans. on Mechatronics* 2009; 14: 718-723.

Tesi di dottorato in Bioingegneria industriale, di Roberto Barone,
discussa presso l'Università Campus Bio-Medico di Roma in data 04/03/2017.
La disseminazione e la riproduzione di questo documento sono consentite per scopi di didattica e ricerca,
a condizione che ne venga citata la fonte.

[44] Cipriani C, Zaccone F, Stellin G, et al. Closed-loop controller for a bio-inspired multi-fingered underactuated prosthesis. In: *IEEE Int. Conf. on Robotics and Automation*, Orlando, Florida, May 2006, pp.2111-2116.

[45] Zhu G, Duan X and Deng H. Hybrid Force-Position Fuzzy Control for a Prosthetic Hand. In: Lee J, Lee MC, Liu H and Ryu JH (eds) *Intelligent Robotics and Applications*. Springer Berlin Heidelberg, 2013, pp. 415-426, 2013.

[46] Pasluosta CF and Chiu AW. Evaluation of a neural network-based control strategy for a cost-effective externally-powered prosthesis. *Assistive Technology* 2012; 24: 196-208.

[47] Mingrino AR, Bucci A, Magni R, et al. Slippage control in hand prostheses by sensing grasping forces and sliding motion. *IEEE Int. Conf on Intelligent Robots and Systems*, Munich, Germany, September 12 - 16, 1994, pp.1803-1809.

[48] Engeberg ED and Meek SG, Adaptive sliding mode control for prosthetic hands to simultaneously prevent slip and minimize deformation of grasped objects. *IEEE/ASME Trans. on Mechatronics* 2013; 18: 376-385.

[49] Sriram G, Jensen AN and Chiu SC. Slippage control for a smart prosthetic hand prototype via modified tactile sensory feedback. In: *IEEE Int. Conf. on Electro/Information Technology*, Milwaukee School of Engineering Milwaukee, WI, 05 Jun - 07 Jun 2014, pp.225-230.

[50] Pasluosta CF and Chiu AW. Modulation of Grasping Force in Prosthetic Hands Using Neural Network-Based Predictive Control. *Artificial Neural Networks*; 2015; 179-194.

[51] Deng XB, Duan XG and Deng H. Disturbance Observer-Based Fuzzy Control for Prosthetic Hands. *Intelligent Robotics and Applications. Springer International Publishing*; 2015; 338-347.

[52] Ciancio AL, Barone R, Zollo L, et al. A bio-inspired force control for cyclic manipulation of prosthetic hands. In: *IEEE Int. Conf. of Engineering in Medicine and Biology Society*, Milan, Italy, August 25-29 2015, pp. 4824-4827.

[53] Gomez G, Hernandez A, Eggenberger Hotz P, et al. An adaptive learning mechanism for teaching a robotic hand to grasp. In: *International Symposium on Adaptive Motion of Animals and Machines*, 2005.

Tesi di dottorato in Bioingegneria industriale, di Roberto Barone,
discussa presso l'Università Campus Bio-Medico di Roma in data 04/03/2017.
La disseminazione e la riproduzione di questo documento sono consentite per scopi di didattica e ricerca,
a condizione che ne venga citata la fonte.

[54] Pastor P, Kalakrishnan M, Chitta S, et al. Skill learning and task outcome prediction for manipulation. In: *Robotics and Automation (ICRA), 2011 IEEE International Conference on*, Shanghai, China May 9-13 2011, pp. 3828-3834).

[55] Stulp F and Sigaud O. Path integral policy improvement with covariance matrix adaptation. *International Conference on Machine Learning* , Edinburgh, Scotland, June 26-July 1 2012.

[56] Stulp F and Sigaud O. Policy improvement methods: between blackbox optimization and episodic reinforcement learning. *Robotics and Computer Vision*, 2012.

[57] Bianco R and Nolfi S. Evolving the neural controller for a robotic arm able to grasp objects on the basis of tactile sensors. *Adaptive Behavior* 2004; 12: 37-45.

[58] Cheng-Hung and Naidu DS. Hybrid control strategies for a five-finger robotic hand. *Biomedical Signal Processing and Control* 2013; 8: 382-390.

[59] Meola V, Caligiore D, Sperati V, et al. Interplay of discrete and rhythmic manipulation movements during development: a policy-search reinforcement-learning robot model. *Trans. on Autonomous Mental Development*, 2016, in press.

[60] Siciliano B. Parallel force/position control of robot manipulators. In: *Robotics Research* 1996. Springer London, pp. 78-89, 1996.

[61] Scherillo P, Siciliano B, Zollo L, et al. Parallel force/position control of a novel biomechatronic hand prosthesis. *IEEE/ASME Int. Conf. on Advanced Intelligent Mechatronics* 2003, 2: 920-925.

[62] Engeberg ED and Meek SG. Backstepping and sliding mode control hybridized for a prosthetic hand. *Neural Systems and Rehabilitation Engineering, IEEE Transactions on* 2009; 17:70-79.

[63] Romeo RA, Cordella F, Zollo L, et al. Development and preliminary testing of an instrumented object for force analysis during grasping. *IEEE Int. Conf. of Engineering in Medicine and Biology Society*, Milan, Italy, August 25-29 2015, pp: 6720 - 6723.

[64] Bullock I and Dollar AM. Classifying Human Manipulation Behavior, *IEEE International Conf. on Rehabilitation Robotics*, 2011.

Tesi di dottorato in Bioingegneria industriale, di Roberto Barone,
discussa presso l'Università Campus Bio-Medico di Roma in data 04/03/2017.
La disseminazione e la riproduzione di questo documento sono consentite per scopi di didattica e ricerca,
a condizione che ne venga citata la fonte.

[65] Ciancio AL, Zollo L, Baldassare G, Caligiore D, Guglielmelli E. The role of learning and kinematic features in dexterous manipulation: a comparative study with two robotic hands. *International Journal of Advanced Robotic Systems*, vol. 10, pp. 1-21, 2013.

[66] Kurita Y, Ueda J, Matsumoto Y, Ogasawara T. CPG-Based Manipulation: Generation of Rhythmic Finger Gaits from Human Observation. *IEEE International Conference on Robotics and Automation*, pp. 1209-1214, 2004.

[67] Ozawa R, Arimoto S, Nakamura S, Bae JH. Control of an object with parallel surfaces by a pair of finger robots without object sensing. *IEEE Transactions on Robotics*, vol. 21, pp. 965-976, 2005.

[68] Peerdeman B, Fabrizi U, Palli G, Melchiorri C, Stramigioli S, Misra S. Development of prosthesis grasp control systems on a robotic testbed. *IEEE International Conference on Biomedical Robotics and Biomechatronics*, pp. 1110-1115, 2012.

[69] Zhang W, Zhao D, Chen Q, Du D. Linkage under-actuated humanoid robotic hand with control of grasping force. *In International Asia Conference on Informatics in Control, Automation and Robotics*, vol. 2, pp. 417-420, 2010.

[70] Jo J, Kim SK, Oh Y, Oh SR. Contact force control of a robotic hand using F/T sensory feedback with a rigid object. *IEEE International Conference on Automation Science and Engineering*, pp. 436-441, 2012.

[71] Sutton RS, Barto AG. Reinforcement learning: An Introduction, Cambridge MA, USA: *The MIT Press*, 1998.

[72] http://www.prensilia.com/index.php?q=en/node/40

[73] Zollo L, Roccella S, Guglielmelli E, Carrozza MC, and Dario P. Biomechatronic design and control of an anthropomorphic artificial hand for prosthetic and robotic applications. *IEEE/ASME Transactions On Mechatronics*, vol. 12, 418-429, 2007.

[74] Post M. Physical Examination of the Musculoskeletal System. *Year Book Medical Publishers*, Chicago, 1987.

[75] Smurr LM, Gulick K et al. Managing the Upper Extremity Amputee: A Protocol for Success. *JHT*. 2008; 21:160-76

Tesi di dottorato in Bioingegneria industriale, di Roberto Barone,
discussa presso l'Università Campus Bio-Medico di Roma in data 04/03/2017.
La disseminazione e la riproduzione di questo documento sono consentite per scopi di didattica e ricerca,
a condizione che ne venga citata la fonte.

[76] Stocker D, Neufeld A. A Pilot Study Examining Repetitive Strain Injuries in People with Limb Loss. *Proc. Myoelectric Controls*, Fredericton NB, Institute of Biomedical Engineering, University of New Brunswick. 1999; pp. 24-30.

[77] Jones LE and Davidson JH. Save that arm: a study of problems in the remaining arm of unilateral upper limb amputees. *Prosthetics and Orthotics International*, 1999; vol. 23, pp. 55-58.

[78] Gambrell CR. Overuse Syndrome and the Unilateral Upper Limb Amputee: Consequences and Prevention. *JPO* 2008; Vol 20, Num 3, p 126.

[79] Carey SL, Highsmith MJ, Maitland ME. and Dubey RV. Compensatory movements of transradial prosthesis users during common tasks. *Clinical Biomechanics*, 2008 23(9), 1128-1135.

[80] Mell AG, Childress BL, Hughes RE, The effect of wearing a wrist splint on shoulder kinematics during object manipulation. 2005; *Arch. Phys. Med. Rehabil.* 868, 1661-1664.

[81] Zinck A. *The investigation of compensatory movements in prosthesis users and the design of a novel wrist.* [master's thesis] [Fredericton (Canada)]: University of New Brunswick; 2008

[82] Atkins DJ, Heard DCY, Donovan WH. Epidemiologic overview of individuals with upper-limb loss and their reported research priorities. *J Prosthet Orthot* 1996; 8:2-11.

[83] Bertels T, Schmalz T, Ludwigs E. Objectifying of functional advantages offered by wrist flexion. *J Prosthet. Orthot.* 2009; 21(2):74-78.

[84] MacPhee B. Examining the prosthetic function and body behaviour of prosthesis users performing Activities of Daily Living. [master's thesis]. [Fredericton (Canada)]: University of New Brunswick; 2007.

[85] Berselli G and Vassura G, Design solution and methods for robotic hands that can help prosthetic hands development, pp. 78-91, 2012.

[86] Cutti A, Parel I, Luchetti M, Gruppioni E, Rossi N and Verni G. The psychosocial and biomechanical assessment of amputees fitted with commercial multi-grip prosthetic hands. pp. 59-77, 2012.

Tesi di dottorato in Bioingegneria industriale, di Roberto Barone,
discussa presso l'Università Campus Bio-Medico di Roma in data 04/03/2017.
La disseminazione e la riproduzione di questo documento sono consentite per scopi di didattica e ricerca,
a condizione che ne venga citata la fonte.

[87] NASA, "ANTHROPOMETRY AND BIOMECHANICS," [Online]. Available: hrrp:// msis.jsc.nasa.gov/sections/section03.htm.

[88] Garrett JW. The adult human hand: some anthropometric and biomechanical considerations. *Human Factors*, pp. 117-131, 1971.

[89] Ottobock, "Prosthetics Upper limb," [Online].

[90] Touch Bionics, «Flexion wrist,» Dicembre 2014. [Online]. Available: http://touchbionics.com/sites/default/files/files/flexion20wrist%20Product%20Sheet.pdf.

[91] Aizawa J, Masuda T, Koyama T, Nakamaru K, Isozaki K, Okawa A and Morita S. Three-dimensional motion of the upper extremity joints during various activities of daily living. *Journal of Biomechanics*, pp. 2915-2922, 2010.

[92] Ryu J, Cooney WP, Askew LJ, An KN and Chao YS. Functional ranges of motion of the wrist joint. *Journal of hand surgery*, pp. 409-419, 1991.